DEVELOPMENT OF HYBRID ELECTRIC POWERTRAIN OF REDESIGNED VOLKSWAGEN CRAFTER WITH ONLINE DATA ACQUISITION SYSTEM

Thesis for the Degree of Doctor of Philosophy (PhD)

Aminu Babangida

Supervisor: Dr. Péter Tamás Szemes

University of Debrecen
Doctoral Council of Natural Sciences and Engineering
Doctoral School of Informatics
Debrecen, 2025

Hereby I declare that I prepared this thesis within the Doctoral Council for Natural Sciences and Engineering, Doctoral School of Informatics, University of Debrecen in order to obtain a PhD Degree in Engineering at Debrecen University.
The results published in the thesis are not reported in any other PhD theses.
Debrecen, 2025.03.03

.....
signature of the
candidate

Hereby I confirm that Aminu Babangida candidate conducted his studies with my supervision within the Information Technology Systems and Networks with Industrial applications Doctoral Programme of the Doctoral School of Informatics of University of Debrecen between 2021 and 2025. The independent studies and research work of the candidate significantly contributed to the results published in the thesis. I also declare that the results published in the thesis are not reported in any other theses.
I support the acceptance of the thesis.
Debrecen, 2025.....

.....
signature of the
supervisor

DEVELOPMENT OF HYBRID ELECTRIC POWERTRAIN OF REDESIGNED VOLKSWAGEN CRAFTER WITH ONLINE DATA ACQUISITION SYSTEM

Dissertation submitted in partial fulfilment of the requirements for the doctoral (PhD) degree in Informatics

Written by: Aminu Babangida certified Mechatronics Engineer

Prepared in the framework of the Information Technology Systems and Networks with Industrial applications Doctoral Programme of the Doctoral school of Informatics of University of Debrecen

Dissertation Supervisor: Dr. Péter Tamás Szemes

The official opponents of the dissertation:

Dr. .....
Dr. .....

The evaluation committee:

chairperson:	Dr. .....
members:	Dr. .....
	Dr. .....
	Dr. .....
	Dr. .....

The date of the dissertation defence: 20 .....

Contents

List of Figures

List of Tables

Abstract

The function of energy management strategy (EMS) in electric vehicles (EVs) is to ensure the optimal performance conditions of the vehicles in terms of fuel economy and toxic gas emissions. In the Volkswagen (VW) hybrid powertrain of the Department of Vehicles Engineering, a 2.0 turbocharged direct injection common rail diesel engine (TDI CR) is integrated with a permanent magnet synchronous electrical machine (PMSM) to minimize vehicle consumption and gas emissions. This dissertation presents the development of the hybrid VW Crafter implemented with a novel methodology based on an online data acquisition (DAQ) approach for the analysis of vehicle controller area network (CAN) bus for electrical drives.

To facilitate the feasibility of transforming a conventional internal combustion engine (ICE) powered vehicle into a hybrid, the vehicle CAN bus data is collected using LabVIEW software, which is based on the hardware-in-the-loop (HIL) method, decoded with the help of a database (DBC) file and analyzed by redesigning the Crafter based on the data measurements conducted and complemented by the model-in-the-loop (MIL) method on the basis of the physical background plant descriptions of the vehicle components with a computer-aided simulation (CAS) in MATLAB/Simulink/Simcape environment.

This dissertation analyzes the vehicle's traction using its mathematical background descriptions to validate its exact power source as a trade-off between vehicle size, battery size, engine, vehicle mass, driving range, and fuel consumption as well battery capacity fade over time and its life cycles. Thus, in the context of the technical requirements and design considerations, the Crafter is evaluated and validated to achieve VW's performance objectives set at the beginning of the vehicle design and construction. Moreover, EMS using a proportional integral derivative-based genetic algorithm (GA-PID), proposing an integral time absolute error (ITAE) as a fitness function, is developed to allocate load demand to the power source, reducing fuel consumption and carbon (IV) oxide (CO_2) emissions. Hence, the pure, conventional, and hybrid versions of the vehicle are developed and compared. The effectiveness of the proposed EMS is verified by the proportional integral-based particle swarm optimization (PSO-PI) and fractional order proportional integral derivative (FOPID) control strategies for the hybrid powertrain. This research reduces fuel consumption, CO_2 emissions and energy consumption by 68.620%, 70.840%, and 25.080%, respectively. The contributions of this research have been published in international conferences and journals.

Acknowledgements

I wish to thank my supervisor, Dr. Péter Tamás Szemes, for his insightful contribution and constructive criticism towards the success of my research throughout this journey. I would not have achieved this without his valuable advice, effort, and mentoring. I also wish to acknowledge the head of the doctoral program, Prof. Dr. Sztrik János, for his insightful and moral support towards my success throughout this journey. Similarly, I want to thank the Dean of the Engineering Faculty, Prof. Dr. Géza Husi, and the head of the doctoral school, Prof. Dr. Baran Sándor, for their support and a conducive atmosphere for my academic success. I must acknowledge all Engineering faculty staff, especially Prof. Dr. Korondi Péter and Szabolcs Sándor Diós and the faculty of Informatics staff, for their tireless support and encouragement throughout my studies. I want to thank my wife, Amina Sani Lawan, and my newborn son, Mahmud Aminu Babangida, who was born in Hungary and has brought immense joy to our lives. Their patience, emotional support, and physical presence have been invaluable to me, and I appreciate everything they do.

Publications

1. Kunya, A. B., Mundu, M. M., Babangida, A., and Szemes, P. T. (2025). MPC based Frequency Control of an Autonomous Microgrid Integrated with Electric Vehicles. Results in Engineering, 104727. https://doi.org/10.1016/j.rineng.2025.104727.

2. Omer Ghareeb AWJ, Babangida A, Szemes P. T. (2025). Dynamic Modeling and Optimization of Permanent Magnet Synchronous Electrical Machine Propulsion Powertrain at Different Modeling Levels. Acta Polytechnica Hungarica. 22 (3). https://doi.org/10.12700/aph.22.3.2025.3.3.

3. Babangida, A., Korondi, P., Diós, S. S., and Szemes, P. T. (2024, September). Development of Meta-Heuristic Optimization Based Control of Redesigned VW Crafter Hybrid Vehicle. In 2024 IEEE 21st International Power Electronics and Motion Control Conference (PEMC) (pp. 1-6). IEEE. https://doi.org/10.1109/PEMC61721.2024.10726405.

4. Babangida, A., and Szemes, P. T. (2024). Dynamic Modeling and Control Strategy Optimization of a Volkswagen Crafter Hybrid Electrified Powertrain. Energies, 17(18), 4721. https://doi.org/10.3390/en17184721.

5. Neamah HA, Dulaimi M, Silavinia A, Babangida A, and Szemes P. T. (2024). Development of a Volkswagen Jetta MK5 Hybrid Vehicle for Optimized System Efficiency Based on a Genetic Algorithm. Energies. 17(5):1116 https://doi.org/10.3390/en17051116.

6. Babangida A, Light Odazie CM, and Szemes P. T. (2023). Optimal Control Design and Online Controller-Area-Network Bus Data Analysis for a Light Commercial Hybrid Electric Vehicle. Mathematics. 11(15):3436. https://doi.org/10.3390/math11153436

7. Babangida, A., Odazie, C. M. L., and Szemes, P. T. (2023, June). Fuel economy simulation and development of an online data acquisition system with hil method for a vw crafter hybrid car. In 2023 IEEE 32nd International Symposium on Industrial Electronics (ISIE) (pp. 1-4). IEEE. doi:10.1109/ISIE51358.2023.10227931.

8. Maaruf, M., Babangida, A., Almusawi, H. A., and Szemes, P. T. (2022). Neural network-based finite-time control of nonlinear systems with

unknown dead-zones: Application to quadrotors. Journal of Robotics and Control (JRC), 3(6), 735-742.. https://doi.org/10.18196/jrc.v3i6.15355

9. Babangida, A., Husi, G., and Szemes, P. T. (2022). Bond Graph Modeling, Simulation, and Control of Permanent Magnet Linear Synchronous Motor: PMLSM Motor Based EVs Applications. Recent Innovations in Mechatronics, 9(1), 1-9. https://doi.org/10.17667/riim.2022.1/3.

10. Babangida, A., and Szemes, P. T. (2022, September). Energy consumption simulation and economic benefit analysis for a light duty urban commercial electric vehicle. In 2022 IEEE 20th International Power Electronics and Motion Control Conference (PEMC) (pp. 667-672). IEEE. doi:10.1109/PEMC51159.2022.9962881

11. Babangida, A and Szemes, P. T. (2021) Electric Vehicle Modelling and Simulation of a Light Commercial Vehicle Using PMSM Propulsion. HUNGARIAN JOURNAL OF INDUSTRY AND CHEMISTRY, 49 (1). pp. 37-46. https://doi.org/10.33927/hjic-2021-06

12. Babangida, A., and Szemes, P. T. (2021). Electric Vehicle Modeling and Simulation of Volkswagen Crafter with 2.0 TDI CR Diesel Engine: VW Vehicle 2020 Based PMSM Propulsion . Recent Innovations in Mechatronics, 8(1), 1-6. https://doi.org/10.17667/riim.2021.1/1.

Chapter 1

Introduction

1.1 Background of Research and Motivation

This chapter presents the motivation and background for designing the hybrid electrified powertrain for the VW Crafter 35 Einzelkabine mittlerer Radstand 103 (VW Crafter EIKA MR103); manufactured in 2020, and its topology, the establishment of the vehicle and 2.0 TDI CR diesel ICE, and the review of the current state of literature in the area of electric and hybrid cars.

1.1.1 Hybrid Powertrain Technology Evolution

In past decades, ICE emissions have been one of the chronic environmental concerns that causes global warming and dangerous air pollution. Gas-powered vehicles have been the source of this negative trend. For example, light commercial vehicles and passenger cars made about 16% and 3% of Europe's total CO_2 emissions. To reduce this negative trend, a CO_2 emission standard was set in the framework of 2019/631 European Union (EU) regulations for new vehicles and passenger cars. With this stricter target, the emissions from the latest passenger cars and commercial vehicles were reduced by 27% and 10%, respectively, from 2019 to 2022. The European Parliament and the Council on 19 April 2023 amended the regulations regarding the CO_2 emissions standards for the new commercial vehicles and passenger cars to comply with the EU's ambition of reaching climate neutrality by 2050. This target would strengthen the emissions standards from 2030, which will set the target for reducing CO_2 emissions by 100% from 2035 onward [1]. Two critical pathways can be adapted to scale down the green house gas (GHG) emissions: fuel consumption reduction (increasing energy efficiency)

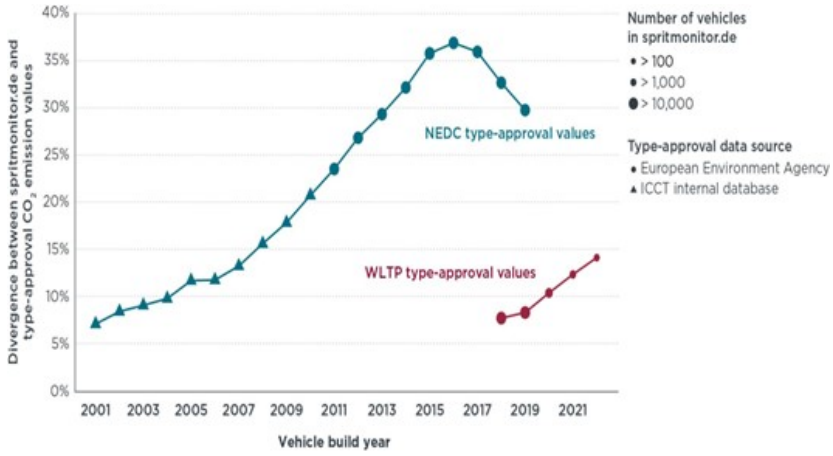

Figure 1.1.1: Fuel Consumption and Emission Standard [3]

and reduction in the CO_2 emissions [2].

The significance of fuel consumption research in vehicles has been underscored in [4, 5], highlighting its relevance in advancing sustainable solutions in transportation networks. It represents the maximum allowable amount of fuel that a vehicle can use over a specified distance (typically 1 kilometer) [6]. This fuel consumption evaluation considers vehicle weight, driving conditions, road conditions, frontal area, and environmental factors. Hence, for strict emission requirements for each type of vehicle to comply with European emissions standards [6], the "Worldwide Harmonized Light Vehicle Test Procedure (WLTP)", which is closer to replicating the real-world driving scenario [7], was introduced by the EU to standardize global carbon dioxide emissions and fuel consumption, replacing the "New European Driving Cycle (NEDC)" test procedure [6]. In 2022, it was discovered that the difference between real-world fuel and the official consumption and emissions of carbon dioxide values has increased to 14%, which is higher than the one announced by the manufacturers, despite introducing the new test procedure (WLTP) [3]. Therefore, this must be adequately addressed so as not to compromise with the requirements of the European emissions standards. Figure 1.1.1 above shows the approved difference between the hybrid and ICE vehicles' real-world fuel consumption and emissions of CO_2 [3]. The EU emission standard spelt out in the regulation from 2020 to 2024 for commercial vehicles was 147 gCO_2/km, while the passenger cars was 95 gCO_2/km based on the NEDC test profile. On the other hand, the CO_2 emission targets based on the WLTP test procedure for the commercial vehicles were 93.6 gCO_2/km from

2024 to 2029 and 49.5 gCO_2/km from 2030 to 2034. While for the passenger cars, the emission targets were 153.9 gCO_2/km from 2025 to 2029 and 90.6 gCO_2/km from 2030 to 2034 [1]. Thus, the WLTP test procedure, in addition to the Real Driving Emissions (RDE) test, was introduced in January 2022, which must be passed by newly registered cars. This is known as the Euro 6 d (EU6d) emissions standard, tougher real-world testing, adopted to ensure the generation of much cleaner new diesel cars [8].

From the research context, the above mentioned challenges can be mitigated by the development of electric models [9]. Consequently, the automotive industry has put efforts in top gear and has spanned various research institutions, especially transportation and environmental researchers, to strive for an alternative and clean energy source. Electric vehicles (EVs) have been widely adopted as environmentally friendly vehicles [10], [11], [12], making them an emerging research area and became the key selling point for electric car dealers. Therefore, EVs have been embraced and continued to be adopted as a lasting solution to eliminate GHG emissions [13]. However, the main issues in developing EVs are the limited ranges of operation, the long charging time, their limitation in terms of energy density, and difficulty in accessing electricity in remote areas, which can be restrictive [14], [15], [16].

The historical development of EVs can be categorized into stages. Starting from the 1900s, electric cars were in use, particularly in big cities, due to EVs' limited range of operation. Their production peaked in 1912 [17]. Therefore, the use of EVs was only favored in big cities. On the other hand, many countries did not have sufficient electrical power infrastructures to meet the widespread adoption of EVs [18]. However, the development of extended modern road transportation with a massive expansion of the network of petrol stations had led to the enormous production of cars with the ICE. Therefore, in this early stage of history, cars with ICE were preferred due to the mass production, which led to lower prices [19].

In this early stage, electric and hybrid cars were developed, such as general motors electric vehicle 1 (GM's EV1) and Toyota's Prius. Ten years later, Tesla cars became the most popular in the vehicle market. Meanwhile, the global increase in charging locations occurred worldwide, and the involved engineers and scientists recorded intensive improvement in the batteries. Nowadays, nations worldwide offer a wide range of manufacturing hybrids, plug-in hybrids, and full EVs, and they subsequently look forward to developing future cars [19]. However, the combined disadvantages of full EVs and ICE cars prompted the research on hybrid electric vehicles (HEVs), which dominate sales market for electrified vehicles [20]. HEVs combine

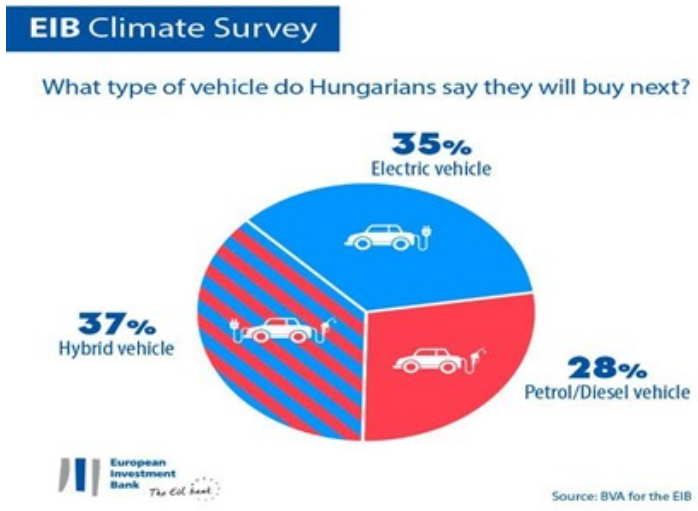

Figure 1.1.2: Statistical Consumer Survey [29]

electrical machine and engine technology [21, 22], consume less fuel and lower costs than their conventional counterparts [23, 24, 25]. Hence, HEVs are highly energy efficient and aim to reduce fuel consumption [26, 27], and achieve carbon neutrality [28]. Moreover, reducing fuel consumption and toxic gas emissions has been vital in Europe's fight against climate change. Hence, hybrid vehicles have been preferred due to their advantages over full EVs and ICE vehicles by most customers of EVs in Europe, with particular reference to the data recorded in Hungary. Figure 1.1.2 above shows the results of the survey conducted by the European Investment Bank (EIB) around 2022 in Hungary on the use of hybrid vehicles over full electric and petrol/diesel vehicles. The survey results show that 37% of the Hungarians in Europe prefer hybrid vehicles (and it is up to 39% by the Europeans in general), 35% prefer full electric and 28% prefer ICE vehicles [29].

The above-analyzed state of literature motivates the need for hybrid electrified powertrain technology for the proposed vehicle in this research. Therefore, finding an optimal vehicle consumption rate is one of the cornerstones to adopt an appropriate control algorithm to save energy consumption and reduce carbon dioxide emissions. In general, research and development activities on the vehicle's consumption and the associated emissions are essential to ensure that the designed cars comply with European standards and consumer emerging mobility needs. Fuel consumption, fuel economy,

and energy are measured in liter per 100 kilometers (L/100 km), mile per gallon (MPG), kilometer per liter (km/L), kilowatt hour per 100 kilometer (kWh/100 km), respectively.

1.1.2 Establishment of VW Hybrid Crafter

VW Crafter is a light-duty commercial vehicle manufactured by Volkswagen. The VW Crafter was firstly developed in 2006 by car manufacturing company in Germany. Initially, this brand type took over the VW large transporter (LT) nameplate, which was inaugurated in 1975 [30]. However, the first Crafter issued was manufactured in the Mercedes-Benz Ludwigsfelde and Düsseldorf plants [30]. A French car designer, Laurent Boulay, is responsible for the frontal design of the Crafter, which takes advice from the Volkswagen Constellation [30]. The VW Crafter establishment process took place in two generations: the first generation (2006-2017) and the second generation (2017 to date). Subsequently, the VW Crafter has been revised into different versions. The VW Crafter van had a gross weight of 3500 kg and was approximately reduced to 2758 kg after transformation to pick-up style. The early generation of the VW Crafter was characterized by 5-speed automatic and 6-speed manual transmissions. In comparison, the latest design has up to 8-speed automatic transmission systems. Figure 1.1.3 shows the conventional version of the VW before integration with an electrical machine.

Since the reference vehicle in this research is a commercial vehicle, fuel consumption is of paramount importance. Based on the manufacturer's information, VW Crafter has an average fuel consumption of 11.69 Liters/100 kilometers (L/100 km) and 309 gCO_2/km emissions with a 2.5 L TDI diesel engine [31]. Later, the 2.5 L diesel engine was replaced by the most efficient 2.0 L TDI engines, and the vehicle consumption was reduced to 8.89 L/100 km and 235 gCO_2/km emissions [32]. According to the manufacturer datasheet, the proposed vehicle in this research has an average consumption of 10 L/100 km and associated carbon dioxide emissions of 223 gCO_2/km based on the latest test procedure. The toxic gas emissions and the use of fossil oil have been eliminated with the advent of electric Crafter (e-Crafter) in 2018. The e-Crafter has a gross weight of 2502 kg, a battery with a 35 kWh rated capacity, and a 90 km/h top speed [33]. Short operation range, longer charging time, and lower energy density would limit its popularity in the vehicle market.

This research presents the development of the hybrid powertrain (VW Crafter 35 EIKA MR103, 2020 manufactured) using the model-based ap-

Figure 1.1.3: Establishment of VW Crafter [30]

proach (MIL method) transition and physical assembly process of the VW Crafter of the faculty of engineering at the University of Debrecen from the conventional diesel-powered drivetrain to hybrid, introducing a novel methodology of experimental vehicle CAN Bus analysis acquired through a NetCAN Plus hardware devices (HIL method). This new approach formed the basis for the vehicle transformation for the optimal consumption and reduction of the CO_2 emissions. The physical assembly process of the VW Crafter started from construction to assembly, as investigated and led by a research group of the faculty of engineering in [30]. The engineering faculty unveiled the real transformation of this vehicle within the framework of the TKP project funding scheme. A new gearbox was designed based on gear ratios, incorporating the PMSM electrical machine (Parker motor), which was assembled on the rear wheel and activated by a switching mechanism. Therefore, the hybrid vehicle runs as a pure electric, conventional, and hybrid via the switching mechanism. Figure 1.1.4 shows the architecture of the VW Crafter integrated with the electrica drive and the online data acquisition (DAQ) system and Figure 1.1.5 shows the assembled vehicle. The vehicle monitoring system aims to conduct the electric drive test using the framework of the online measurement system via Netcan Plus 110 hardware. Moreover, a commonly used diagnostic tool known as VAG-COM diagnostic system (VCDS) was utilized to investigate the engine drive part, which accounts for the complete data analysis of the proposed vehicle. The details of the assembly process, gearbox design, and experimental analysis are presented in Chapter Four, covering the complete hybrid vehicle testing, development, and control.

The VW Crafter is proposed for this research due to its widespread adop-

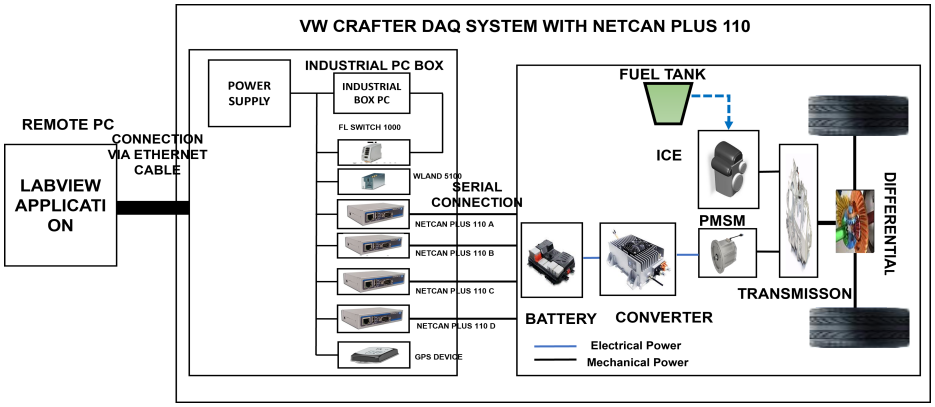

Figure 1.1.4: Architecture of Redesigned Crafter with DAQ System [34]

tion in European countries as a light-duty commercial vehicle, particularly suitable for urban goods transportation. The aim is to leverage both the benefits of a fully electric Crafter and a gas-powered one while keeping away from the disadvantages of the two. Its versatility, efficient performance, and eco-friendly features render it an ideal choice for businesses and individuals across various regions. However, the ICE-powered Crafter is plagued by high fuel costs, high fuel consumption, and toxic gas emissions that are detrimental to the environment compared to hybrids. However, the full-electric version is limited by its short range of operation and prolonged charging duration, which can hinder business logistics and individual purposes. To address these challenges, this dissertation proposes redesigning the conventional vehicle, leveraging the synergy between the 2011 Nissan Leaf battery pack and the PMSM electrical drive. The three-mode operation of this vehicle enables optimized performance, catering to varying torque requirements, thereby enhancing its suitability for light-duty applications in urban settings, benefiting both individual users and logistics operations.

1.1.3 Establishment of 2.0 TDI ICE

The vehicles' engines manufactured from 2006 to 2010 were based on the VW manufacturing company, i.e. 2.5 L diesel, 5-cylinder, TDI ICE [30]. This engine was characterized by having a displacement of 2.459 L, the updated common rail technology. It has a piezoelectric actuated injector that facilitates the direct injection of the fuel for the cylinder. To comply with Euro 4 emission standards, a diesel particulate filter (DPF) was incorporated into VW Crafter [30]. However, the engine in question had an issue of turbo

Figure 1.1.5: Assembled Vehicle [30]

failure, which motivated and necessitated its upgrade in 2010. This was accompanied by another updated engine that utilized diesel exhaust fluid (DEF) together with DPF, which was inconsistent with Euro 5 emission standards [30]. Nevertheless, another better version was unveiled in 2012, which was a 2.0 TDI engine. This version has become popular in many VW vehicles due to its high output torque, better fuel economy, and reduced toxic gas emissions compared to the old version [30].

This motivates the use of 2.0 TDI CR in the latest-designed vehicles which is in conformity with the emission standard of Europe. Therefore, the ICE for the Crafter in this research is 2.0 TDI, characterized by having a 1968 cm^3, 8–900 km range, and 70 L tank capacity.

1.2 VW Hybrid Powertrain Topology

There has been an effort to reduce the greenhouse effect by encouraging the transition from cars with ICEs to electric and hybrid vehicles. Electric cars are classified into three categories [35]. However, they can be classified in some cases based on the battery capacity [36] or engines technology [37]. These include plug-in hybrid electric vehicles (PHEVs), battery EVs (BEVs), and HEVs. Hybrid electric vehicle (HEV) is further classified into Parallel Hybrid Electric Vehicle (PHEV), Series Hybrid Electric Vehicle (SHEV), and Series-Parallel Hybrid Electric Vehicle (SPHEV). Battery electric vehicles (BEVs) or simply EVs, use battery as the source of energy required to propel the vehicle. The battery supplies the power to the electrical machine to produce the torque translated into vehicle movement. The capacity of the

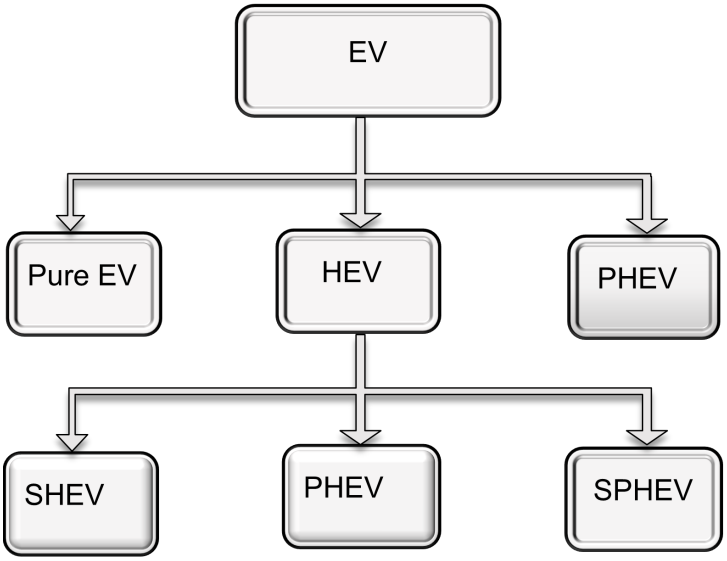

Figure 1.2.1: Classification of EVs

battery is a factor that determines the range to be covered by the vehicle [38].

Therefore, accurate electric vehicle (EV) parameters are crucial in the modeling approach, and obtaining them is the primary step. In this dissertation, the fixed parameters used have been sourced from the manufacturer's manual for the proposed vehicle. The proposed VW Crafter is a plug-in hybrid electric vehicle integrated with a synchronous machine electrical drive. Specifically, the combustion engine drives the front wheels, while the e-motor powers the rear wheels. As the name suggests, PHEVs can be recharged from an external power source [38]. Contrary to ordinary HEVs, battery of the PHEV is rechargeable. As described in this research, the types of EVs can be summarized as shown in Figure 1.2.1. In a series configuration, the electric generator is driven by the ICE. The generator performs two functions: Charging the battery as well powering the electrical machine (motor) that propels the vehicle's wheel. However, both the ICE and the motor are connected to a mechanical transmission to propel the vehicle for parallel powertrain. Meanwhile, the series-parallel hybrid incorporates a power-split device (planetary gear) that transmits electrical or mechanical power to the vehicle.

In this research, the VW Crafter was studied based on different types of EVs configuration and complexity levels. The conventional, parallel, series

and series-parallel topology of the powertrains as briefly introduced in this section. However, we focused on the detailed analysis of traditional, pure electric, and parallel hybrid powertrains based on real measurement data from the VW Crafter hybrid vehicle. Therefore, other types of EV-based VW Crafter as described in this section will be further elaborated and considered in future studies.

1.2.1 VW Crafter Mechanical Powertrain

Despite the considerable paradigm shift and increased penetration towards transportation electrification, ICE vehicles are still on our transportation network. This research designs the VW vehicles' conventional powertrain and uses it as a benchmark to investigate the fuel consumption and CO_2 emissions of the proposed hybrid vehicles. As stated in [39], one of the importance of simulating the powertrain-based ICE is that it allows us to evaluate the engine parts strength and durability, reliability and wear lubricated contacts of the engine parts, noise, and vibratory interaction of the powertrain with the body of the vehicle. The components of the mechanical powertrain consist of the ICE and the drivetrain [40]. The conventional VW Crafter is propelled by a 2.0 L TDI diesel engine with a maximum power of 103 kW (with DAUA engine code). A 6-speed manual gearbox is integrated with the gearbox controller. In [41] the performance of the ICE was assessed by the three essential parameters: the engine maximum power, the efficiency, and the engine displacement in liters. Figure 1.2.2 shows the conventional powertrain architecture as a front-wheel drive (FWD) for the VW Crafter. However, in real-world operating conditions, the FWD is preferred more in terms of fuel economy, while the real-wheel drive (RWD) is preferred in terms of performance [42]. In this research, the vehicle was simulated in RWD mode, assuming that the performance and fuel consumption characteristics remain comparable to the actual all-wheel drive (AWD) or FWD configurations. Hence, the detailed mechanical powertrain components consists of the engine, the fuel tank, the clutch (in case of the manual transmission), the gearbox, and the differential [40].

1.2.2 VW Crafter Electric Powertrain

The earlier version of e-Crafter 2018 model with 35.8 kWh battery capacity, had average consumption of 21.54 kWh/100 km [43]. However, due to payload and other external environmental factors, the e-Crafter with a model

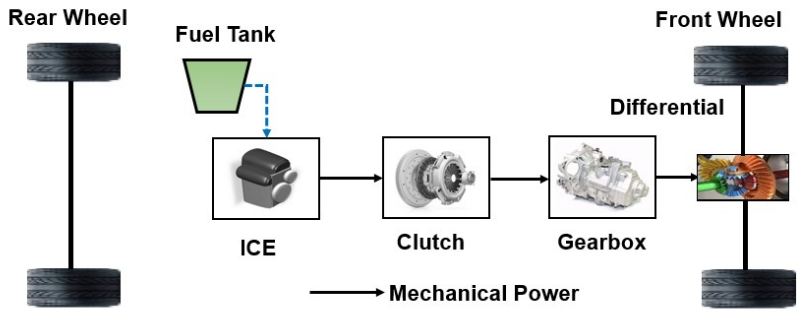

Figure 1.2.2: Conventional Powertrain Architecture

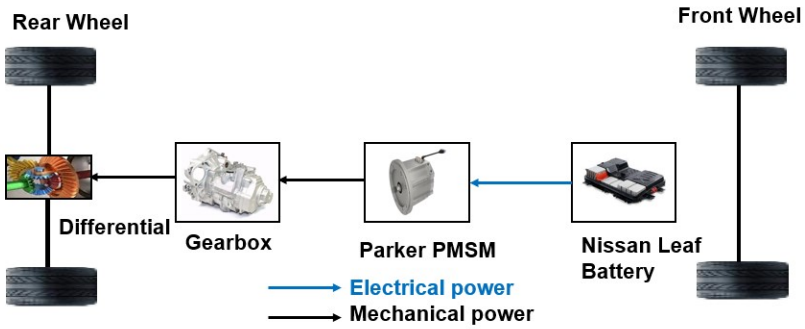

Figure 1.2.3: VW e-Crafter Powertrain Architecture

manufactured from 2018 to 2023 with the same battery capacity had an average energy consumption of 31.2 kWh/100 km based on data collected from 62 users. This is according to the VW model with 0603 manufacturer key and car global domain (CGD) type key numbers [44]. According to the other source, the VW manufactured in 2020 had an energy consumption of 29.1 kWh/100 km [45]. Therefore, this shows an increase in energy consumption based on the measured data from the manufacturer and the real measured data.

This motivates the need to develop an appropriate control algorithm to ensure that power and energy are managed at some optimal level that gives some extension of a wider kilometer of the e-Crafter. Figure 1.2.3 shows the simplified e-Crafter block diagram as RWD. It consists of the vehicle body, the gearbox, the electric motor, and the battery.

1.2.3 Parallel Hybrid Powertrain

Parallel HEVs have been developed to meet the users' and market demands, where there is high demand for performance and drivability [46], with a rapid growth from 2021 [47]. In parallel HEV, the engine and the electric motor propel the vehicle. There has been a decrease in fuel consumption and emissions with the advent of parallel hybrid vehicles. The studies in [48, 49] mentioned a significant improvement in the fuel consumption and CO2 emission for the parallel hybrid propulsion vehicle in compliance with a single-shift transmission system-based WLTP profile. The study in [50] stated that the parallel HEV produces the power of either the engine, the electrical machine, or both, while the torque produced combines the two. Figure 1.2.4 shows the block diagram of the proposed VW Crafter PHEV with the individual components before implementing the DAQ system. The following are the advantages associated with PHEV:

- It is very efficient due to limited energy losses.
- It is suitable for highway driving because it uses engine power directly.
- It consumes less fuel than the conventional ICE vehicles.
- It uses the electric motor as a generator to recharge the battery during the generative braking, significantly improving fuel efficiency.
- It has reduced costs because the motor can be used as a generator.

However, one of the disadvantages of the PHEV is its complexity in terms of design.

In PHEV, like the purely electric, the three-phase electric motor acts in both motoring and generating modes. The model consists of the following subsystems: the battery, the drive controller, which consists of the two control loops as in the case of the purely electric vehicle; the engine subsystem, the engine controller subsystem which is used to control the torque of the engine; the three-phase PMSM motor subsystem which consists of the three-phase inverter, the gate driver and the torque sensor; the longitudinal controller which is used to convert the driver input to load command.

1.2.4 Series Hybrid Powertrain

The VW Crafter has also been configured in the SHEV topology. The SHEV powertrain consists of a generator, an engine, and an electric motor. The

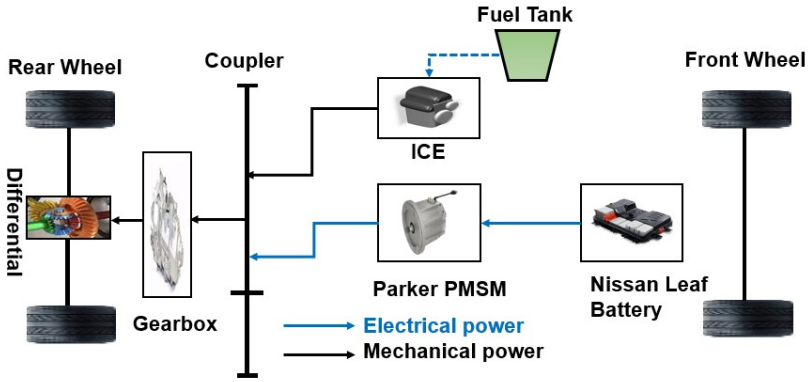

Figure 1.2.4: Parallel HEV Powertrain Architecture

engine drives the generator, which charges the battery and powers the electric motor that moves the vehicle. Therefore, in the case of this powertrain, the vehicle receives mechanical power directly from the electrical machine. Figure 1.2.5 shows the series powertrain topology. The SHEV is the simplest in terms of the energy management and configuration compared to the other types [51, 52].The SHEV has following advantages:

- The connections in SHEV are less complex than in PHEV.
- It is suitable for urban driving since the vehicle receives motor power directly.
- The driving conditions do not affect the engine's performance.

While the disadvantages are as follows:

- It is not suitable for highway driving.
- Short driving range.
- Increased cost due to the large motor and battery capacity requirement. Using generator adds to its cost compared to PHEV.
- Less efficient than PHEV.

The series model consists of the following subsystems: The Nissan Leaf battery, the driver inputs, the longitudinal vehicle controller, the DC-DC converter used to modulate the voltage of the battery, the three-phase

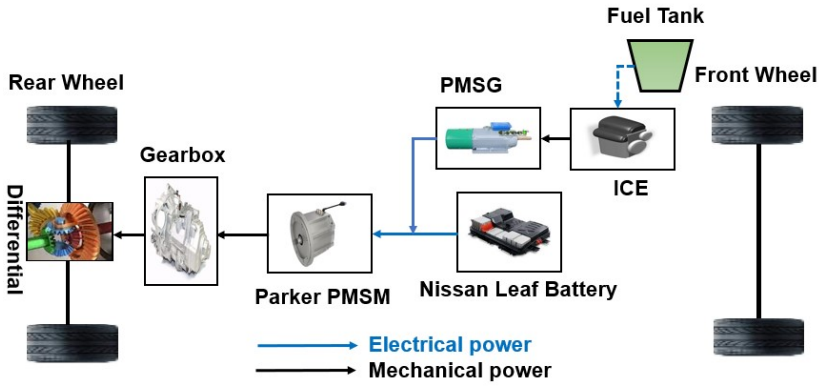

Figure 1.2.5: Series Hybrid Powertrain Architecture

permanent magnet synchronous generator (PMSG), the engine, the three-phase PMSM, and its three-phase inverter drive, the gate driver, the drive subsystems, the transmission system comprising the gearbox, the vehicle dynamics subsystems consisting of the vehicle body, the tires modeled based magic formula of pacejka, the friction brakes both for front and rear wheels and the sensor subsystem. There is no mechanical connection between the internal combustion engine and the vehicle's wheel in a series hybrid. The engine drives the three-phase permanent magnet generator, and the generator then charges the battery and powers the three-phase PMSM.

1.2.5 Series-Parallel Hybrid Powertrain

Series-parallel HEV combines the advantages and disadvantages of the SHEV and PHEV. In this configuration, the engine can provide power to the vehicle's wheel independently, just like in PHEV, or the electric motor can provide power to the vehicle's wheel, just like in the case of SPHEV. Toyota Prius is an example of this type of hybrid topology. The following are the advantages of SPHEV:

- Efficient in terms of performance.
- Uses less fuel.
- It has less energy loss.
- It has better traction.

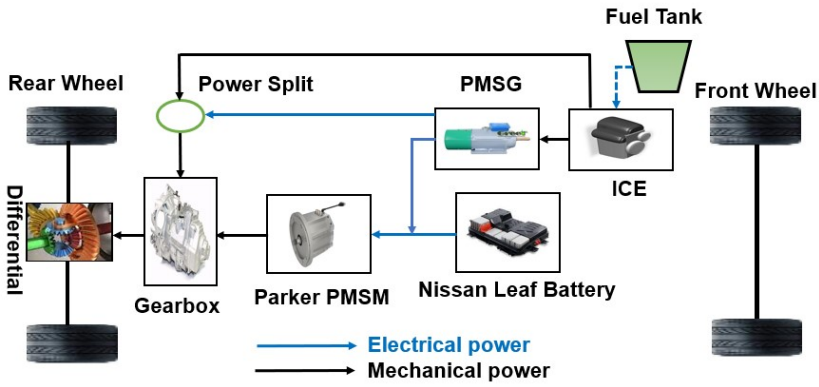

Figure 1.2.6: Series-parallel Powertrain Architecture

The following are the disadvantages of SPHEV:

- It is more expansive.
- Higher maintenance.
- Complex control system.

Figure 1.2.6 shows the VW Crafter series-parallel hybrid vehicle, which is more complex since it integrates both the series and parallel topologies. The model consists of many subsystems: the Nissan Leaf battery; the electrical subsystem, which comprises the DC-DC converter; the three-phase interior permanent synchronous generator and its three-phase inverter drive; the gate driver, and the sensor; the three-phase PMSM and its three-phase inverter drive, the gate driver, and the sensor; the control subsystem comprises the vehicle controller, the three- PMSM drive controller, the PMSG drive controller, and the combustion engine controller; the power split subsystem, the transmission system, and the vehicle subsystem comprising the vehicle body, the tire model, the brakes, and the sensor subsystems. The descriptions of the types of electric vehicles were studied based on the VW Crafter. Further research will be conducted based on these classifications, which is beyond the scope of this disseration.

1.3 Research Objectives

This research aims to design a hybrid vehicle-based VW Crafter, leveraging the experimental data obtained from the CAN bus system of the vehicle.

The objective is to transform the vehicle from the conventional to hybrid operated diesel engine and electric modes, and the specific objectives are as follows:

1. Designing the conventional VW Crafter powered by a 2.0 TDI CR diesel engine with a 6-speed manual transmission based on the MIL method.

2. Designing the pure VW Crafter EV powered by a PMSM propulsion system.

3. Designing the hybrid vehicle-based VW Crafter by integrating the electric motor-based PMSM propulsion system.

4. Comparing the fuel consumption between the conventional and hybrid powertrains.

5. Investigating the VW Crafter models at different modeling levels, taking into account the level of complexity and technical differences.

6. Developing an EMS-based GA-PID to minimize fuel consumption and CO_2 emissions. The vehicle controller will be optimized so that the vehicle speed successfully tracks the reference trajectory. The controller allocates the load demand to the power source.

7. Using LabVIEW to perform vehicle monitoring via CAN bus (HIL method) and real-time analysis of the CAN bus messages in and out of VW Crafter vehicle with vision systems NetCAN Plus 110 hardware. Therefore, the CAN bus messages are read from the vehicle and saved as a comma-separated values (CSV) file on a personal computer (PC). The CAN bus messages are not in human-readable form. Therefore, these raw CAN messages will be decoded with the help of the DBC file to provide an engineering meaning for the data.

Therefore, by achieving these objectives, this dissertation contributes to the development of sustainable solutions in transportation electrification.

1.4 Problem Statements, Research Contributions and Claims

Due to the growing demand to minimize the dependence on fossil fuels and improve the fuel economy, HEVs are now under rapid development. This

research aims to develop dynamic models of electric and hybrid vehicles at different levels of fidelity and ensure that power and energy are managed at an optimal level that extends the vehicles to a broader kilometer. The vehicle in this study is based on a 2020 VW Crafter and is suitable for the HIL testing. The vehicle industry has made a significant effort to transition from ICE vehicles to electric vehicles [53], as also emphasized in the context of various keynote speeches and research communities (2022 and 2024 IEEE Power Electronics and Motion Control Conferences). Since the 21st century, the increasing trend of EVs has focused on renewable energy, the impact of transportation systems on the climate due to greenhouse gas emissions, and many other related issues. As a result, EVs have been identified as a solution to climate change. More so, modern electric vehicles have achieved a safer transportation network by eliminating the traditional vehicles' GHG emissions and fuel consumption. However, the main problems in developing EVs include:

- Limited ranges of operation.
- Long charging times.
- Limitations in terms of energy density.
- Difficulty accessing electricity in remote areas.

These disadvantages pose significant obstacles to widespread adoption, necessitating more research activity to address these issues and improve the overall performance and practicality of EVs. Hence, the development of HEVs offers a more sustainable solution by reducing the emissions and fuel consumption and improving the driving range.

Over the years, several control methods have been proposed for HEV powertrains to realize optimal performance, including the vehicle's range extension, traction system current control, direct current (DC) bus voltage regulation, etc. However, intricate nonlinearity and other external effects make it challenging to develop an effective controller for energy management suitable for the vehicle powertrain. The vehicle controller is a classical proportional integral derivative (PID) controller. The PID controller has been widely applied due to its simplicity and practicality for mechatronic devices and industries. Linear control techniques like PID may not be a suitable control candidate for EVs due to the system's complexity and nonlinear effects inherent in the system, which may affect its performance. To address this challenge, an optimization method is necessary to enhance

the PID controller to manage the power and energy at an optimal level, extending the range of the vehicle. This study proposes an improved PID controller based on genetic algorithm (GA-PID) as an alternative control method to optimize the vehicle's energy and fuel consumption.

In modern vehicles, Electronic Control Units (ECUs), like the engine control unit, airbags, and more, are interconnected using the CAN bus system, a message-based protocol designed to reduce costs and complexity by minimizing dedicated electrical wiring between the ECUs. The CAN bus communication protocol incorporates features like message validation and arbitration, ensuring reliable data exchange. However, interpreting raw CAN bus data from vehicle ECUs poses a significant challenge. The raw messages contain hexadecimal CAN frames that require decoding into physical values (scaled engineering values like Volts, km, km/h, etc.) for meaningful analysis. To develop efficient EVs that match the performance of conventional combustion engines, evaluating existing vehicle performance using CAN bus data is crucial. This research collects CAN Bus messages from a VW Crafter using a LabVIEW software-designed system and Vision Systems NetCAN 110 hardware for real-time performance evaluation. This data helps vehicle manufacturers determine the optimal motor and battery capacity for electric vehicles that meet standard requirements. This research uses the data collected as a reference for the design of conventional, pure and hybrid powertrains for the reference vehicle, enabling a comprehensive comparison of the simulation and experimental results. Therefore, the primary contributions of this dissertation compared to existing works are as follows:

1. The thermal performance and capacity fade (degradation) of the 2011 Nissan Leaf battery over time and through various life cycles have been investigated in its first and second life cycles, using a realistic current profile at a 5 C-rate. The simulated battery still maintains 60.3% of its remaining capacity in its first life with a 56% fading rate per 1000 cycles at an operating temperature of 29.30 °C.

2. For the first time, this research investigates the optimal design of the VW Crafter as a trade-off between vehicle size, battery size, engine, vehicle mass, driving range and consumption.

3. This research designs different VW Crafter physical models (simplified and extended) levels, considering technical differences and complexity levels. The simplified model accounts for the transmission losses and

the computational burden of the analytical approaches adopted in the existing literature. This method enables a more effective and accurate investigation of the optimal fuel economy of the proposed vehicle. The extended model takes into account a full-scale model of the components of electric vehicles.

4. Energy efficiency of over 90% has been achieved, reducing energy consumption by 16.81% for the electric mode compared to the measured data, which surpasses many existing studies.

5. Compared to the required traction of 21.354 kWh/100 km, this study has achieved an energy gain of 5.124 kWh/100 km and 9.194 kWh/100 km based on the enhanced PID controller, translating to a 24% and 43.06% efficiency gain for the electric and hybrid modes.

6. This dissertation demonstrates a successful transformation of the VW Crafter for the first time from conventional to hybrid electrified powertrain, focusing on the realization of optimal tracking performance and robustness.

7. Although the VW Crafter has been considered in [30], it was based on the physical transformation and assembly process of the vehicle. This research proposes an improved PID controller to optimize system efficiency for optimal fuel economy and reduced CO_2 emissions. Thus, this research reduces fuel consumption by 68.620%, CO_2 emissions by 70.840%, and energy consumption by 25.080%.

8. Contrary to the existing literature, for example [54], [55], [56], [48], [57], [58], [59], [60], this research uses LabVIEW software in the framework of a new methodology to establish online vehicle CAN bus data analysis facilitated by NetCAN Plus 110 hardware based on a standard frame J1939 CAN protocol.

In general, this research contributes to the advancement of the field of electric vehicles, offering innovative approaches to optimal fuel consumption and data collection methods. Therefore, the research claims are summarized as follows:

1. Tractive force analysis is a basis for improving vehicle safety, design, fuel and energy consumption.

2. The successful transformation of the conventional VW vehicle into a hybrid demonstrates a significant contribution to transportation electrification that advances the understanding and application of hybrid vehicle technologies as a viable solution to environmental problems.

3. The physical modeling method is a multi-domain approach in a single simulation environment that accounts for the energy transmission losses and lessens the computational burden of complex and analytical approaches in electric vehicles.

4. The simplified model provides a reliable and accurate investigation of optimal fuel economy and accounts for the various technical constraints of hybrid powertrain dynamics compared to the full-scale or complex model.

5. Permanent magnet synchronous electrical machines are ideal choice for 2020 VW Crafter hybrid vehicle, which is in line with current international trends in the context of scholarly discourse in the field of electric and hybrid vehicles.

6. The NetCAN Plus 110 hardware online vehicle monitoring method is a compelling novel approach to establishing a CAN bus data analysis framework in present and future electric cars.

1.5 Review of Literature

This research aims to design the hybrid powertrain of the VW Crafter implemented with the online DAQ system-based HIL method and develop an EMS based on the enhanced PID control algorithm to reduce the fuel consumption of the vehicle. This section presents a comprehensive survey of the current results in the context of the recent state-of-the-art technology in the field of electric and hybrid cars. Therefore, through literature analysis as well as research background, the research claims, contributions, and limitations of this work compared to the existing scholarly knowledge are identified and addressed.

1.5.1 Energy Management Strategy

Over the years, energy management systems (EMSs) have received extensive attention in the vehicle industry and from across the scientific research, like

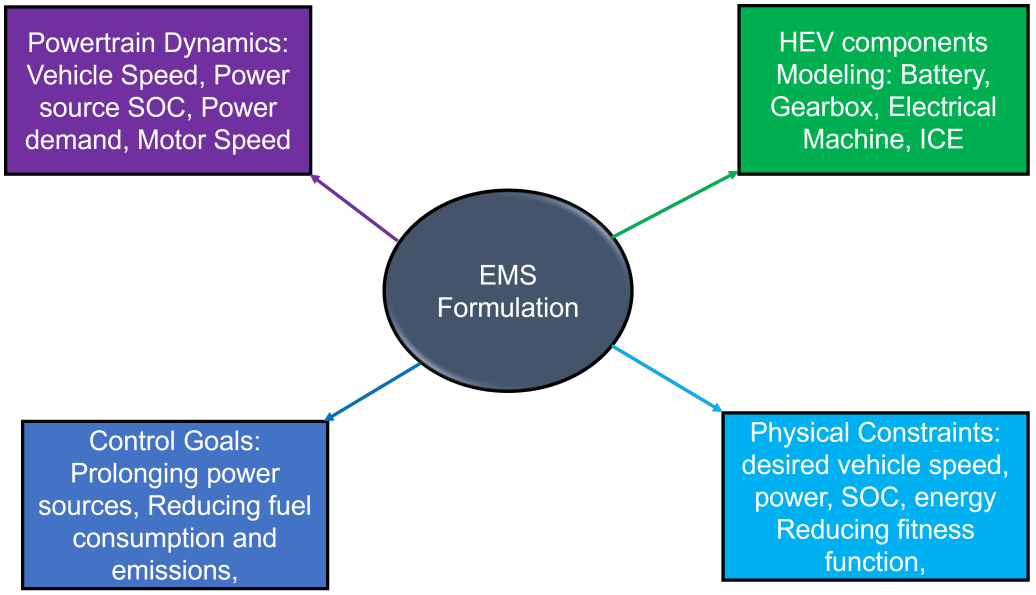

Figure 1.5.1: EMS Formulation adopted from [67]

[61], [62], [63], [64], ensuring the effective and efficient performance of HEVs in terms of both their optimal fuel economy and components durability, as well as improving drivability and HEV's user experience [65]. From the aspect of components durability, they handle the issue of energy storage devices degradation like batteries. However, from the fuel aspect, they reduce the fuel consumption [66]. The aforementioned characteristics are the control objectives for EMS in HEVs [67]. Hence, the optimization problem of the control strategy for energy management in HEVs is formulated based on the components of the HEV, the physical constraints, the control objectives and the dynamics of the powertrain, as shown in Figure 1.5.1, modified from [67]. The EMS is divided into three [68], [69], [70]: the rule-based, the optimization-based and the learning-based, and the pros and cons of each category have been discussed in the literature [71] and in-depth analysis of each [72]. In some context, the EMSs are classified into online and offline [72]. Figure 1.5.2 shows the common classification of the EMSs and Table 1.1 presents the summary of the main approaches and their pros and cons.

The rule-based strategies are based on predefined rules applied to control energy allocation and consumption in HEVs. In other words, the rule-based optimization problem is formulated as an optimization task on the basis of a predefined set of rules. Therefore, they are commonly used mainly depending

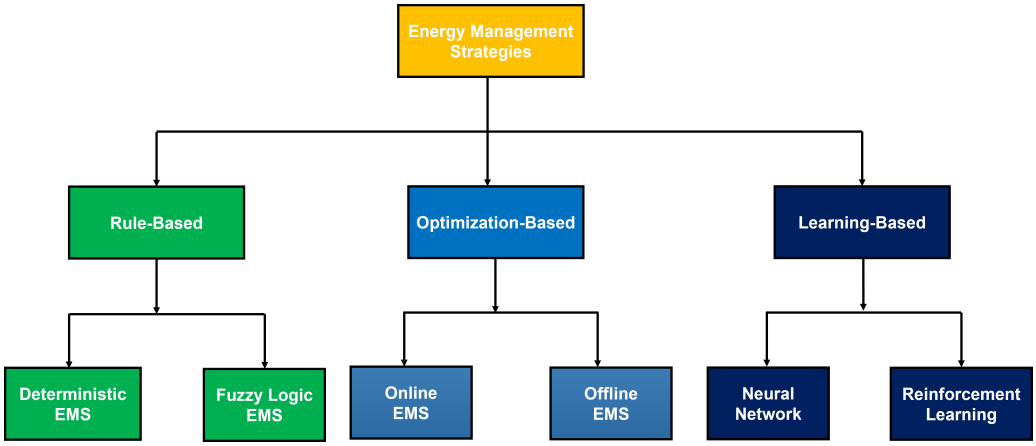

Figure 1.5.2: EMS Classification adopted from [73]

on the look-up tables and the pre-tuned rules [76]. Rule-based EMS consist of deterministic and fuzzy logic approaches [75]. The deterministic approach is based on the logical rules employed to split power among the power sources [71], and consists of filtering, classical, and heuristic controls. The Fuzzy rule-based approach distributes power among the power sources using fuzzy rules [71] and consists of conventional and adaptive controls [77]. The optimization-based approach is formulated using a mathematical optimization technique to enhance fuel efficiency or minimize fuel consumption and reduce emissions in HEVs and consists of online and offline methods [73]. The optimization-based techniques include GA, PSO, dynamic programming (DP), stochastic dynamic programming (SDP), robust control (RC), game theory (GT), evolutionary algorithm (EA), simulated annealing (SA), anti-bee, anti-colony, bacterial memetic algorithm (BMA), virus evolutionary genetic algorithm (VEGA), battery assistance optimization (BASO), model predictive control (MPC), and so on. While the learning-based leverages machine learning (ML) and artificial intelligence (AI) like reinforcement learning (RL) and neural networks (NN) [75]. This approach obtains an optimal solution by using a larger historical dataset and real-time driving-related data, and it does not require the precise model data of the system [71]. The application of EMS in EVs and HEVs aims to minimize fuel consumption, maximize fuel efficiency, and reduce emissions, thereby contributing to sustainable transportation solutions. According to the current state of the literature, two or more approaches are being hybridized to enhance performance; for example, a rule-based PID control approach can be combined with an optimization-based

Table 1.1: Summary on EMSs, Pros, and Cons

EMSs	Summary	Pros	Cons
Rule-Based [71, 74]	Based on the predefined logical rules according to the characteristics and operation mode of the HEV system .	Simple to implement and it is very robust EMS.	Varying driving conditions make it less adaptable.
Optimization-Based [73]	Mathematical optimization approach is utilized to reduce fuel consumption.	Handles complex driving conditions.	The practicality of the solutions cannot be guaranteed.
Learning-Based [75]	leverages machine learning like AI and NN for energy management.	It is flexible.	Requires large training data and processing power.

approach to improve fuel economy in HEVs. Therefore, the literature review in this study focuses on the control methods that deal with fuel consumption for HEVs.

In the early stage of the control strategies for fuel consumption in hybrid vehicles, linear control techniques such as PID and linear quadratic regulator (LQR) have been published in the literature [78], [79], [80], [81]. However, linear controllers are not suitable candidates against uncertainties and disturbances, rely heavily on the precise model, and cannot accurately capture the complexity of the dynamics of hybrid vehicles. To address these limitations, these controllers have been modified and enhanced to meet the expectations of reduced emissions and fuel consumption in the field of electric vehicles. For example, particle swarm optimization based PID (PSO-PID) was proposed in [82] for optimal fuel consumption, differential evolution (DE-PID) and bat algorithm (BA-PID) in [83], PID based fuzzy logic (Fuzzy-PID) in [84], GA-PID in [85], and dynamic programming based LQR (DP-LQR) in [86]. In recent years, the application of fractional-order controllers in the system's dynamics has gained popularity due to their promising potential to improve control performance and robustness [87, 88]. In effect, fractional-order PID-

based jaya optimization algorithm (JOA-FOPID) was utilized to reduce fuel consumption in [89] and FOPID-PSO in [90]. The increasing demand for hybrid vehicles has sparked pioneering works in control theory, exploring more advanced, cutting-edge, and robust nonlinear control techniques from across the scholarly contexts, for examples, [63], [91], [92], [93], [94]. These controllers have been applied in HEVs to mitigate the effect of disturbances, handle the issue of nonlinearities, and enhance performance.

Fuzzy logic controller (FLC) is one of the powerful control tools applied in HEVs. It has many industrial applications [95], such as anti-lock brake control [96] and transmission shift control [97] . In [98], the FLC was proposed for power-split HEV and fuel consumption was reduced by 27%. T. Basima et al. in [99] applied FLC in HEV and controlled the battery charge thereby reducing the fuel consumption. The study in [100] proposed the FLC as an EMS for HEV and the results of simulation proved the FLC as an alternative and valuable control strategy. Another study in [101] proposed an adaptive neuro fuzzy inference system (ANFIS) to reduce the fuel consumption in HEV. However, the real-time implementation of this proposed strategy is challenging [102]. In [103], the FLC was proposed for four-wheel independent drive EV to split the power between the electrical machines to improve fuel consumption under real driving conditions. In [104], an adaptive-weight GA based FLC was developed to improve the HEV energy efficiency. The proposed control method is promising in reducing the travel cost by 15.18%. In [105], the FLC was proposed and used as a benchmark compared to the recent EMSs to optimize fuel consumption and emissions in HEVs. The results of the study proved the FLC is an alternative and viable control strategy for optimal fuel consumption in HEVs.

MPC is another promising control method proposed for optimal fuel consumption in HEVs. There is a growing adoption of MPC to improve fuel economy in the context of HEVs [106], as an advanced approach [107], to reduce fuel consumption [108], with a satisfactory results [24]. The MPC has been applied in the field of control theory, such as, in autonomous vehicle [109] and full electric vehicles [110]. In [111], MPC was proposed to control the vehicle speed and torque for better fuel economy and fewer emissions. In [112], the MPC was proposed to improve drivability for parallel HEV. Two MPCs were developed: The MPC with hard and softened constraints. The simulation results demonstrated the superiority of the MPC with softened constraints. Another study in [113] suggested a mixed-integar MPC (MI-MPC) for the optimal economy of parallel HEV. The results of the study showed that the proposed strategy is suitable for HEV's fuel consumption.

In [114], a scenario MPC was proposed, and the same reduction in fuel consumption as nominal MPC was achieved with a full preview of the behavior of the driver in the future. In [115], the MPC and ANFIS controllers were proposed to reduce the fuel consumption in HEV. The simulation results indicated a decrease in the calculation time of the EMS by 23.5% and a 6.12% reduction in fuel consumption. MPC relies on accurate predictions of the behavior of the system dynamics, and unpredictable input disturbances are difficult to be handled. As a result, it is sensitive to tuning the parameters, and therefore, poor prediction could worsen the performance of the HEVs.

NN has been widely used for optimal fuel economy in HEVs. The study in [70] proposed recurrent NN (RNN) to reduce HEV fuel consumption. The fuel consumption was reduced by about 4% and 5% for charge-sustaining and charge-depleting strategies compared to the rule-based strategy as a baseline technique. In [116], back propagation NN (BPNN) was proposed to predict an optimal fuel economy in HEV. The aim of the study was to improve the databases of fuel consumption monitoring on the basis of mobile phone data. The study in [117] proposed NN and multiple linear regression to predict fuel consumption for HEV. The simulation results had proven NN to be a better control strategy. In [118], the NN on the basis of a surrogate model, was proposed to increase the range for a range-extended light commercial vehicle based on the optimal fuel economy. The fuel consumption was reduced by adopting different loading conditions. In [119], the NN was proposed to reduce the fuel consumption for plug-in HEV. The proposed algorithm demonstrated excellent performance with only 2.41% worse than the DP approach. In [120], integrated energy management strategy-based approximate dynamic programming (ADP) and NN were proposed to reduce the fuel consumption for autonomous HEV. The simulation results showed an improvement in the fuel economy of 7.4%, 4.6%, and 11.8%, based on the three case studies.

Other control methods that have been adopted for the optimal fuel consumption in HEVs are sliding mode controller (SMC), disturbance observer (DO), backstepping control, deep learning (DL), reinforcement learning (RL), deep reinforcement learning (DRL), adaptive controls, passivity-base controls, differential flatness-based controls, feedback linearization controls, DP control, game theory controls, prescribe performance controls, fault-tolerant controls, resilient controls, and many more. Some of the above mentioned control methods have been applied by many articles, while some of them only a few. Other control techniques like prescribe performance, fault-tolerant, resilient controls that have no been applied yet to study fuel consumption and CO_2 emissions in hybrid vehicles. In [121], the SMC and proportional integral

(PI) were applied as the energy management stratgies for the HEV. The study in [122] proposed multi-agent deep reinforcement learning (MADRL) based on the testing platform of software-in-the-loop (SIL) as the energy management for HEV. The proposed control technique saved up to 4% and 23.5% of energy compared to the single-agent and the conventional rule-based systems, respectively. In [123], DO was proposed base on traction control and estimated the frequency in a specific range. The PI control method was used for disturbance rejection. The proposed controller was proven to be effective in improving the energy efficiency of the HEV.

In this research, a GA-PID is proposed as energy management to reduce the fuel consumption of the VW Crafter. In addition, PSO-PID and FOPID are applied to verify the effectiveness of the baseline controller. GA has been widely adopted due its global search feature and ability to handle multi-optimization problem while PSO is characterized by its fast convergence capability less parameter tuning [124]. Over the years, PID control algorithms have been widely applied in industrial process controls due to their simplicity, robustness, and practicality for real-time applications. The application of the PID control strategy has been relevant throughout history due to its intuitive approach to practical implementation in industrial and commercial mechatronics products. The PID control algorithm still remains a widely recognized and useful approach in many scientific communities [125]. These features make the PID-based EMS a natural choice for the VW Crafter.

Some of the advanced control strategies discussed in the literature, such as NN, MPC, ANFIS, FLC, etc. can be challenging to implement in real-world applications, such as electric vehicles. The application of NN in HEVs could be computationally intensive due to the large training dataset and the power requirement. The application of optimization-based EMS, such as GA and PSO, will be challenging in simple practical driving scenarios. The prediction and control horizons in MPC are challenging to handle, as poor prediction can significantly worsen control performance. Moreover, nonlinear controllers, such as adaptive, are excellent for energy management but are often sensitive to parameter tuning [34]. However, linear control algorithms, such as PIDs, are not suitable candidates for energy management in complex dynamic systems like EVs and HEVs due to the nonlinear effects that may compromise optimal performance. Therefore, subjecting the classical strategy to an optimization problem framework is typically necessary to achieve optimal fuel economy, reduced emissions, and extended vehicle range [34]. The classical PID controller for the VW Crafter may not yield satisfactory performance due to the system's nonlinearity. Therefore, integrating the vehicle controller

(PID) with an optimization-based strategy (GA) is an ideal and suitable control tool to minimize fuel consumption and CO_2 emissions or maximize efficiency for the HEV.

1.5.2 Vehicle CAN Bus System

The CAN protocol is utilized to transmit/receive messages between our vehicles' ECUs. The CAN bus is the best standard for vehicular networks used in the automotive industry. This vehicle CAN bus system is developed in the vehicle network systems to monitor vehicle parameters such as the engine speed, fuel consumption, temperature, vehicle, motor speed, etc., from remote areas [126]. The CAN was developed beginning of the 1980s by Bosch. The CAN protocol was accepted worldwide, and nowadays, car manufacturers include CAN in their car models. It is generally regarded as a broadcast bus that operates at speeds of up to 1 Mbit/s and a payload size of up to 8 bytes [80]. The CAN bus connects all the ECUs in the automobiles, usually transmitted at an average transmission speed of 500 kbps. Moreover, the message arbitration and message validation design elements of the CAN Bus communication protocol assist the CAN bus in achieving the reliability criterion. Instead of complex wiring, it consists of two wires, CAN low and CAN high (Figure 1.5.3), which transmit information from one ECU to the next. The ECUs would check the data transmitted on the CAN network, and each ECU accepts or ignores it, depending on whether that message was specifically for a particular ECU or next (Figure 1.5.4) [127].

Technically, CAN bus can be described in two layers: the physical (international organization for standardization (ISO 11898-2) and data link (ISO 11898-1). The physical layer defines the electrical signal levels, cable impedance and types, and the requirements of the node, etc. The ISO 11898-2 shows the baud rate so that the CAN notes should be connected through the two-wire bus having baud rates of a maximum of 1 Mbit/s—the Cable length, between 500m (125 kbit/s) and 40 m (1 Mbit/s). Moreover, the CAN bus should be terminated using a 120-ohm resistor [127]. As CAN Bus is used in most of today's vehicles, the following are the benefits of using in our vehicles [127]:

- The ECUs communicate easily via a single wire (CAN bus) network instead of the traditional complex wiring systems. This reduces cost, weight, and errors.
- Data can easily be accessed via the CAN bus. All the networks of

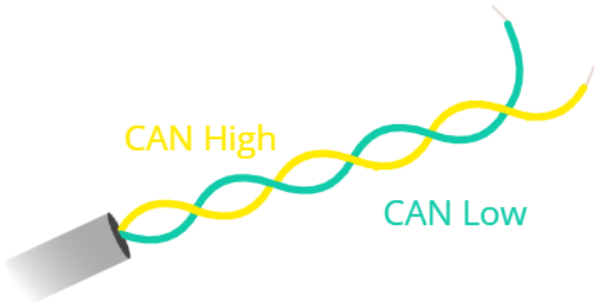

Figure 1.5.3: CAN Bus [127]

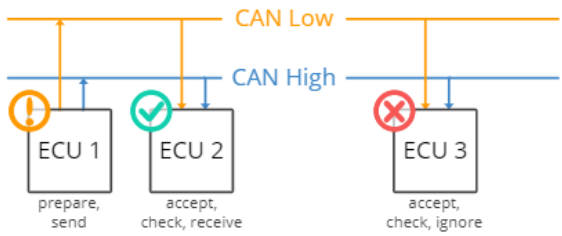

Figure 1.5.4: Vehicle ECUs with CAN Bus [127]

ECUs can be communicated together using a single entry with the CAN bus system, which enables data logging, central diagnostics, etc.

- It provides robust performance against disturbances (such as electrical and electromagnetic).
- It is very efficient.

The standard CAN bus frame consists of 11 CAN identifiers (CAN IDs), which is CAN 2.0A. The communication is made through the CAN bus

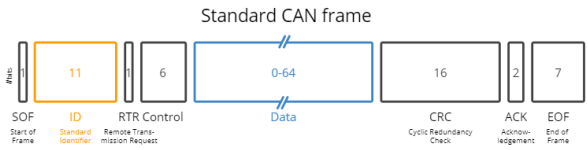

Figure 1.5.5: Standard CAN Frame [127]

frames. Figure 1.5.5 shows the standard CAN frame example. The CAN ID and the data are highlighted [127]. The SOF means the start of the frame, The ID is the fame identifier in which the lower values will have priority, and RTR stands for remote transmission request, which shows the data is sent or requested by the node. Data contains the data bytes (CAN signals). The Cyclic Redundancy Check (CRC) safeguards data integrity. The control has the data length code (DLC) from 0 to 8 bytes. The ACK shows whether data is received correctly by the node. End of frame (EOF) shows the end of the CAN frame [127]. However, the main issue in decoding the CAN messages is understanding raw CAN data from the vehicle's various ECUs. The CAN frames, which consist of the CAN data in hexadecimal and are not human-readable, must be decoded and analyzed into physical values [80].

1.5.3 On-Board Diagnostics Version II

The on-board diagnostics version II (OBD-II) provides access to the real-time status of the vehicle's data [128], including vehicle speed, engine speed, temperature, pressure, etc. In other words, it is a standardized vehicle protocol that allows us to extract diagnostic trouble codes (DTCs) and real-time data facilitated through the OBD-II connector (Figure 1.5.6) [127]. The OBD-II port, typically 16 pins, is generally located under the dashboard in most vehicles. When there is an issue with a car, an OBD-II diagnostic tool is used to diagnose the problem. When the tool is connected to the car via the OBD-II interface, it sends an OBD-II request, and the car responds with DTCs to address the problems or the requested data, such as fuel consumption and speed [127].

The structure of the OBD-II frame expedites the communication between the ECU and the OBD-II scanner (diagnostics tool). Like the CAN bus frame, it consists of several fields organized to facilitate data transmission in our automobiles [129]. Figure 1.5.7 the standard OBD-II frame structure that is precisely aligned with the CAN protocol. As shown, the OBD-II frame consists of two main parts: the CAN ID (identifier) and the CAN data with a particular reference to the CAN protocol. The identifier in OBD-II is used to differentiate between the requested message (ID: 7DF) and the responded message (ID: 7EF or 7E8). The # byte is the number of bytes or length of the remaining data on the frame, ranging from 03 to 06. The mode specifies the request being sent. It typically ranges from 01 to 0A. The parameter ID (PID) identifies the data being sent or requested in the message. With PID, messages such as engine speed, vehicle speed, etc. will be identified. The A,

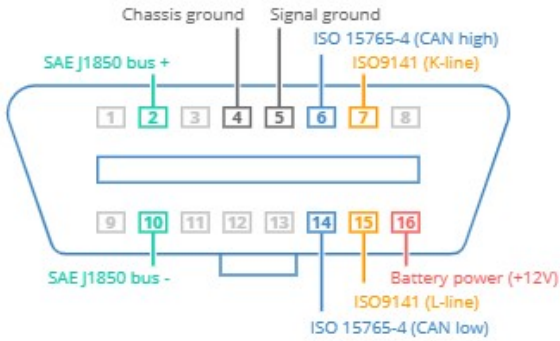

Figure 1.5.6: OBD-II Connector [127]

OBD2 Frame

Identifier	#bytes	Mode	PID	A	B	C	D	Unused
(e.g. 7E8)	03	41	0D	32	AA	AA	AA	AA
CAN ID	CAN Data							

Figure 1.5.7: Standard OBD2 Structure Frame [129]

B, C, and D represent the data bytes, which are in hexadecimal while the data byte represents the actual values of the data. The OBD-II scanners (diagnostic tools) facilitate the understanding and interpretation of these messages for users [129].

From a research point of view, several studies have been conducted on the vehicle CAN bus to decode the raw CAN data for real-time analysis. In the early stage of technological development, conventional methods such as the OBD-II scanner interface [56], CAN edge [127], VCDS [130], OBD-II-Dewe 101 [131] etc., were adopted. The vehicle's performance for optimal performance and diagnosis and the fuel consumption were investigated [56]. In [132], an accurate and practical model (machine learning algorithm models trained with real-world driving cycles) was developed for fuel consumption estimation based on OBD data, with help of a high precision flow meter.

However, to keep up with the latest technological advancement, the CAN bus data collection method and analysis from our automobiles should continue to support more advanced applications to make it faster, easier, efficient and to meet vehicle's standard safety requirements. In [133] , real-world vehicle data was recorded using data loggers, extracting information (fuel consumption) from the vehicle's CAN bus system. The study in [48]

performed an experimental and numerical investigation of the optimal fuel economy on the basis of ISO-15765-4-CAN protocol. Therefore, there is an improvement in performance using the hybrid system on local routes with a higher proportion of city driving conditions, even though there is a slight decrease in the overall efficiency of the electrical system. The study in [134] conducted an evaluation of the driving behaviour through CAN bus data collection. In their study, the deep learning and machine learning models were leveraged to employ a naturalistic driving dataset. In [135], the vehicle CAN bus data was read using libpanda library in C++ to provide rich sensor data. In [136], a deep neural network (DNN) was proposed for energy optimization for electric vehicle. The proposed DNN approach was used for CAN bus and various media control for effective performance. In [60] a DAQ system was proposed to record velocity, displacement and current every 100 milliseconds (ms) on the basis of the XU4 odroid board in an electric vehicle. The validation was carried on the basis of the comparison between the real and numerial mathematical model data. In [58], a standalone CAN bus data logger was proposed, which was optimized to record CAN bus data anytime the tractor engine was on. In [59], a vehicle was simulated, and the CAN bus network was designed based on the HIL system for the HEV for optimal performance. It could be proved from simulation and experimental findings that the desired performance in terms of load split between the power sources and speed control stability was achieved.

1.5.3.1 Technical Challenges in Data Acquisition

Data acquisition is essential for various industrial applications, including healthcare monitoring, environmental monitoring, manufacturing processes, financial market analysis, and scientific research [137] —for example, vehicle monitoring—as numerous contributions have been published [56]. However, there are technical challenges, such as errors that can occur in the data acquisition process, as it cannot always be error-free or flawless, which could compromise the data and pose challenges due to various factors, including data quality, data integration, and the need for real-time processing [137]. The error in CAN bus happens due to the number of reasons, such as noise, faulty cables, incorrect termination, incorrect setting of the baud rate, and when the CAN nodes are not functioning properly. Therefore, identifying these errors is critical for ensuring the continuity in the CAN bus system. Therefore, it is necessary to devise an error-handling approach that identifies and rejects messages containing errors to enable the sender to rebroadcast or

retransmit the message. This error-handling method also aids in identifying and disconnecting CAN nodes that contain messages that pose errors [127].

The practical method of handling errors in CAN bus messages requires technical knowledge and practical skills, which have been described in [138] . For example, monitoring system performance requires diagnostic software for the early detection of issues. To detect signal interference, an oscilloscope is utilized. Error frame analysis requires knowledge of the CAN protocol or diagnostic software, and so on [138]. Other measurement uncertainties, such as a malicious attack by internal or external factors on the CAN bus, can be handled by the use of the deep neural network (DNN) as in [139]. In this research, an online DAQ system implemented via the standard CAN frame protocol, such as J1939, using a novel approach of interconnecting four sets of NetCAN Plus 110 hardware, wireless local area network (WLAN), factory line (FL) switch, and global positioning system (GPS) device has been adopted to facilitate data collection. Errors due to the software and hardware issues were faced. For the hardware, the error was due to loosened cables in the CAN bus node. This issue was resolved by performing a continuity test and reconnecting the wires. The software issue was caused by the error frames and broken lines displayed in the output of the CAN bus message. This issue was resolved by using LabVIEW software on the host PC. The signal integrity was verified with the help of an oscilloscope.

1.6 Research Structure

The research structure is as follows: Chapter Two describes the battery energy storage modeling and traction analysis for the VW Crafter. The detailed 2011 Nissan Leaf battery pack is investigated, and its capacity fade over time and life cycles, based on its system-level performance, has been examined. This gives rise to the development of Chapter Three. This necessitates properly selecting the electrical machine based on the energy and power demands presented in Chapter Two. Chapter Three presents the design, modeling, and control of electrical machines at different levels of complexity, as well as e-crafter design. The integration of chapters two and three gives rise to the complete development of the VW Crafter in its three modes of operation, i.e., electric, engine, and hybrid modes, as presented in chapter four. Chapter Four presents the development of the VW hybrid vehicle. Chapter Five presents the summary, conclusion, and recommendations for future developments.

Chapter 2

Energy Storage Modeling and Traction Analysis

2.1 Introduction

This chapter presents the background information about the energy sources: the traction batteries in EVs, the mathematical model of the 2011 Nissan Leaf battery pack, its equivalent circuit and the battery pack simulation for capacity fade analysis over time and its life cycles for the VW Crafter application in this research. In this chapter, the analysis of the tractive force for the VW Crafter is presented. This is done to ensure the torque needed to propel the vehicle. This ranges from the power and energy requirements of the prime mover (engine or electrical machine) to the vehicle wheels.

2.2 Battery Background

The function of the battery in the powertrain is to supply energy for the whole vehicle. With the advancement of battery technology, different types of batteries have been developed over the years. Therefore, the battery is a delicate component that affects the EVs dynamic performance, safety, and economy. The battery provides power to electrical devices using an electrochemical reaction between two or more cells. The battery features include specific energy, auto-discharge rate, charging time, capacity rate (C-rate), operational conditions, and toxicity [140]. The reversibility conditions of the electrochemical process are the determining factors of the battery capacity. The battery capacity (in kilowatt-hour, kWh or Ampere-hour, Ah)

is a critical characteristics representing the maximum amount of electrical energy a battery can store and deliver. It decreases the usage of electrodes or electrolytes. However, the C-rate of the battery is a measure of the discharge of the battery relative to the battery's peak capacity, or it simply represents the charging or discharging rate. The battery type used as the primary power source significantly affects the EVs' and HEVs' driving range and performance. The commonly used types of batteries in EVs and HEVs include nickel-based, sodium-based, lithium-ion, and lead-acid [140].

However, batteries are divided into primary and secondary. The secondary battery is the most popular used for vehicular technology. Other essential characteristics of the battery are the state of charge (SOC), the depth of discharge (DOD), and the state of health (SOH). The SOC of a battery is defined as the percentage the battery is charged. Therefore, the battery is fully charged if it is 100 % and completely discharged when it is 0 %. The Ah is the current rated capacity of the battery. It tells us how much the amount of current a battery gives in one hour. The percentage discharged by the battery is its DOD. It is inversely proportional to the battery SOC. Typically, a 2011 Nissan Leaf battery pack with a 67 % DOD, 24 kWh rating, this means the discharge should not exceed 16.08 kWh out of 24 kWh rated capacity. The kWh capacity of the battery is the amount of energy stored. It is the continuous power output that the battery gives in one hour. The SOH is the useful life of the battery. C-rating is an essential characteristic to consider when buying a battery. It is used for labelling the current capacity of the battery. Suppose a 40 Ah rated capacity battery is fully charged and has a 1 C rating. This battery would give a current of 40 A in one hour. However, if the battery is discharged at a 2 C rating, it would provide a current of 80 A in 30 minutes.

This research battery pack is based on lithium-ion batteries (LIBs). In recent years, the research on LIBs has attracted attention and is widely implemented in EVs today and in the future [141], due to their superiority in power density [142]. In 1996, the lead-acid battery pack was used in general motors EVs. However, the presence of lead in this type of battery chemistry makes it heavy, limiting the on-vehicle energy storage. It also has a short lifespan, causing its capacity to degrade. At that time, a nickel-based battery pack was developed and featured in General Motors EV1, which was launched in 1999 and had a longer lifespan and capacity than the lead-acid battery pack. The nickel-based battery pack was used for the Toyota Prius in 1997. LIBs have been the basis for EV rebirth, which started when the Tesla Roadster was launched in 2008. In the past years, LIB chemistry has

used manganese and cobalt as the primary metals [143]. Table 2.1 presents a different battery chemistry used for EVs applications, where E_s and P_s are the specific energy and power of the batteries.

Table 2.1: Electric Vehicle Batteries adopted and modified from [144]

Type	E_s **[Wh/kg]**	P_s **[W/kg]**	**Applications**
Lead-acid	30∼50	150∼200	Suzuki Alto
Nickel-based	35∼80	150∼450	Toyota RAV4L
Amb.-Temp. Lithium	120∼300	200∼450	Nissan Leaf
Sodium-beta	115∼200	120∼250	BMW AG
High-Temp. Lithium	130∼180	240∼400	-
Metal/Air	75∼250	100∼200	Mercedes-Benz
Zinc/Halogen	65∼75	60∼110	Toyota EV-30

2.3 The 2011 Nissan Leaf Battery Pack

The Nissan Leaf battery pack consists of 48 modules, each with four cells; There are two pairs in series pairs in parallel, totaling 192 cells in the pack. The battery has a nominal voltage of 360 V and a capacity of 24 kWh. Each cell's nominal, maximum, and discharge voltages as well as the current capacity are 3.75 V, 4.2 V, 2.5 V, and 33.1 Ah, respectively. The maximum voltage of the entire pack is 403.2 V, the maximum capacity of 66.2 Ah, and the power of more than 90 kW. The collaboration between Nissan and NEC corporation, AESC, manufactured Nissan Leaf battery cells.

Table 2.2 presents the parameters of the battery pack according to cells, modules, and the whole pack. The battery pack is made of 48 modules that are connected in series. The total weight of the battery pack is 293.9 kg, and it has an energy density of 81.65 Wh/kg. Suppose the cell's rated capacity is 33.1 Ah at 0.3 C for 3 hours when discharging. In that case, this entails that the rated capacity of 33.1 Ah or 155.194 Wh/kg per cell or 66.2 Ah or 24 kWh per pack is available when the cell or the battery pack is discharged at a 0.3 C rate of 9.93 A per cell or 19.86 A per pack for 3 hours. Under normal driving conditions, the 0.3 C rating is typically close to the battery's discharge current. Other C rating ratings can be specified based on the applications and the total current requirements [34].

Table 2.2: 2011 Nissan Leaf Battery Cell, Module, and Pack Technical Specifications [34]

Parameters	Cell	Module	Battery Pack
Number of Cells	1	4	192
Voltage [V]	3.75	7.5	360
Current Capacity [Ah]	33.1	66.2	66.2
Energy Capacity [kWh]	0.124	0.4965	24
Volume [L]	0.445	2.365	494.2
Weight [kg]	0.799	3.8	293.9
Energy Density [Wh/kg]	155.194	130.66	81.65
Energy Density [kWh/kg]	0.155	0.131	0.08165

2.4 Modeling of the Battery Pack

To derive the mathematical model of the battery, we consider it as an example of a spontaneous electrochemical redox reaction that is doing electrical work, converting chemical energy and generates an EMF. Therefore, the Nissan Leaf battery can be modeled as in [145, 143] as follows:

$$\begin{cases} V_r^0 = -\frac{\Delta G^0}{nF} \\ V_b = V_r^0 - \frac{RT}{nF} log_e Q_R - \Omega_d \\ V_b = V_r^0 - \frac{RT}{nF} log_e Q_R - R_b I_b, \Omega_d = R_b I_b \end{cases} \tag{2.4.1}$$

Where ${V_r}^0$ is the no-load open circuit voltage of the battery cell, ΔG^0 is the change in the Gibbs free energy, n is the number of moles, F is the Faraday's constant, R is ideal gas constant, Q_R is the reaction quotient, T is the temperature, Ω_d is the ohmic drop, R_b is the cell resistance, I_b is the cell current, and V_b is the cell voltage. The battery cell voltage can be expressed as a function of the logarithmic, linear and exponential drops with the capacity, no-load reversible voltage, and ohmic drop with the current [143], as follows:

$$V_b(I_b, y) = {V_r}^0 - A log_e(B \cdot y) - K \cdot y - F e^{G(y - y_3)} - R_b I_b \tag{2.4.2}$$

Where y is variable related to DOD, SOC, capacity y_3 is the value when the exponential drop starts, A, B, K, F, and G are the constant determined by

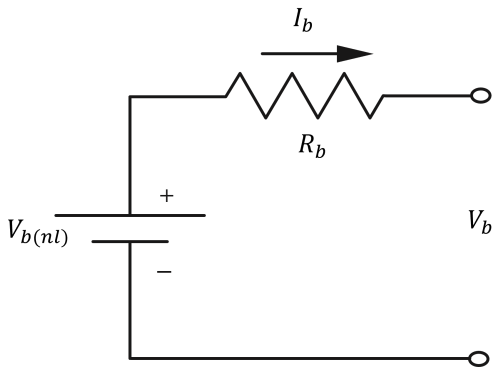

Figure 2.4.1: Battery Equivalent Model [143]

the curve fitting [143]. Equation (2.4.2) can be expressed as a function of the DOD as follows:

$$\begin{cases} V_b(I_b, DOD) = V_r{}^0 - Alog_e(B \cdot DOD) - K \cdot DOD - Fe^{G(DOD-DOD_3)} - R_b I_b \\ V_b(I_b, DOD) = V_b(nl)(DOD) - R_b I_b \\ V_b(nl)(DOD) = V_r{}^0 - Alog_e(B \cdot DOD) - K \cdot DOD - Fe^{G(DOD-DOD_3)} \end{cases} \tag{2.4.3}$$

Therefore, the above equation can be represented by the general equivalent circuit in Figure 2.4.1.

2.4.1 MATLAB Model and Detailed Analysis

For the battery pack, if N_m is the number of modules which is 48, V_bp is the voltage of the battery pack, I_bp is the current of the battery pack, and R_bp is the resistance of the battery pack, C_b is the battery capacity, C_r is the battery remaining capacity, N_c is the total number of cells in the pack, C_{re} is the battery pack residual capacity, C_I is the battery pack initial capacity, and C_{Ah} is the current capacity of the battery pack. Therefore, we can obtain the following models as related to the entire battery pack:

$$\begin{cases} V_{bp} = 2 \cdot N_m V_b \\ I_{bp} = 2 \cdot I_b \\ R_{bp} = N_m \cdot R_b \\ C_b = N_c \cdot V_b \cdot I_b \\ C_r = \frac{C_{re} \cdot C_I}{C_{Ah}} \end{cases} \tag{2.4.4}$$

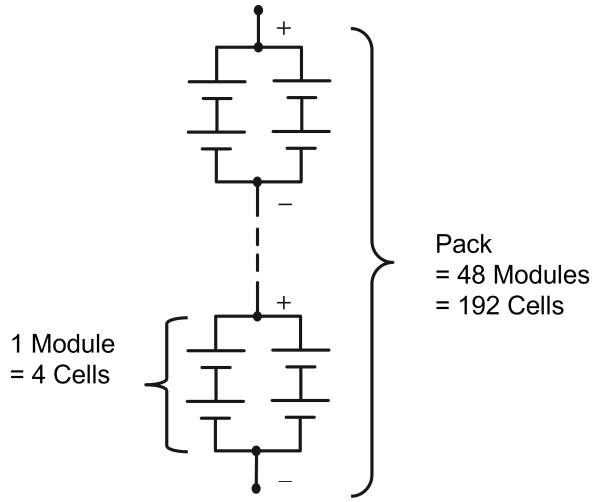

Figure 2.4.2: Nissan Leaf Battery Pack [143]

The Nissan Leaf battery pack was simulated in MATLAB/Simulink based on the modeling concept presented in Figure 2.4.2. The simulated pack is shown in Figure 2.4.3 which contains the 48 modules. In each module, there are 2 series, pairs in parallel cells. The detailed battery pack was simulated to validate the simulated results, which should be close to the real-life situation of our battery pack for the VW Crafter. We took each cell of the battery and studied its discharge characteristics. Figure 2.4.4 shows the characteristics of the battery per cell or Figure 2.4.5 per pack , whose nominal current discharge characteristics at 0.3 C-rate is 9.93 A or 19.86 A as previously described. Therefore, the recommendation for each cell discharged voltage is 2.5 V, as shown in Figure 2.4.4, while for the pack, the recommended voltage is 250 V. In three hours, the Nissan leaf battery can provide the regulated discharge limit in the nominal area. This shows that the battery functions well at a given C-rating, delivering a current of 9.93 A per cell or current of 19.86 A for the battery pack. Up to 2-5 C-rating can be used for a car-sized battery pack.

To reduce the complexity of the detailed model, the battery pack was compressed into a system-level model, enabling real-time operation. The system-level model captures the behavior of the detailed model, making it suitable and easy to integrate into our hybrid powertrain. Since the battery is an integral part of the powertrain, it is necessary to ensure its safe operation under thermal effects and to understand how its capacity fades over time or with its cycles of operation. Its prediction is worth billions to the energy

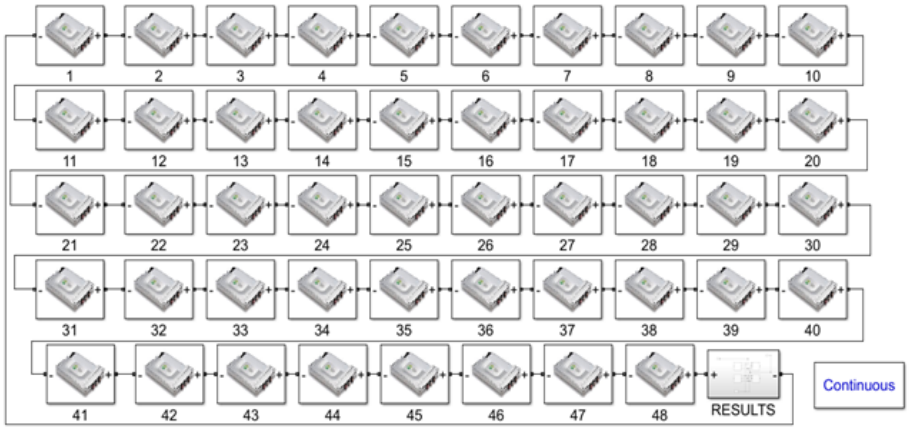

Figure 2.4.3: Simulated Nissan Leaf Battery Pack [34]

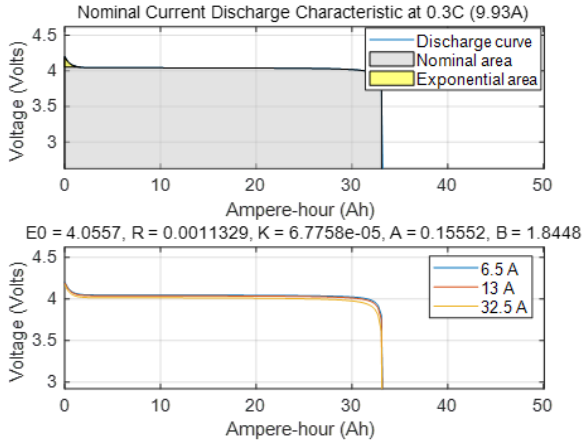

Figure 2.4.4: Cell Discharge Characteristics [34]

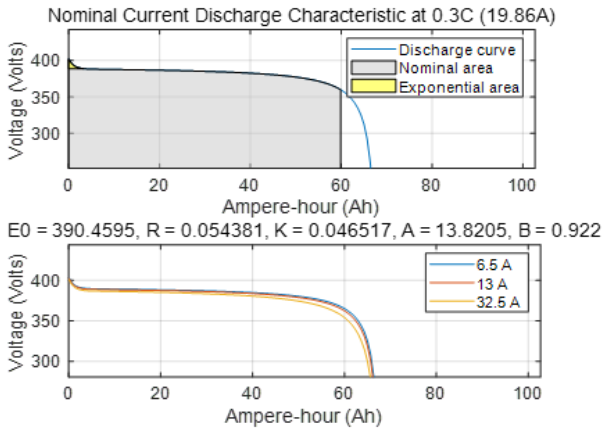

Figure 2.4.5: Pack Discharge Characteristics

storage, automotive, and aviation industries [146]. Hence, in this section, we simulated the battery to investigate its capacity fade and to compare the results with adopted data from the real test. Figures 2.4.6 and 2.4.7 show the simulation results for the 2011 Nissan Leaf battery pack, including SOC, capacity fade, temperature, current, voltage, and power. These results were modeled at the system level to investigate its performance prior to integration into our traction application. Therefore, Figure 2.4.6 shows the SOC of 0.603 from an initial of 1, which means 60.3% from an initial SOC of 100%, temperature of 54.3 °C from the initial ambient temperature 25 °C, and capacity remaining of 39.92 Ah from the total capacity of 66.2 Ah and this means 26.28 Ah faded away. If we assume the battery was 100% fully charged and was in its 100% SOH. In this case, the SOC and SOH will be temporarily aligned in the same context.

In practice, the SOC and SOH would be different metrics for evaluating our battery conditions. However, in terms of thermal effect performance, we observed a temperature increase of 29.30 °C, which is normal for the battery pack in this duration without a cooling system. There is an optimal operating temperature for the lithium ion battery, which ranges from 15 to 35 °C. Therefore, lower or higher temperatures often affect battery performance, leading to degradation [147]. Thus, the battery capacity was reduced to 39.92 Ah, equivalent to 14.472 kWh of remaining available capacity, despite the long duration of 3600 seconds. This does not present a serious capacity fade because, with 14.472 kWh available, the vehicle can cover approximately 74 km if its consumption per 100 km was 19.51 kWh. Furthermore, with only

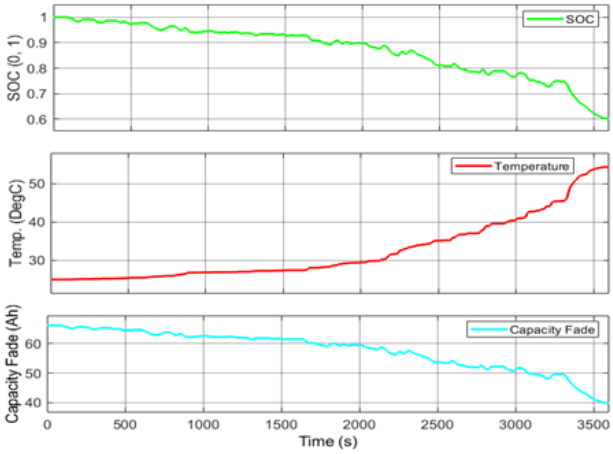

Figure 2.4.6: Battery SOC, Temperature, and Capacity Fade Over Time

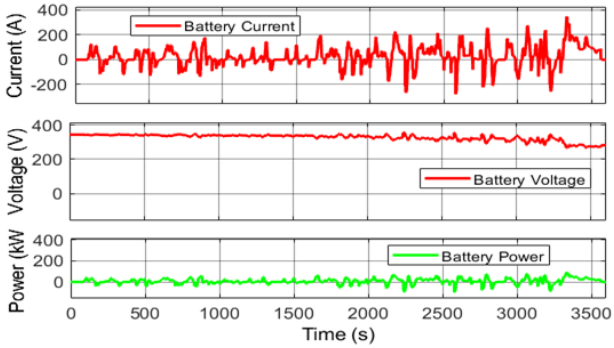

Figure 2.4.7: Battery Current, Voltage, and Power

$60 - 67\%$ capacity remaining, the retired battery can function well for 12 to 20 years in second life [148]. If the 2011 Nissan Leaf battery had 1800 cycles in their first life for the EV application, the simulated battery in our analysis degraded by 26.28 Ah in approximately 715 cycles with a 56% fading rate per 1000 cycles. However, according to the aging test conducted on two battery cells in [148], the battery completed 7380 cycles. Therefore, with a remaining capacity of 30 Ah in 4200 cycles [148], the capacity of our Leaf battery reduced to 39.92 Ah in approximately 5589 cycles with a fading rate of 7.1% per 1000 cycles in second life. However, our application is still in its first life that lasts 8 years.

Moreover, based on the realistic current profile that can be handled by the high-voltage (HV) EV battery, this was applied to test the battery (typically

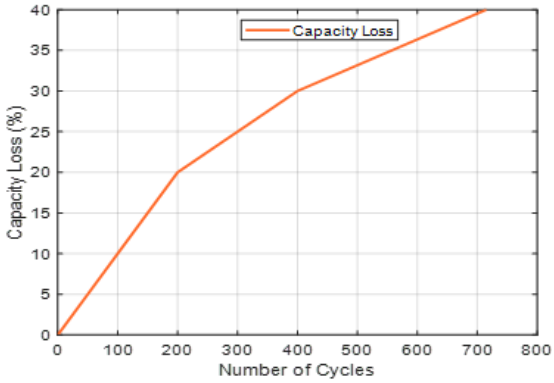

Figure 2.4.8: Battery Capacity Loss Per Life Cycles

in the range of a 2-5 C rate). Figure 2.4.7 shows the battery current of 347 A, power of 92.11 kW, a maximum voltage of 357.5 V and a minimum voltage of 265 V. These results are as expected even without the experimental validation. The 2011 Nissan Leaf battery is capable of delivering a power of over 90 kW (3.75 C) [148], with a maximum (charged) and minimum voltage (discharged) of 403.2 V and 250 V for the pack, respectively, based on our initial requirements. The 2011 Nissan Leaf battery could deliver up to 246 A (3.75 C) in its first life [148]. Figure 2.4.8 shows the battery capacity loss in percentage (approximately 40%) against the 715 life cycles plotted with help of interpolation in MATLAB.

2.5 VW Crafter Traction Analysis

A force needed to propel the vehicle is called the tractive force. This force is usually due to the friction between the wheels of the vehicle and the surface of contact with the road. The frictional force in question depends on the properties of the surface, the sliding conditions between the surface of the road and the wheels of the vehicle, and the weight of the vehicle. Therefore, when the vehicle wheels are propelled by the prime mover and the friction force is large enough, the vehicle moves forward. However, in this situation, when the prime mover does not drive the vehicle wheels, the friction force is not large enough, and the vehicle does not move. In this situation, the vehicle slides over the road surface due to the limiting value of the friction force between the wheel and the surface. Therefore, various resistive forces acting on the vehicle are considered when calculating the tractive force [149].

In recent years, only a few articles have worked on the traction energy required for the propulsion of vehicles, as well as the power demand and the factors affecting it [150]. However, we briefly introduced this concept [151] in the vehicle dynamics study modeling of the VW Crafter. According to the literature available in Google Scholar, IEEE Xplore, Web of Science, and Science Direct, many articles and PhD theses have considered traction analysis for ICE and electric vehicles, but there is no specific analysis on traction energy and the factors affecting it as related to the exact power source. This thesis provides a detailed analysis of the tractive force required to propel the vehicle. The excess tractive force for the VW Crafter has been presented based on the Taylor series. The excess force has been formulated in the frequency domain on the basis of Laplace Transformation. The tractive force equals the sum of all other resistance forces acting in opposite directions. The analysis of the tractive force gives rise to the total traction required to estimate the exact power source needed for the vehicle. The tractive force equals the sum of all other resistance forces acting in opposite directions. The analysis of the tractive force gives rise to the total traction required to estimate the exact power source needed for the vehicle. The tractive force is equal to the sum of all other resistance forces acting in opposite directions. In other words, the algebraic sum of all the forces acting on the vehicle, as shown in Figure 2.5.1, is zero.

2.5.1 Dynamic Modeling for Tractive Force Calculation

The VW Crafter is modeled by considering the free body diagram (FBD) with the resisting forces that oppose it on the basis of its longitudinal dynamics, as shown in Figure 2.5.1. The tractive force is expressed as in [145]:

$$\begin{cases} F_{tr} = F_A + F_r + F_{grade} + F_a \\ F_A = 0.5 \cdot \rho C_d \cdot A_F \cdot V^2 \\ F_r = wC_{rr} \cos\theta \\ F_{grade} = w \cdot \sin\theta \\ F_a = m \cdot a \\ P = F \cdot v \\ E = P \cdot t \end{cases} \tag{2.5.1}$$

From equation (2.5.1), F_{tr}, F_A, F_r, F_{grade}, F_a, C_d, A_F, v, C_{rr}, θ, m, a, E, P, t are the tractive force, wind resistance force, rolling resistance force,

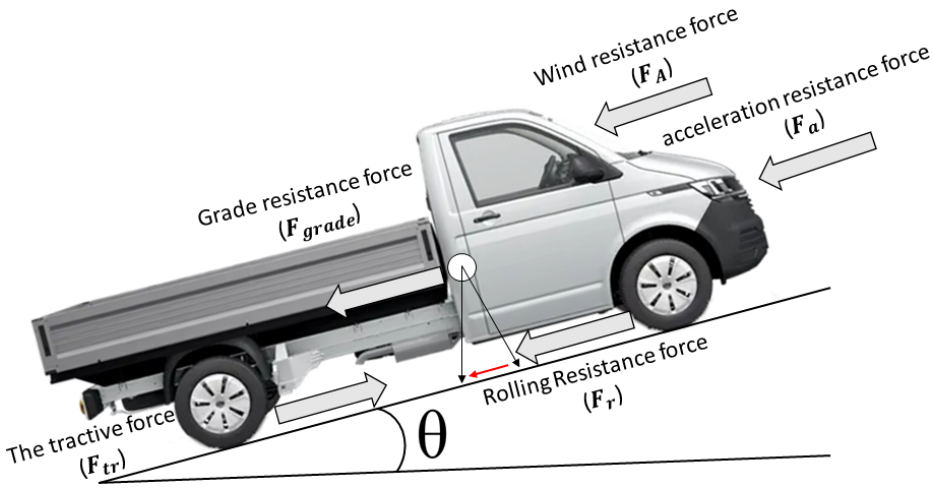

Figure 2.5.1: VW Crafter Resistance Forces [34]

grade resistance, force due to acceleration, drag coefficient, rolling resistance coefficient, inclination angle, mass of the vehicle, acceleration of the vehicle, vehicle total tractive energy, vehicle tractive power (which is the product of force and velocity), time. [34]. The tractive torque and power are related by the following expressions:

$$\begin{cases} T_{tr} = F_{tr} r_t \\ P_A = F_A v \\ P_r = F_r v \\ P_{grade} = F_{grade} v \\ P_a = F_a v \\ P_{total} = P_A + P_r + P_{grade} + P_a \end{cases} \tag{2.5.2}$$

Where r_t is the radius of the vehicle's tire, T_{tr} is the tractive torque, which is the actual torque propelling the vehicle wheels, P_A is the power required to overcome the wind resistance force, P_r is the power needed to overcome the force of rolling resistance, P_{grade} is the power needed to overcome the force due to grade resistance, P_a is the power that overcomes the acceleration resistance, P_{total} is the total actual power needed to propel the vehicle. The mathematical formulations described are used to get the appropriate battery pack and the electrical machine that will be used for designing the ICE, electric, and hybrid version of our vehicle. Figure 2.5.2 shows the MATLAB model of the vehicle dynamics system used for validation of the power and energy requirements

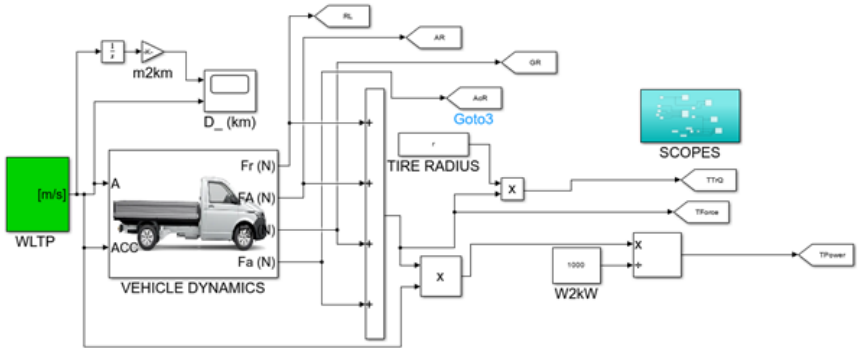

Figure 2.5.2: Vehicle Dynamics MATLAB Model

Table 2.3: The VW Crafter General Technical Specifications [34]

Parameters	**Values**	**Symbols [Unit]**
Length	5.986 - 7.319	l [m]
Width	2.040	w [m]
Height	2.355 - 2.798	h [m]
Curb Weight	2159 - 2196	W_c [kg]
Gross Weight	3500	W_g [kg]
Front Axle	1	T_F [m]
Rear Axle	1.346 - 1.901	T_R [m]
Tire Radius	0.357	r_t [m]
Center of Gravity	0.785	CG [m]
Frontal Area	4.05	A_F $[m^2]$
Rolling Resistance	0.013	C_{rr} [-]
Drag Coefficient	0.3	C_d [-]
Air Density	1.225	ρ $[kg/m^3]$
Acc. due to Gravity	9.81	g $[m/s^2]$
Engine Displacement	1968	D $[cm^3]$
Bore x Stroke	0.081 x 0.0955	BxS [m]
Number of Valves	16	v [-]
Compression Ratio	16.2:1	CR [-]
Engine Peak Power	103	P_{ICE} [kW]
Gearbox	6-Speed, Manual	-
After Treatment System	DPF	-

Table 2.3 presents the general technical specifications for the VW Crafter used in this research. We calculated the tire radius from Table 2.3 specification for the vehicle (205x75 R16), using the following equations expressed in [34]:

$$\begin{cases} AR = \frac{h_s}{w_s} \cdot 100\ \% \\ r_t = r_m + h_s \end{cases} \tag{2.5.3}$$

Where h_s, AR, r_m, and w_s are the section height, aspect ratio, rim radius, and section width. Based on the formula, the section height would be 0.15375 m, and the tire radius would be 0.357 m.

2.5.2 Excess Tractive Force Using Truncated Taylor Series

If the tractive force of the VW Crafter is expressed as:

$$F_{tr} = wC_{rr}\cos\theta + w\sin\theta + 0.5\rho C_d A_F v^2 + ma \tag{2.5.4}$$

Assuming the Crafter is on a level road, then the trative force is:

$$F_{tr} = 350.389 + 0.7442v^2 + 2868.32\frac{d}{dt}V \tag{2.5.5}$$

Equation (2.5.5) is nonlinear. Therefore, this equation can be linearized about $v_0 = 20$ km/h using truncated Taylor series:

$$\begin{cases} v^2 = 2v_0 v - {v_0}^2, v_0 = 5.56[m/s] \\ v^2 = 11.12v - 30.91 \\ F_e = F_{tr} - F_r + F_A \\ F_e = 8.276v + 2868.32\frac{d}{dt}v \end{cases} \tag{2.5.6}$$

Where F_e is the required excess tractive force, which can be formulated in frequency-domain based on transfer function by using Laplace transform where the force is the input and the vehicle speed as the output. The excess tractive force model for the vehicle is shown in Figure 2.5.3. The traction requirement analysis was achieved using equation-based methods while the electric vehicle components were modeled using physical model-based methods. Consequently, Equation (2.5.5) was linearized using a truncated Taylor series to obtain the excess tractive force at the maximum allowable speed of 20 km/h. However, when the vehicle speed is increased to 120 km/h or

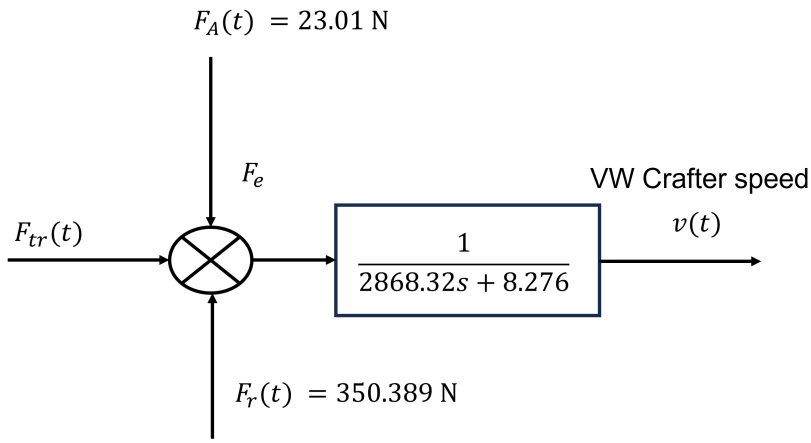

Figure 2.5.3: VW Crafter Exess Tractive Force

the maximum speed of the VW Crafter, which is approximately 158 km/h (98 mph), the tractive force is expected to increase. To ensure safe design, it is essential that this increased tractive force does not exceed the maximum allowable traction limit. In this study, the vehicle speed was analyzed beyond the 20 km/h limit. The 20 km/h speed limitation in this research is typically suitable for urban drives with specific speed restrictions, such as those encountered during events like the annual flower festival in Hungary. Therefore, it is necessary to generalize the traction analysis, as the proposed hybrid vehicle components in this study are designed to operate beyond this speed limit and are often utilized in similar vehicle models that require higher speed capabilities.

2.5.3 Detailed Traction Analysis

Figure 2.5.4 shows the tractive force against the vehicle speed for the VW Crafter at different values of the vehicle speed (0-20 km/h), assuming that the vehicle is on a level road. The 20 km/h is maximum speed allowed for the vehicle in both diesel and electric modes. This is because the vehicle was developed mainly for the flower festival that is held in the city. Usually, a speed limiter is used to set the desired speed. Therefore, in this thesis, we proposed a different speed range in more realistic driving scenarios to investigate the energy demand. Hence, the vehicle was tested beyond this speed limit using the WLTP test procedure, to estimate the exact power requirement for the vehicle in a more real-world driving scenario. The

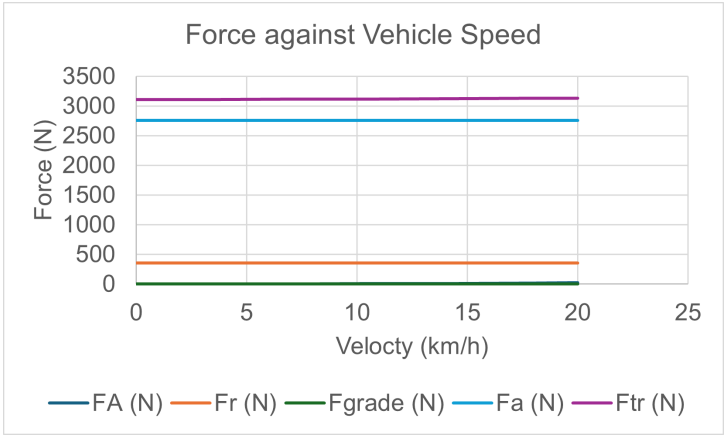

Figure 2.5.4: Tractive Force Analysis due to a Level road

aerodynamic resistance force and the tractive force were observed to increase as the speed of the vehicle increases. At the same time, other resistance forces remain constant, which is evident on the basis of the mathematical relations of the forces, such as the vehicle speed and the vehicle slope. Therefore, the total actual tractive torque that would be required on our Crafter wheel is 1118.384 Nm for a tractive force of 3132.73 N.

If we assume that the vehicle is RWD, the electrical drive mode is active or if we assume that the vehicle is FWD, the diesel mode is active, or in hybrid mode, and the torque at the vehicle's wheel is:

$$\begin{cases} F_{th} = \frac{i_x \cdot i_0 \cdot T_E \cdot \eta_P}{r_t} \\ F_{max} = \phi \cdot w \end{cases} \tag{2.5.7}$$

T_E, ϕ, F_{max}, i_x, F_{th}, i_0 are motor or engine torque, coefficient of adhesion between the tire of the vehicle and the surface, maximum total tractive force allowed for the Crafter, the transmission's first gear ratio, the theoretical total tractive force, the gear ratio of the final drive of the transmission. If the peak torque of ICE is 340 Nm, and the first gear ratio of the transmission is 5.06. Then, based on the equation, the theoretical force would be 17,001 N. For the efficient design, we took the transmission efficiency as 0.9 or 90% when the final gear ratio of the final drive is 3.92. However, the maximum allowed total tractive force was calculated to be 21,644.78 N. Therefore, when comparing these forces, it was observed that the maximum total tractive force allowed was greater than the total theoretical torque. This indicates there was a safe vehicle design, so the vehicle would not experience any slip.

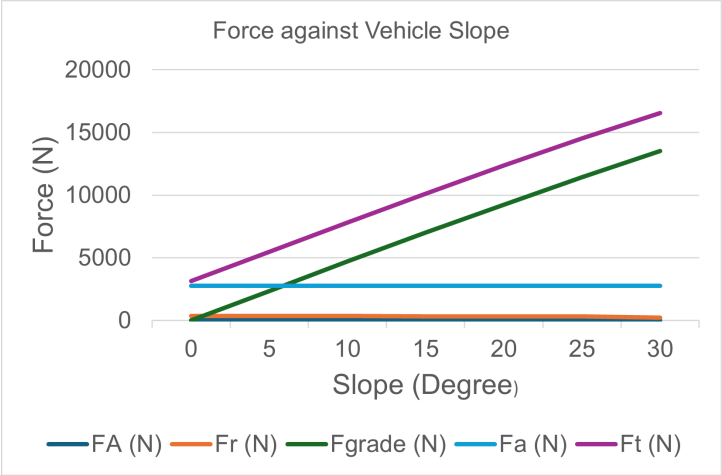

Figure 2.5.5: Vehicle Tractive Force due to Slope

Therefore, we developed the equation-based MATLAB model of the VW Crafter based on the mathematical background of its dynamics descriptions to validate the accuracy of the power source proposed for the vehicle.

However, when the vehicle is inclined, normally up to the sloping angle of 30^0, the forces acting on the vehicle are shown in Figure 2.5.5. As the angle increases, some of the forces, such as the tractive and gradient forces were increasing and so also the power and torque requirement. While the rolling resistance force was decreasing. In this case, the torque and power requirement would be large. If the maximum tractive force is 16613.61 N then the tractive power would be around 92.368 kW and tractive torque would be 5931.059 Nm. This is why Parker electrical machine with peak power of 82.3 kW, ICE with 103 kW and 2011 Nissan Leaf battery pack delivering a power of 90 kW are the right choice for this type of hybrid vehicle. The detailed technical specifications of the proposed the electrical machine are presented in Chapter Three. However, since the tractive power is directly proportional to the tractive force, a similar diagram for the tractive power analysis as shown in Figure 2.5.6 was obtained.

After analyzing the vehicle at a constant speed of 20 km/h, we proposed a top speed of 120 km/h, which is more realistic than the initial 20 km/h. This speed varies depending on the manufacturing year and the engine configuration [152]. The e-Crafter has a top speed of 90 km/h [33], and only 80 km/h is allowed [153]. For this design, we chose 120 km/h. Although all these speeds that we proposed to test the vehicle are constant, the power or

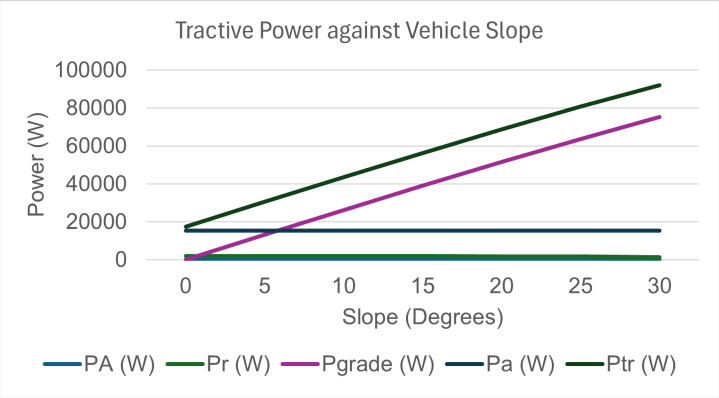

Figure 2.5.6: Vehicle Tractive Power due to Slope

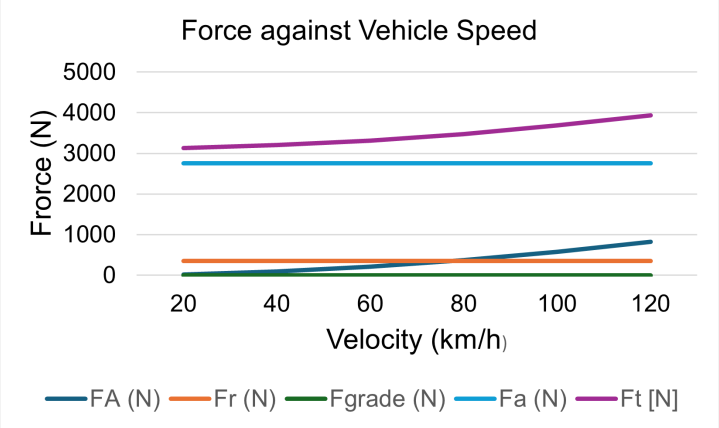

Figure 2.5.7: Vehicle Tractive Force at 120 km/h

energy demand would be higher compared to the drive cycles that account for the acceleration and deceleration driving behavior, as well as the average speed. Figure 2.5.7 shows the tractive force and other resistance forces at the vehicle speed of (20-120 km/h). At 120 km/h, the total tractive force was found to be 3,936.44 N and the tractive torque was 1405.31 Nm when the tractive power was 131.20 kW. When we consider a maximum speed of 90 km/h for the e-Crafter, the tractive force and torque were 3574.85 N and 1,276.22 Nm, respectively. Therefore, the tractive power would be 89.37 kW. However, when the vehicle was inclined at 30^0 at the maximum speed of 120 km/h, the total traction was 17,417.31 N and 6,217.988 Nm, respectively. Therefore, for the conditions of the level road and steep terrain, there is a safe design.

To design the vehicle under the influence of the drive cycle, we adapted a real-world test profile such as a WLTP as a reference speed for the vehicle. The MATLAB model in Figure 2.5.2 was developed for this purpose. Hence, Figures 2.5.8, 2.5.9, and 2.5.10 show the resistance forces, the total tractive force and torque, as well as the total tractive power. Figure 2.5.11 shows the speed set-point based on the WLTP in m/s or (131 km/h top speed) with 23.26 km, the distance covered by the vehicle. Therefore, since the distance is more closely related to energy and fuel consumption, we corrected the distance and computed the vehicle consumption based on the standard of 100 km (i.e. L/km, kWh/km, L/100 km, or kWh/100 km). WLTP is a drive cycle commonly used for fuel consumption, as it better replicates real-world driving conditions. It has a maximum speed of 131 km/h, which is approximately 36.3889 m/s. Therefore, we used this drive cycle to simulate the vehicle at 1800 seconds. The vehicle covered 23.26 km. Based on the simulation results, the force due to rolling resistance was found to be 351.7 N, the force due to aerodynamics was 989.9 N, the grade force was found to be 0 N, and the acceleration resistance force was found to be 6,361.6 N. The total tractive force and torque were 5,407 N and 1,930 Nm, respectively, as shown in Figure 2.5.9, with the WLTP drive cycle in 1800 seconds. Based on the maximum total tractive force allowed and the tire radius, the maximum total tractive torque allowed would be 7,727.186 Nm, much greater than the simulated torque of 1,930 Nm. This also proves that there was a safe vehicle design.

Moreover, the total tractive power based on the simulation was 79.85 kW as shown in Figure 2.5.10 in addition to the individual power due to the resistance forces. The power due to the rolling resistance (P_r) was found to be 12. 83 kW, the power due to the aerodynamic resistance (P_A) was 36.11

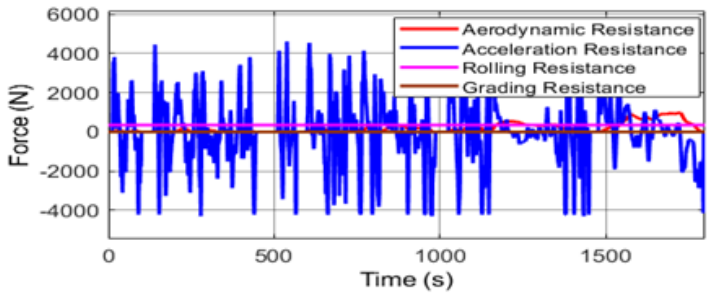

Figure 2.5.8: Simulated Resistance Forces [34]

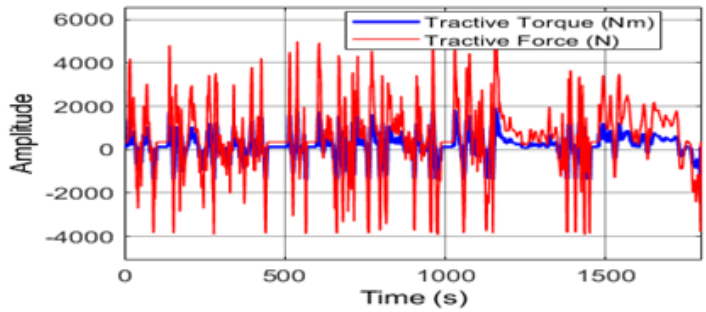

Figure 2.5.9: Tractive Torque and Force [34]

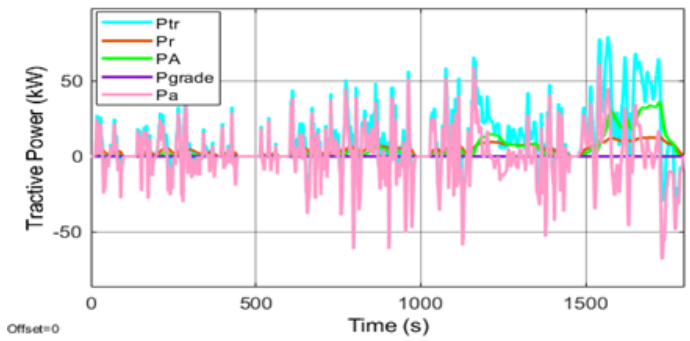

Figure 2.5.10: Tractive Power

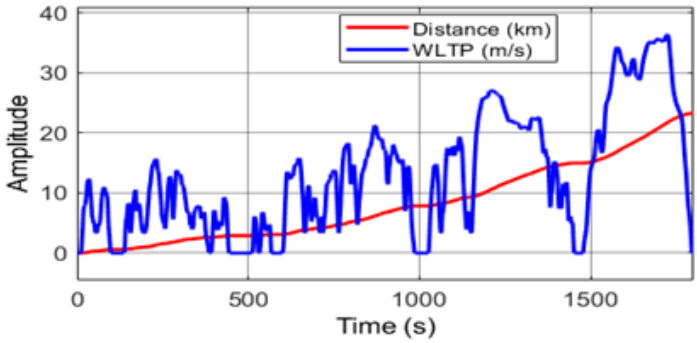

Figure 2.5.11: WLTP Reference and Distance

kW, the power due to the grade resistance (P_{grade}) was 0, and the power due to the acceleration resistance (P_a) was 61.55 kW, respectively. The sum of the power due to the acceleration and deceleration of the vehicle (both motoring and generation) should be the total tractive power. Therefore, in this thesis, the power source requirement was validated based on two reference inputs: firstly, the WLTP drive cycle, replicating the real-world driving cycle. In other words, we proposed a speed that is above the limit of the maximum speed allowed for the vehicle (i.e., 20 km/h) because this does not mean that the vehicle could not operate above the limiting speed. A speed limiter is usually incorporated to serve this purpose. Most diesel engines, in particular, are capable of high speed. For example, the ECU is set up to 200 km/h for golf. Secondly, the speed is 20 km/h (This is the limiting speed allowed in either diesel or electric mode). Hence, if we consider the vehicle's gear ratios, the maximum power and torque requirement of the engine and motor designed based on 103 kW, 340 Nm and 82.3 kW, 173 Nm output requirements, were the right choice. This is a safe design vehicle even when considering 30^0 sloping which had a maximum tractive force of 16,613.61 N and the tractive torque was 5,931.059 Nm which is much less than the permissible value.

2.5.3.1 Sensitivity Analysis on the Vehicle Traction

In sensitivity analysis, we investigate how the coefficients of rolling resistance, vehicle mass (e.g Figure 2.5.12), and frontal area impact energy consumption and tractive force, making it a suitable framework for assessing risk, evaluating the applicability of the results, and verifying the reliability of our model. To correlate this, alternative methods relevant to vehicle dynamics are

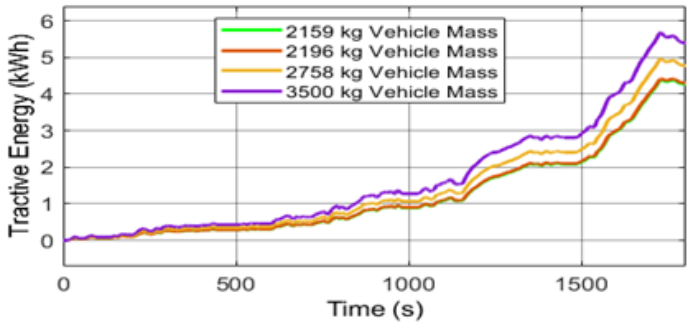

Figure 2.5.12: Tractive Energy for Different Mass

analyzed in detail in the subsequent section of this thesis, which includes a SWOT analysis. To perform this analysis, data obtained from the drive cycle (WLTP), which replicates real-world driving conditions, were used. In addition, we tested the vehicle based on the NEDC, which yielded an energy consumption of 20.045 kWh/100 km, compared to the WLTP, which gave 21.354 kWh/100 km. Therefore, the detailed vehicle design included the NEDC as a test procedure in Chapter Four for comparison, as most manufacturers in Europe specify consumption and emissions in terms of the two commonly used drive cycles, as well as highways. Figure 2.5.12 shows the tractive energy of the vehicle changing with the vehicle masses, such as 2159 kg, 2196 kg, 2758 kg, and 3500 kg. We know that the VW Crafter has different masses, from curve to gross weight. The conversion from the van with 3500 kg to pick-up usually changes the vehicle's weight. In this dissertation, we used 2758 kg weight because the weight was further reduced even after the conversion to pick-up. Considering the weight of the 2011 Nissan Leaf battery and other electrical devices, we estimated the vehicle's weight to be around 2758 kg. However, the traction energy was analyzed based on the vehicle's mass and different front areas to validate the energy requirement taking into account battery size, engine, and electrical machine. Since the vehicle mass was reduced when converted to pick-up style, protected covers are assumed to be equal to the weight of the electrical drives, which may increase the vehicle mass above the curb weight but less than the gross weight.

Figure 2.5.13 shows the total tractive energy changes with the frontal area. Therefore, energy consumption is affected by the size and mass of the vehicle components. Figures 2.5.14 and 2.5.15 show the effect of the coefficients of rolling radius on energy consumption and tractive force. The

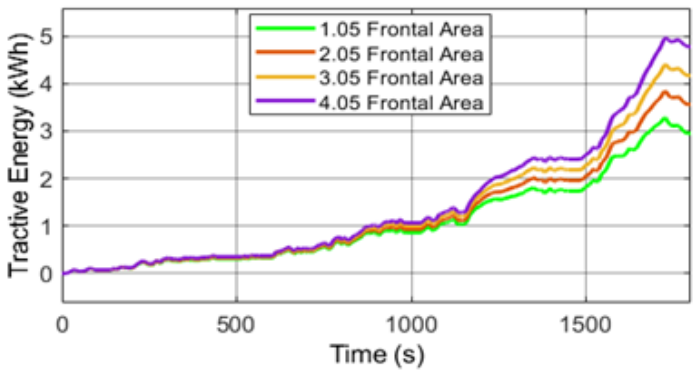

Figure 2.5.13: Tractive Energy for Different Frontal Area

rolling radius coefficient has been experimentally found in a laboratory test in Hungary to vary between 0.01 and 0.025, which falls within the range of typical asphalt road conditions [154]. The magnitude of the coefficient of the rolling radius ranges from 0.001 to 0.4 and depends on the ratio and magnitude with respect to the deformation of the road surface and the tire, and increases with the temperature of the road surface by 13% when the temperature rises to 60 °C [154]. Therefore, the energy consumption depends on the tire-road contact conditions.

Table 2.4 presents the total tractive energy and force as a function of vehicle mass, indicating the direct relationship between vehicle mass and energy consumption, as well as tractive force. Therefore, even at high speeds of 131 km/h, the energy consumption remains within the maximum capacity of the 2011 Nissan Leaf battery per 100 km for all mass cases, except for the 3500 kg scenario. In this case, the energy consumption marginally exceeds the battery capacity by 0.458 kWh/100 km, representing a 1.873% increase. The recent version of the e-Crafter has 90 km/h, and this vehicle was limited to 20 km/h. Furthermore, just like in the case of vehicle mass, the tractive energy also changes with the vehicle's front area. While Table 2.5 presents the total tractive energy and force values when the mass was fixed and frontal areas of the vehicle changed. This shows that the vehicle range, energy consumption, tractive force, and emissions are affected by the vehicle size, engine size, battery size and mass. Therefore, this gives an avenue to investigate the vehicle's traction as a trade-off between the vehicle size, battery size, engine, vehicle mass, driving range, and consumption. Moreover, Table 2.6 presents how the coefficient of rolling resistance affects the tractive force and the vehicle's energy consumption. We considered different values

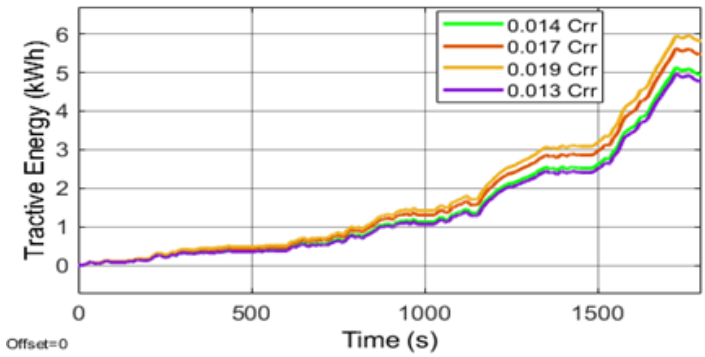

Figure 2.5.14: Tractive Energy for Different Rolling Radius Coeff.

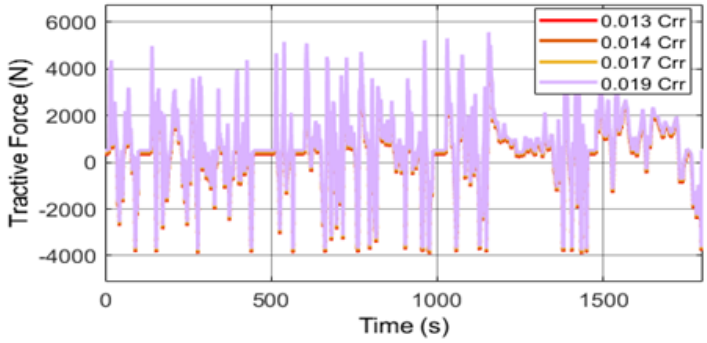

Figure 2.5.15: Tractive Force for Different C_{rr}

of the rolling resistance coefficient and observed how it affects the critical vehicle parameter. However, the coefficient value varies according to the region and tire-road conditions, such as snow, wet asphalt, dry asphalt, and others. Therefore, considering this design of the VW Crafter, it is necessary to utilize the appropriate energy source components such as the battery and electrical machine in the case of pure electric and the engine in the case of the hybrid, taking into account the losses in the driveline, battery, and the electrical drive sections. There are very few authors according to the literature that have worked in this critical area of research such as A. Saleem et al. in [150].

It was observed, based on the results presented in the tables and the MATLAB results shown in the Figures, that the coefficient of rolling resistance and the vehicle mass affect the tractive force and energy consumption. Hence, for the comprehensive sensitivity analysis, we proposed a commonly used chart called a Tornado to visually illustrate how energy consumption and tractive

Table 2.4: Tractive Energy and Force Changing with Mass

Mass [kg]	**Tractive Force [N]**	**Energy [kWh/100 km]**
2159	4241	18.852
2196	4313	19.007
2758	5407	21.354
3500	6853	24.458

Table 2.5: Tractive Energy and Force Changing with Area

Area [m^2]	**Tractive Force [N]**	**Energy [kWh/100 km]**
1.05	5381	14.106
2.05	5390	16.513
3.05	5399	18.929
4.05	5407	21.354

Table 2.6: Tractive Energy and Force Changing with C_{rr}

C_{rr}	**Tractive Force [N]**	**Energy [kWh/100 km]**
0.013	5407	21.354
0.014	5435	22.066
0.017	5516	24.187
0.019	5570	25.602

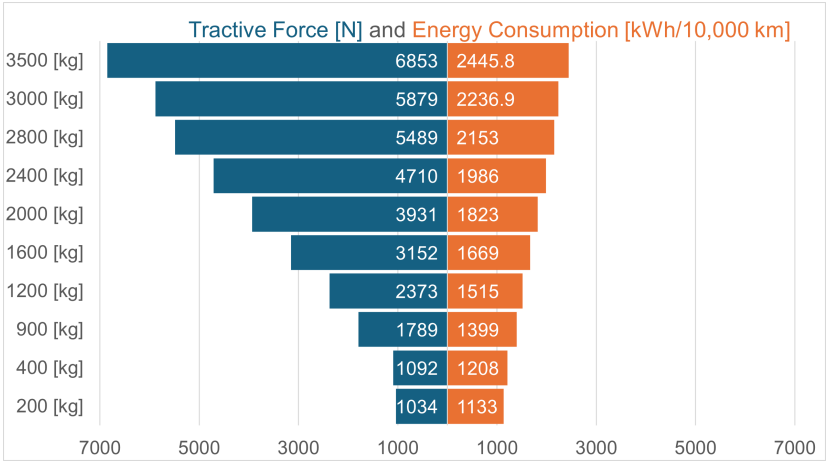

Figure 2.5.16: Tornado Chart for Sensitivity Analysis

force are affected by vehicle mass. However, to make the energy consumption more visible on the cart, we corrected the unit of the energy consumption from kWh/100 km to kWh/10,000 km. Figure 2.5.16 shows sensitivity analysis of the tractive force and the energy consumption according varying vehicle mass using Tornado chart. Therefore, to get the energy consumption in the standard unit, the value must be divided by 100 km. For example, from Figure 2.5.16, 2445.8 kWh/10 000 km is equivalent to 24.458 kWh/100 km, as presented in Table 2.4. It should be noted the vehicle mass in the range (2800-3500 kg) is within the range of the practical mass of the proposed vehicle. The remaining masses were chosen to effectively demonstrate the vehicle's impact on energy consumption and tractive force. Therefore, based on the results presented in this research, data presented in the manufacturer's datasheet [43], real-world tests conducted by users of similar vehicle models [44], and the measured data discussed in Chapter Five, the energy consumption and tractive force presented in this thesis accurately replicates the real-world physical behavior under long-term operating conditions. This was validated by testing the developed model under realistic driving scenarios, including higher speeds and long distances.

2.5.3.2 SWOT Analysis

Figure 2.5.17 shows the SWOT (strengths, weaknesses, opportunities, and threats) analysis of the vehicle dynamics study (analytical and simulation-based approaches) presented in this chapter. The analytical approach is based

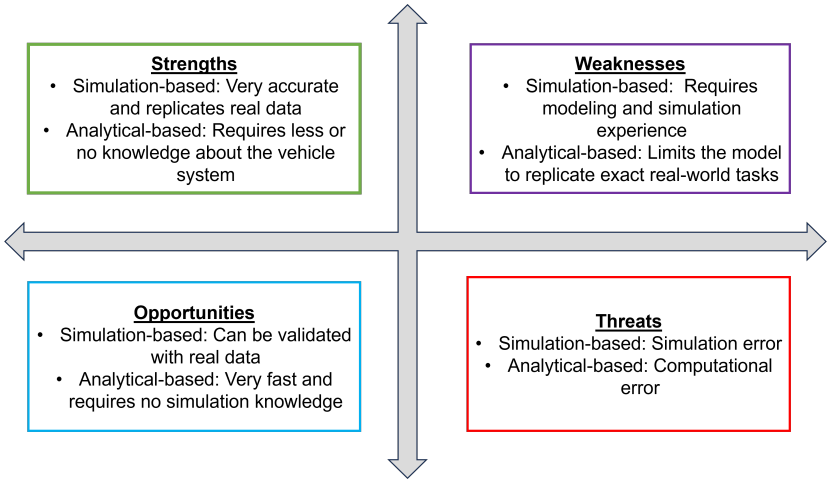

Figure 2.5.17: SWOT Analysis for VW Crafter Dynamics

on the computation of the tractive force, torque, and power requirements of the VW Crafter, as described at the beginning of subsection 2.5.3. The simulation is based on the use of MATLAB software (MathWorks, R2024a) to simulate the vehicle dynamics behavior based on the drive cycle as a reference velocity. The simulation-based approach is more accurate because it requires software (MATLAB) to do tasks. Therefore, it is computationally error-free. It also replicates real-world data because it applies real driving scenarios, which take into account, for example, the motoring and generation actions of the powertrain or during the regenerative braking of the vehicle. In addition, the simulation-based could be directly validated with the real data because the achieved results (energy consumption) were close to the manufacturer or experimental data as presented previously. Nevertheless, it can be limited by simulation errors, such as arithmetic errors and solver errors. On the other hand, the analytical approach does not require knowledge of the vehicle system. It only requires the parameters and Newton's equations of motion to study the dynamic behavior of the vehicle. Additionally, it is very fast and can be used even without prior knowledge of simulation analysis software. However, the analytical-based approach can be limited by computational error which could lead to in accurate presentation of the traction requirement of the vehicle.

2.6 Conclusion

The complex battery pack simulation provides a detailed simulation of each cell and module. Therefore, to reduce the complexity of the entire pack due to low simulation time and to make the system faster, the detailed model has been compressed into a system-level model that replicates the detailed model behavior in real-time and provides an effective simulation environment for the battery management system. The battery has been simulated over a realistic current profile. The thermal performance and capacity fade (degradation) of the 2011 Nissan Leaf battery over time and number of life cycles have been investigated in its first and second life cycles, using a realistic current profile at a 5 C-rate. The simulated battery still maintains 60.3% of its remaining capacity in its first life with a 56% fading rate per 1000 cycles at an operating temperature of 29.30 °C. The 2011 Nissan Leaf battery presented in this chapter will be used in the coming chapters for the development of EVs and HEVs in this research. The proposed control strategy is expected to enhance the battery capacity, extend its range, and manage energy consumption at an optimal level.

For the vehicle powertrain to meet the design requirement, it must be analyzed on the basis of the intended operating environment. Therefore, the vehicle must be able to overcome the resistance forces acting in the opposite direction for it to move forward. This is in line with the vehicle's power or torque requirement. Therefore, the thesis analyses the total tractive force needed to propel the vehicle either in electric, hybrid, or conventional modes, at different speeds, sloping angles, front area, and mass to choose the proposed vehicle's exact power source. The thesis investigated a trade-off between vehicle size, battery size, engine, vehicle mass, driving range, and consumption. Consequently, a 2.0 L TDI CR diesel engine, which complies with the EU6d emissions standards, with a CR fuel technology, capable of providing a maximum power of 103 kW, will be utilized. The hybrid version will be developed by cooperating the combustion engine with the 2011 Nissan Leaf battery, capable of providing a power of more than 90 kW, 24 kWh nominal capacity and a Parker PMSM electrical machine (82.3 kW/53.5 kW maximum power/rated power).

The exact energy required per 100 km of distance covered to be consumed by the proposed VW Crafter was found to be 21.354 kWh/100 km validated from the actual data of the similar model, specified at 21.54 kWh/100 km, which will help determine if there is an efficiency gain when the actual vehicle is developed based on the proposed optimization techniques in the

coming chapters. Hence, in the context of the vehicle technical requirements and design considerations, the VW Crafter was evaluated and validated to achieve the performance goals. A comprehensive sensitivity analysis, based on a Tornado chart, has been conducted to investigate how changes in key parameters, such as vehicle mass, affect energy consumption at higher speeds, including those based on the WLTP, thereby extending the applicability and relevance of our model to real-world tasks. In addition, the modeling approaches adopted related to the dynamics of the proposed vehicle have been compared using a SWOT analysis to confirm the reliability and understanding of our chosen methods.

Chapter 3

Electric Drives Dynamics and e-Crafter Simulation

3.1 Introduction

The proper choice of electrical drive for industrial application is critical, especially in the field of electric and hybrid vehicles. Many electrical machines have been used in traction applications, from direct current machines (DCMs) to alternating currents (ACs), typically asynchronous machines (for example, Induction machines (IMs), synchronous (for example, permanent magnet synchronous machines), such as permanent magnet synchronous motors (PMSMs) and brushless direct currents (BLDCs). Currently, most of the electrical machines used in most cars for traction applications are PMSMs or permanent magnet ACs (PMACs) due to their high efficiency and power density and their ability to maintain constant speed over a range of speeds. However, switched reluctance (SRMs) and induction machines are seen to be increasingly applied in traction applications. The mathematical descriptions, the MATLAB models, and the pure model of the electrified powertrain of the VW Crafter are presented in this chapter. Both brushless direct currnt (BLDC) and PMSM machines were utilized to power the vehicle for performance comparison.

3.2 Permanent Magnet Synchronous Motor

The PMSM, which is referred to as a three-phase permanent magnet alternating current (PMAC) motor, has been widely employed as a traction motor

for transportation electrification due to its high efficiency and power density and ability to provide constant power over various speeds. However, PMSM can also be called BLDC motor in other contexts used by the electrical machine control community. Specifically, the PMAC is commonly called the PMSM. The major difference between the PMSMs and BLDCs is their back electromotive force (EMF) voltages shape. The PMSM has been adopted in EVs and HEVs to overcome the disadvantage of conventional DC electrical machines. The recent permanent magnetic materials and the sophisticated electronics control structures have made traction electrical machines more efficient and possess highly compact designs [155].

Electrical machines have been known to be the heart of electric vehicles. The study in [155] compared various traction machines, like the induction motor (IM), BLDC machine, and PMSM, to determine the best electrical machines for use in traction applications. The PMSM is the most efficient, cost-effective, and compact size. The PMSM is categorized into interior PMSM (IPMSM) and surface-mounted PMSM (SPMSM).

This research applies PMSM, whose three-phase stator, a three-phase AC supply voltage, feeds the winding of the machine, in which a revolving magnetic flux is established in the air gap (Figure 3.2.1). Hence, the electrical machines adopted for traction applications, especially for industrial-sized vehicles, should have smooth and perfect rotation over the entire operating speed range. In effect, the control of its torque should be fully achieved even at zero speed. This research adopts a complex control strategy called field-oriented control (FOC) to control the motor. This control method has been applied to eliminate the shortcomings of its BLDC motor counterpart control method due to the torque ripple and lack of maximum torque during the commutation process of the trapezoidal control. The maximum torque is needed in order to improve performance that perfectly suits traction applications.

At the same time, the PMSM is gaining popularity in traction applications due to its advantages in terms of control strategies and overall performance compared to the IM, which has much more complex dynamics. Two models of the PMSM for the vehicle were developed: Simplified and detailed models. Therefore, computed electrical losses from the detailed three-phase model were utilized for modeling the electric vehicle at simplified modeling level without considering the detailed model's power electronics and other complexity. Hence, the energy equivalent model was implemented on the basis of torque-speed envelope to abtract the complex model at system level performance. [145].

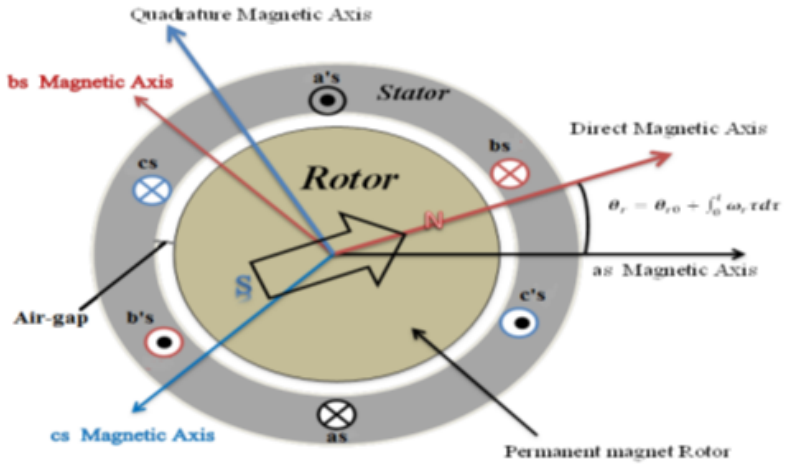

Figure 3.2.1: PMSM Structure [145]

3.2.1 PMSM Detailed Modeling

The detailed modeling of the PMSM is applied based on the following assumptions. The sinusoidal Magnetomotive Force (MMF) was distributed in the air gap. 2. There was a restriction in the saliency according to the rotor position. 3. hysteresis and saturation were ignored. 4. A balanced 3-phase supply voltage was assumed. 5. Assuming that the back EMF was sinusoidal [145]. Therefore, the three-phase voltages can be expressed as in [145] as follows:

$$\begin{cases} V_A = \frac{d}{dt}\Psi_A + I_A R_s \\ V_B = \frac{d}{dt}\Psi_B + I_B R_s \\ V_C = \frac{d}{dt}\Psi_C + I_C R_s \end{cases} \tag{3.2.1}$$

Where Ψ_A, Ψ_B, Ψ_C and I_A, I_B, I_C are the flux linkages and three-phase currents and R_s is the phase resistance, respectively. Therefore, if L_s is the phase inductance, the rotor coupling flux linkage is expressed as:

$$\begin{cases} \Psi_A = L_s I_A + \Psi_r \cos\theta \\ \Psi_B = L_s I_B + \Psi_r \cos(\theta - \frac{2\pi}{3}) \\ \Psi_C = L_s I_C + \Psi_r \cos(\theta + \frac{2\pi}{3}) \end{cases} \tag{3.2.2}$$

Thus, with help of the $d-q$ frame of reference, the model of the electrical machine can be represented in d_q rotating reference frame [145]:

$$\begin{cases} V_q = R_s I_q + \omega_r \lambda_d + \frac{d}{dt}\lambda_q \\ V_d = R_s I_d - \omega_r \lambda_q + \frac{d}{dt}\lambda_d \end{cases} \tag{3.2.3}$$

In which:

$$\begin{cases} \lambda_q = L_q I_q \\ \lambda_d = L_d I_d + \lambda_r \end{cases} \tag{3.2.4}$$

Hence, equation (3.2.3) will be:

$$\begin{cases} V_q = R_s I_q + \omega_r \left(L_d I_d + \lambda_r\right) + \frac{d}{dt} L_q I_q \\ V_d = R_s I_d - \omega_r L_q I_q + \frac{d}{dt}\left(L_d I_d + \lambda_r\right) \end{cases} \tag{3.2.5}$$

Thus, the electromagnetic torque will be given as:

$$T_e = \frac{3}{2}\frac{P}{2}\left(\psi_r I_q + \left(L_d - L_q\right) I_d I_q\right) \tag{3.2.6}$$

Therefore, in equation (3.2.6) P stands for the number of pole pairs. Also, the q-axis inductance is equal to the d-axis inductance. Hence, equation (3.2.6) will now be expressed as:

$$T_e = \frac{3}{2}\frac{P}{2}\left(\psi_r I_q\right) \tag{3.2.7}$$

Table 3.1: Three-Phase PMSM Parameters

Parameters	**Values of Parameters**	**Symbols [Unit]**
Stator Resistance	0.0317	$R\ [\Omega]$
d-axis Inductance	0.000389	$L_d\ [H]$
q-axis Inductance	0.000389	$L_q\ [H]$
Rotor Flux	0.112	$V_s\ [Weber]$
Number of Pole Pairs	4	$P\ [-]$
Rotor Type	Salient Pole	-

Table 3.1 presents the estimated parameters of the three-phase PMSM. The parameters of the electrical machines can be obtained based on the manufacturer datasheet. Moreover, the parameters can be obtained based on the hardware set-up (Taxes Instruments) to estimate accurate parameters

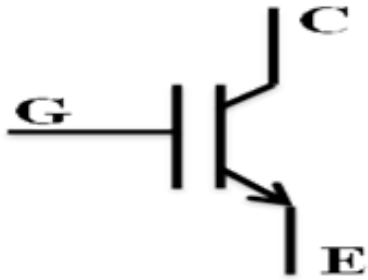

Figure 3.2.2: IGBT Symbol [156]

that suit the real-life application of the required traction application or from the analysis of the detailed electromagnetic simulation. However, the machine parameters were adjusted based on trial and error to match the requirements and operating conditions.

3.2.2 PMSM Drives

The PMSM drives consist of the DC-DC converter (which was installed to protect onboard devices for the Crafter while it is optional in some cases at the simulation level), three-phase inverter, controllers, and the gate driver. The DC source, which provides power to the motor through a DC-DC converter (if present), provides the voltage suitable for the inverter, which converts the DC voltage into three-phase AC power. There are three PIs in the PMSM control loops: two PIs in the inner loop regulate the current vectors, while in the outer loop, one PI controls the motor speed. In this research, we adopted the simulated losses for the PMSM energy equivalent model. Therefore, both the detailed three-phase PMSM and the simplified model were applied for the Crafter.

3.2.2.1 Insulated Gate Bipolar Transistor

Insulated gate bipolar transistor (IGBT) is a type of transistor used as a switching device for the three-phase inverter to energize the three-phase winding of the motor. The control system is responsible for generating the signals for the inverter switches on the basis of the desired motor speed or torque. Since there are three phases, and two phases are energized simultaneously, just like in the case of the commutation process in the BLDC motor, six IGBTs are used for the three-phase inverter. Figure 3.2.2 shows

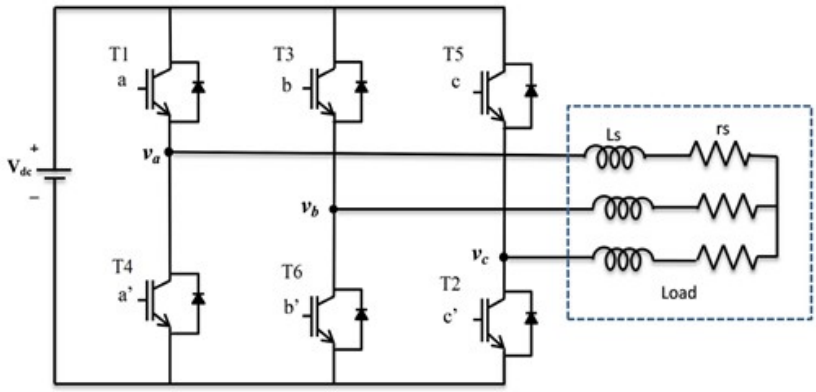

Figure 3.2.3: PMSM Three-Phase Inverter [156]

the symbol of the switch, which is based on a four-layer, two-junction NPNP transistor.

3.2.2.2 Three-Phase Inverter

The inverter is an integral part of the FOC strategy used to convert the DC voltage of the power supply to three-phase AC. The three-phase inverter model consists of the six IGBT switches used to provide pulses generated from the FOC algorithm for energizing the motor phases at the appropriate rotor angle in the sector. The pulse width modulation (PWM) signal controls the motor speed by varying the power delivered. In this application, a space vector pulse width modulation (SVPWM) is commonly used to provide pulses to the IGBT switch of the three-phase inverter for energizing the motor phases. Figure 3.2.3 shows the schematic diagram of the three-phase inverter.

3.2.2.3 Field Oriented Control

The FOC is a complex control strategy utilized to regulate the three-phase PMSM. The overall aim is to produce torque due to its advantages of torque ripple elimination and achieving the maximum torque to improve performance compared to the trapezoidal control in BLCD motors. The FOC approach regulates the vector of the three-phase current which is perpendicular to the rotor angle [157]. Thus, the FOC algorithm should keep the rotor and stator fields orthogonal to each other in order to generate the maximum torque for the PMSM to enhance the performance for efficient performance in our EVs

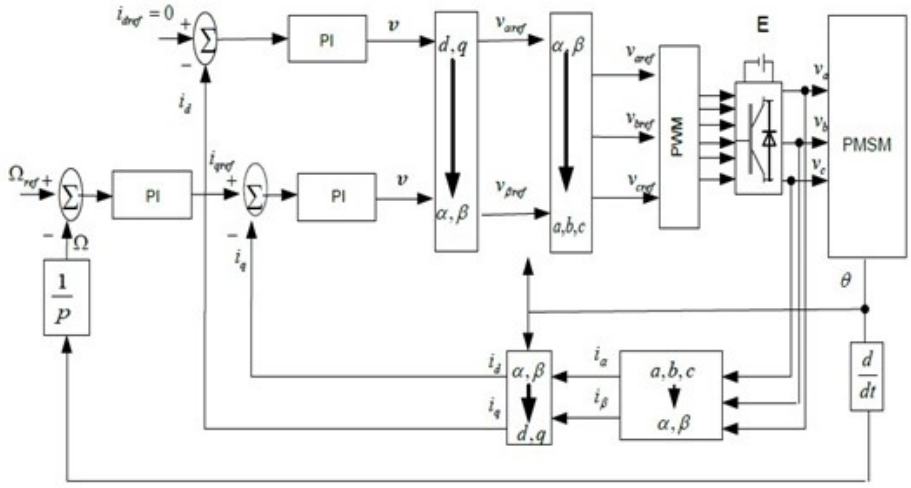

Figure 3.2.4: Three-Phase PMSM FOC Strategy [157]

applications. Figure 3.2.4 shows the three-phase PMSM-based FOC strategy implementation.

The FOC algorithm aims to control the three-phase currents (I_a, I_b, I_c) to regulate the motor's speed and torque. Therefore, instead of handling the sinusoidal three-phase AC currents directly, which could be hard to control by the PID control algorithm, Clarke/Park transformation is used to convert the currents into two DC currents for easier control: quadrature current (I_q) and direct current (I_d). Therefore, the two PIs in the inner loop would control these currents. Hence, one PI is set to maximize the I_q while the other PI is to zero the I_d since I_d is not responsible for producing the motor torque. Consequently, these controllers output the two voltages: (V_q) and (V_d) and inverse Clarke/Park transformation is used to convert them back into three-phase voltages, which fed into the PWM to generate the pulses to the three-phase inverter. At the same time, the outer loop PI controls the motor speed. The three-phase currents are first converted into two stationery reference frame (α, β) having two current, (I_α, I_β) which is expressed based on forward Clarke transformation as in [157] as:

$$\begin{cases} I_\alpha = \frac{3}{2} I_a \\ I_\beta = \frac{\sqrt{3}}{2} I_b - \frac{\sqrt{3}}{2} I_c \end{cases} \tag{3.2.8}$$

Since we need to control the current in a rotating frame of reference, forward

Park transformation is applied [157]:

$$\begin{cases} I_d = I_\alpha \cos\theta_d + I_\beta \sin\theta_d \\ I_q = -I_\alpha \sin\theta_d + I_\beta \cos\theta_d \end{cases} \tag{3.2.9}$$

These two DC currents are fed as reference to the two PIs of the inner control loops which provide the following voltages [157]:

$$\begin{cases} V_q = \frac{2}{3}[V_a \cos\theta + V_b \cos(\theta - \frac{2\pi}{3}) + V_c \cos(\theta + \frac{2\pi}{3})] \\ V_d = -\frac{2}{3}[V_a \sin\theta + V_b \sin(\theta - \frac{2\pi}{3}) + V_c \sin(\theta + \frac{2\pi}{3})] \end{cases} \tag{3.2.10}$$

The reverse Park transformation converts the rotating vooltage vectors (V_d, V_q) into the stationery reference frame (V_α, V_β) and the reverse Clarke transformation converts them into three-phase voltages (V_a, V_b, V_c). However, the reverse Park-Clarke transformation directly converts them into three-phase voltages as expressed in [157] as follows:

$$\begin{cases} V_\alpha = V_d \cos\theta - V_q \sin\theta \\ V_\beta = V_d \sin\theta + V_q \cos\theta \\ V_a = V_\alpha \\ V_b = \frac{-V_\alpha}{2} + \frac{\sqrt{3}}{2} V_\beta \\ V_c = \frac{-V_\alpha}{2} - \frac{\sqrt{3}}{2} V_\beta \\ V_a = V_q \cos\theta - V_d \sin\theta \\ V_b = V_q \cos(\theta - \frac{2\pi}{3}) - V_d \sin(\theta - \frac{2\pi}{3}) \\ V_c = V_q \cos(\theta + \frac{2\pi}{3}) - V_d \sin(\theta + \frac{2\pi}{3}) \end{cases} \tag{3.2.11}$$

The above mathematical formulations describe the FOC algorithm. The electrical losses are computed based on the speed-torque vector specified in the high fidelity model. These computed electrical losses are utilized in the abstracted model of the PMSM in order to speed-up the simulation time and improve the optimization level. Figure 3.2.5 shows the representation of the forward Clarke-Park and reverse Park-Clarke transformation based on the three-phase current and vector axes.

3.2.3 Simplified PMSM Model

The simplified PMSM equivalent model was obtained by abstracting the full-scale model of the three-phase PMSM model that works on the basis of

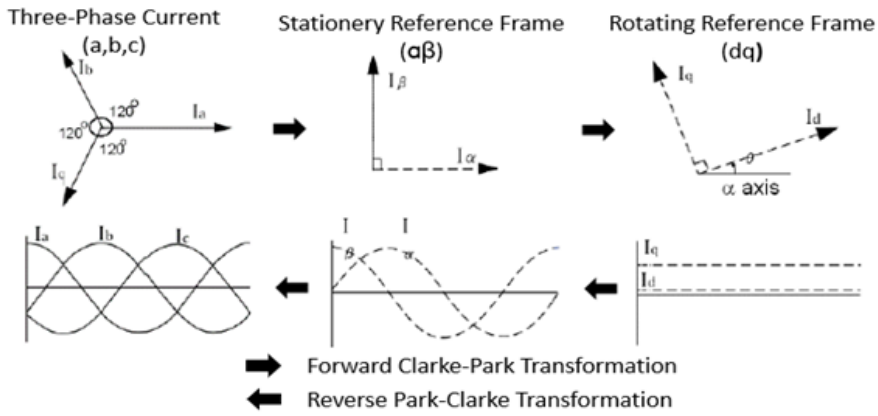

Figure 3.2.5: Park-Clarke Transforms modified from [157]

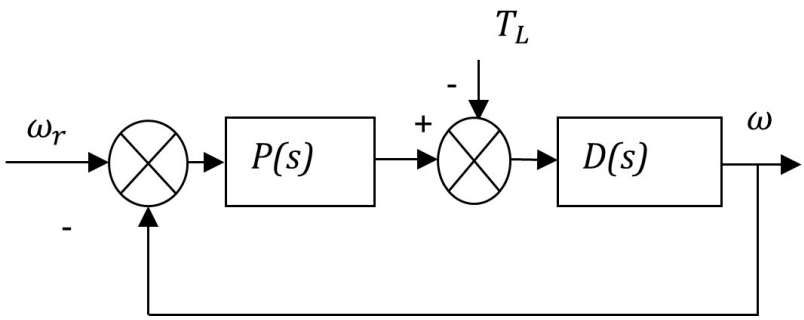

Figure 3.2.6: PMSM Simplified Model [145, 158]

the computed electrical losses. The PMSM model's FOC technique is made of three proportional integral (PI) controllers. Therefore, the two PIs in the inner loops are used to control the two current vectors (such as the I_q and I_d) in the full-scale model. The third PI controller in the outer loop, which controls the motor speed, is maintained in the simplified motor model and works on the basis of the torque-speed envelope.

Considering the simplified model of the PMSM in Figure 3.2.6, we can define the transfer function $D(s)$ from the load torque T_L to the actual motor speed ω and the overall transfer function of the system $G(s)$ as expressed in [145, 158] as follows:

$$\begin{cases} D(s) = \frac{1}{sJ+B} \\ G(s) = \frac{\omega}{\omega_r} = \frac{P(s)(D(s)}{1+P(s)D(s)} = \frac{\alpha}{s+\alpha} \end{cases} \tag{3.2.12}$$

Where ω_r, ω and T_L are the reference, motor speed, and load torque; meanwhile, B, J, α and are the viscosity coefficient and motor inertia, and bandwidth for the speed control, respectively. [145].

$$P(s) = \frac{\alpha}{s} \cdot \frac{1}{sJ + B} \tag{3.2.13}$$

Therefore, we transform equation 4.2.13 into PI controller form of the outer loop from PMSM complex model:

$$\begin{cases} P(s) = \alpha \cdot J + \frac{\alpha \cdot B}{s} = K_p + \frac{K_i}{s} \\ u(t) = k_p e(t) + k_i \int e(t) dt \end{cases} \tag{3.2.14}$$

Where $u(t)$ defines the mathematical expression of the PI controller in time-domain and $e(t)$ is the speed error in time domain. However, the parametric uncertainties present are due to the inertia in mechanical parameters as a result of the changing behaviour at different operating conditions. At the same time, for electrical parameters, a function of the temperature and stator resistance affects the current loop control performance.

3.2.3.1 PMSM Quadrant Operation

The four-quadrant operation of the electrical machine is an operation of the machine based on the speed-torque envelope. It occurs during the machine's motoring and generating actions when the vehicle accelerates and decelerates. The motor is said to operate in the first quadrant when the vehicle accelerates. In this quadrant, both its speed and torque are positive. Hence, the electrical machine converts the electrical energy into mechanical rotational motion, supporting the vehicle's movement when going uphill. The second quadrant operation is the forward braking. In this quadrant of operation, the speed is negative while the torque is positive. This is when the vehicle is coming down the hill. The third quadrant is the reverse acceleration that is when both the positive and torque are negative. However, in this quadrant, the vehicle is going up the hill in the reverse direction. In the fourth quadrant, vehicle is coming down the hill in reserve, that is when the speed is negative and torque is positive. Table 3.2 presents the four quadrant operation of the PMSM.

Therefore, in these operations, the output power of the motor will be positive in the first and third quadrants and negative in the second and fourth quadrants, respectively. Table 3.3 presents the parameters of the

Table 3.2: The PMSM Quadrant Operations [159]

Quadrant	**Quadrant Operations**	**Speed**	***Torque***
1	Forward Acceleration	Positive	Positive
2	Forward Braking	Positive	Negative
3	Reverse Accelerating	Negative	Negative
4	Reverse Braking	Negative	Positive

PMSM based on the maximum or peak and the rated values of the power and torque.

Table 3.3: The PMSM Technical Specifications [80]

Name of Parameters	**Values**	**Symbols [Unit]**
Motor Peak/Rated Power	82.3/53.5	P_m [kW]
Motor Peak/Rated Torque	173/78.6	T_m [Nm]
Motor Peak/Rated Speed	8000/6500	ω_m [rpm]
Time Constant	0.02	τ [s]
Series Resistance	0	R_s [Ω]
Rotor Inertia	0.00039	I_r [$kg \cdot m^2$]
Rotor Damping	0.00001	D_r [$Nm \cdot s/rad$]

3.3 BLDC Electrical Machine

There have been many transitions from conventional to modern electrical machines and control methods, as well as several phases. For example, three-phase BLDC motors, due to their higher efficiency, low maintenance, and electronic control method compared to classical permanent magnet DCs, have replaced conventional DCMs and have been used for many industrial applications, including EVs. The high torque or ability to produce high torque is a unique feature that makes the three-phase BLDC motors commonly used as traction motors. However, with electronic control, the maximum torque is never achieved in BLDCs and is associated with torque and speed ripple. Due to this limitation, another complex control is adopted, known as field-oriented

control (FOC), based on the Clarke/Park transformation typically used to control three-phase PMSMs to produce the required maximum torque and to overcome the issue of speed and torque ripple. The FOC can operate at high speed through a field weakening technique.

Several research studies in the context of scholarly works have been done on BLDC motors in electric vehicles because of their excellent features for traction applications. The study in [160] proposed a BLDC motor for EV and investigated the impact on the DC voltage and state of ripples at the batter's power using a MATLAB simulation environment. The study in [161] proposed a BLDC motor with a rating of 5 kW, 48 V for an EV application, applying PI and ANFIS control techniques for speed control, taking error into account as the essential factor. In [162], a tilt integral derivative (TID) controller was used to control the speed of the BLDC motor, optimizing its torque and speed to improve its real-time control performance for use in electric vehicles. The study in [163] investigated the role of the pole count of the BLDC electrical machine in optimizing its performance in electric vehicle applications. In [164], a BLDC motor was applied at 1.5 kW, 3000 rpm, and 120 V in two- and three-wheeler electric vehicles. The study in [165] proposed PI-based particle swarm optimization (PSO-PI) to control the speed of the BLDC motor for optimal fuel consumption in EV and the proposed method reduced energy consumption by 3.1%.

3.3.1 BLDC Detailed Modeling

The BLDC electrical machine performs excellently in traction applications due to its high power density and efficiency. The method usually employed to control the motor is a complex control strategy called trapezoidal or commutation logic based on the hall sensors' effect that is used for detecting the rotor position in the sector. Unlike traditional DC motors, this motor does not have mechanical brushes and commutated assembly [158]. The complex model considers the detailed three-phase model of the electrical machine, power electronics, and battery storage system. However, the behavior of the electrical machine is modeled in terms of its voltage, back EMF, speed, and torque. In this research, the physical modeling approach in Simscape was used for modeling the motor, but we have to present some mathematical formulations in theory. To describe the mathematical model of the BLDC motor, the equivalent circuit of three phases in Figure 3.3.1 is used. The matrix equation can be used to represent the electrical and mechanical components of the electrical machine. The three-phase currents, I [A], three-

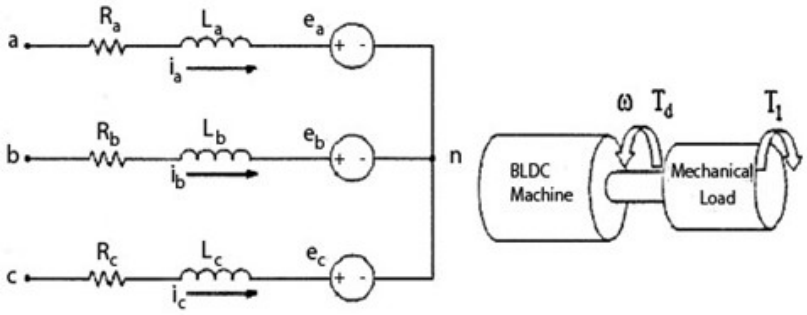

Figure 3.3.1: BLDC Equivalent Circuit [158]

phase voltages, V [Volts], and three-phase back EMFs, E [Volts], are all included in this model. The equations that control the behavior of the motor are expressed as in [158, 166] as follows:

$$\begin{bmatrix} V_a \\ V_b \\ V_c \end{bmatrix} = R \begin{bmatrix} i_a \\ i_b \\ i_c \end{bmatrix} (L - M) \frac{d}{dt} \begin{bmatrix} i_a \\ i_b \\ i_c \end{bmatrix} + \begin{bmatrix} E_a \\ E_b \\ E_c \end{bmatrix} \tag{3.3.1}$$

$$\begin{bmatrix} E_a \\ E_b \\ E_c \end{bmatrix} = K_e \omega_m \begin{bmatrix} F(\theta_e) \\ F(\theta_e - \frac{2\pi}{3}) \\ F(\theta_e + \frac{2\pi}{3}) \end{bmatrix} \tag{3.3.2}$$

Where ω_m is the mechanical speed of the electrical machine expressed as:

$$\omega_m = \frac{d\theta_m}{dt} \tag{3.3.3}$$

Where θ_m stands for the rotor's mechanical angle which refers to the electrical angle (θ_e) [166].

$$T_e = K_t \begin{bmatrix} i_a \\ i_b \\ i_c \end{bmatrix} \begin{bmatrix} F(\theta_e) \\ F(\theta_e - \frac{2\pi}{3}) \\ F(\theta_e + \frac{2\pi}{3}) \end{bmatrix} \tag{3.3.4}$$

$$T_e = J \frac{d\omega_m}{dt} B\omega_m + T_l \tag{3.3.5}$$

Where V_a, V_b, V_c, i_a, i_b, i_c are the three phases voltages and currents in phases A, B, and C, respectively. And R and L are the stator resistance and

inductance, M is the mutual inductance between the phases. Similarly, T_e, J, B, and T_l B, K_t, and $F(\theta_e)$ are the electromagnetic torque, the moment inertia of the rotor, the viscous damping, the torque constant, and function of the back EMF of the position of the rotor, respectively [166].

3.3.1.1 Trapezoidal Complex Control

The complex control method known as commutation logic is the electrical machine control strategy, which is a switching pattern based on the hall sensor for continuous dynamic rotation of the BLDC electric motor. In this control technique, a perfect commutation process is achieved with the correct phases when the control algorithm can detect the exact position of the machine's rotor at any given period and measure it with the help of the hall sensor. The phases of the electrical machine are energized two at a time. The method of energizing the two phases once at a time is the six-step commutation for the full rotation of the rotor for the forward and reverse rotations. The switching patterns for energizing the motor phases based on the motor's forward and reverse motions are presented in Tables 3.4 and 3.5 according to the hall sensors for phases A,B, and C (H_A, H_B, H_C), respectively. However, the four-quadrant operation of the electrical machine describes the motor's motoring and generating actions. The four possible quadrant operations of the BLDC motor can be explained as described in the case of the PMSM electrical machine. In addition, friction and regenerative braking systems are being developed in electric vehicles. Therefore, if the battery is 100%, that is, in its " fullest state", the friction brake can be used to facilitate vehicle stopping. In this case, the regenerative braking is not in effect. However, when the battery is not full, regenerative braking is used. Consequently, the vehicle's kinetic energy is stored as electrical energy and recharges the battery [159].

To obtain the price commutation of the electrical machine and the control, the hall sensors are used to detect the position of the rotor when it is in motion in the sector, which are precisely positioned 120 electrical degrees apart, thus making the controller get the precise stride of the electrical machine. Based on this information, the controller would trigger the stages to follow successive order. In this way, the energized phases produce the required flux, making the rotor rotate. Therefore, the trapezoidal control strategy ensures smooth rotation of the machine based on the control sequence, supplying voltage to its windings.Therefore, the hall sensors for phases A, B, C are represented by H_A, H_B, H_C and the switching sequence for the high and low

Table 3.4: BLDC Machine Forward Switching [158]

H_A	H_B	H_C	C_H	C_L	B_H	B_L	A_H	A_L
1	0	1	0	1	0	0	1	0
1	0	0	1	0	0	0	0	1
1	1	0	1	0	0	1	0	0
0	1	0	0	1	1	0	0	0
0	1	1	0	0	1	0	0	1
0	0	1	0	0	0	1	1	0

sides for phase A are A_H and A_L, and this applies to phases B and C as presented in the switching sequence tables.

Table 3.5: BLDC Machine Reverse Switching [158]

H_A	H_B	H_C	C_H	C_L	B_H	B_L	A_H	A_L
1	0	1	1	0	0	0	0	1
1	0	0	0	1	0	0	1	0
1	1	0	0	1	1	0	0	0
0	1	0	1	0	0	1	0	0
0	1	1	0	0	0	1	1	0
0	0	1	0	0	1	0	0	1

3.3.2 Simplified BLDC Model

The simplified model of the BLDC is similar to that of the PMSM electrical machine. The model is straightforward to apply compared to the complex of the BLDC electrical machine. It contains only the feedback sensor, the PID controller, and the motor itself without taking into account the power electronics. The electrical machine regulated by the PID control is an integral part of the model. The reference speed is sent as an input to the motor, and the actual and reference speeds are compared and sent to the controller. Just like in the case of the PMSM, this model uses a standard configuration. Meanwhile, the inner feedback controls the current, and the outer loop controls the motor's speed. This model is supplied by all the voltage sources

called Vcc. The voltage source is divided into three branches: Vref, Vdir, and Vbrk. The Vref is used to set the speed reference of the motor, while Vdir sets the motor direction, and Vbrk action overrides the voltage from Vref, setting the speed demand to zero and making the motor stop. For the application in this research, the voltage source was modeled using the battery energy storage system.

3.4 e-Crafter Simulation

The development of the VW Crafter hybrid vehicle in this dissertation had taken three stages: The first stage was the development of the pure electric, also called e-Crafter; the second stage was the development of the conventional Crafter; and the third stage was the integration of the two powertrains to form the hybrid version. Electric vehicles have been the compelling solutions to eliminate the GHG emissions and fuel consumption of ICE vehicles, steering industries toward a more sustainable and environmentally conscious trajectory.

Traction electrical machines are an integral part of electric vehicles. Therefore, careful selection must be made to improve the drivability and achieve efficient performance. In this thesis, an e-Crafter has been developed, and its optimal energy consumption has been investigated on the basis of two levels of modeling approaches: simplified and complex, taking into account the level of complexity and technical differences. Despite the disadvantages of pure electric vehicles, as discussed in the literature review section of the dissertation, it is critical to investigate the optimal energy and power consumption of the proposed vehicle and observe the technical impact when transitioning to hybrid. The electrical components of the EV system consist of battery packs, converters, electrical machines, and a control system. The pure e-Crafter uses the Nissan Leaf battery pack as a source of traction energy to drive the vehicle.

Pure electric vehicles have zero emissions and therefore eliminate the overdependency on fuel fuels compared to their counterparts, ICE and hybrid vehicles. Figure 3.4.1 shows the development workflow of the e-Crafter modeling in MATLAB/Simulink/Simscape environment. The conventional VW Crafter was modeled as a pure EV based on the synchronous electrical machines' powertrains (BLDC and PMSM). Therefore, the simplified and complex or extended versions of the energy consumption of the powertrain were studied in this thesis on the basis of qualitative and quantitative findings.

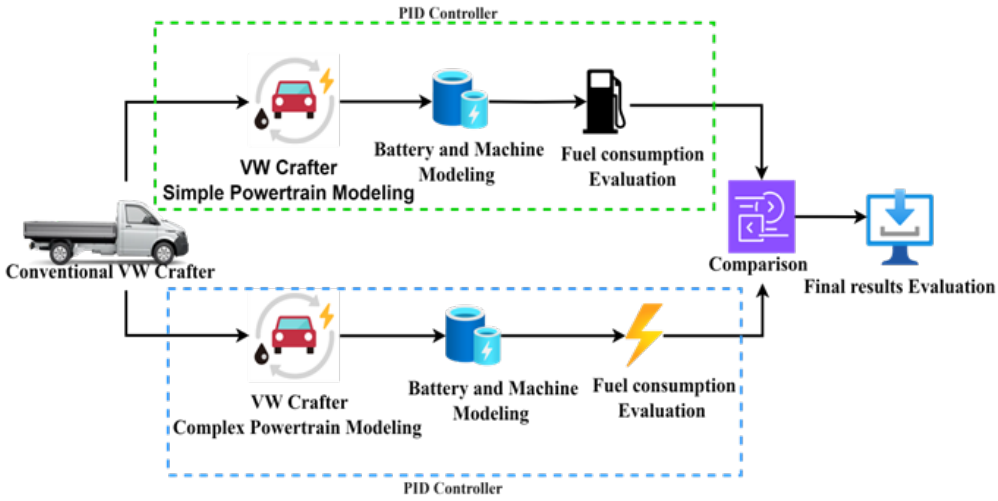

Figure 3.4.1: e-Crafter Development Workflow

Therefore, since the electrical drives based on the proposed electrical machines with the energy source (Nissan Leaf battery) have already been presented, the rest of the components of the electric vehicle are presented in Figure 3.4.1. such as vehicle and tire dynamics are presented in the subsequent sections before the detailed simulation analysis.

3.4.1 Vehicle Dynamics

The study of the behavior of the vehicle in motion is called vehicle dynamics. Vehicle dynamics is studied in longitudinal, lateral, and vertical dynamics. In this research, a longitudinal dynamic of the vehicle is modeled in a MATLAB/SIMSCAPE/Simulink environment. In practical terms, a vehicle not only travels on a level road but also rises and falls on a road slope and around corners [80]. Therefore, Figure 3.4.2 shows the detailed free-body diagram of the vehicle considering all forces and factors, including its suspension systems. The vehicle dynamics described in Chapter Two takes into account the forces and factors acting on the proposed vehicle in order to analyze only the required tractive energy to propel the vehicle. In this chapter, detailed modeling is adopted, taking into consideration a detailed model of the vehicle dynamics. Therefore, the physical modeling approach was adopted to formulate the model of the vehicle dynamics of the VW Crafter on the basis of a half-car model based on the three degrees of

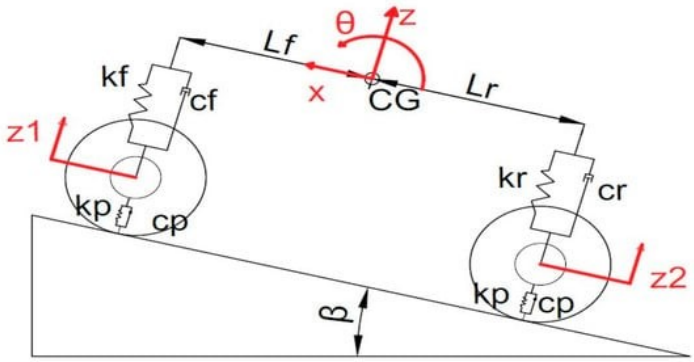

Figure 3.4.2: Vehicle Dynamics [167]

freedom (DOF), such as pitching, bouncing, and advancement. Two degrees of freedom are added, giving stiffness and tire damping as described in [167].

Therefore, the mathematical description of the free body diagram of Figure 3.4.2 based on the Newton's law of motion is described as in [80] is as follows:

$$\begin{cases} m \cdot \ddot{x} = F_x - F_{dx} - F_{gx} \\ m \cdot \ddot{z} = F_{dz} + F_{szF} + F_{szR} - F_{gz} \\ I_{yy} \cdot \ddot{\theta} = -L_f \cdot F_{szF} + L_r \cdot F_{szR} + h \cdot F_x - M_{dy} \\ m_w \cdot \ddot{z_1} = -F_{szF} + F_{s_1} \\ m_w \cdot \ddot{z_2} = -F_{szR} + F_{s_2} \end{cases} \tag{3.4.1}$$

Where F_x is the wheel axis longitudinal force, Fdx is the vertical drag force, F_{gx} is the gravity force component, F_{dz} is the longitudinal drag force, F_{szF} is the elastic force and damping force of the front wheel, F_{szR} is the elastic and damping force of the rear wheel, F_{gz} is the gravity force component, M_{dy} is the drag moment, L_f is the longitudinal distance from the front axle, L_r is the longitudinal distance from the rear axle and h is the C.G height [80]. However, the frictional force is related by the squared difference between vehicles and wind speeds as described in [80]:

$$\begin{cases} F_{dx} = \frac{1}{2} \cdot C_d \cdot \rho \cdot A \cdot (\dot{x} - w)^2 \\ F_{dz} = \frac{1}{2} \cdot C_1 \cdot \rho \cdot A \cdot (\dot{x} - w)^2 \end{cases} \tag{3.4.2}$$

The same condition applied if we consider the drag moment.

$$M_{dy} = \frac{1}{2} \cdot C_{pm} \cdot \rho \cdot A \cdot (\dot{x} - w)^2 (L_r + L_f) \tag{3.4.3}$$

Furthermore, the suspension system and tire damping and elastic force for both front and rear axles are also expressed mathematically as described in [167] as follows:

$$\begin{cases} F_{szF} = -2k_f \cdot (z - z_1 - L_f\vartheta) - 2C_F \cdot (\dot{z} - \dot{z_1} - L_f\dot{\vartheta}) \\ F_{szR} = -2k_r \cdot (z - z_1 - L_r\vartheta) - 2C_r \cdot (\dot{z} - \dot{z_1} + L_r\dot{\vartheta}) \\ F_{s_1} = -k_p x_1 - c_p \dot{x_1} \\ F_{s_2} = -k_p x_2 - c_p \dot{x_2} \end{cases} \tag{3.4.4}$$

Therefore, the parameters used for the vehicle dynamics simulation are presented in Table 3.6.

Table 3.6: The VW Crafter Specific Technical Parameters [34]

Parameters	**Values**	**Symbols [Unit]**
Length	5.986 - 7.319	l [m]
Width	2.040	w [m]
Height	2.355 - 2.798	h [m]
Curb Weight	2159 - 2196	W_c [kg]
Gross Weight	3500	W_g [kg]
Front Axle	1	T_F [m]
Rear Axle	1.346 - 1.901	T_R [m]
Tire Radius	0.357	r_t [m]
Centre of Gravity	0.785	CG [m]
Frontal Area	4.05	A_F [m^2]
Rolling Resistance	0.013	C_{rr} [-]
Drag Coefficient	0.3	C_d [-]
Air Density	1.225	ρ [kg/m^3]
Acceleration due to Gravity	9.81	g [m/s^2]

3.4.2 Tire Dynamics

A tire block from the Simulink/Simscape based on the Pacejika Magic formula obtained through experimental tests was used to model the vehicle dynamics

system. The tire model is formulated using the longitudinal dynamics behavior on the basis of four coefficients such as B, C, D, and E. The tire model is formulated considering that it is a rigid set with the wheel, which is in variable and constant conditions of the road, evaluating its rolling resistance, slip and inertia [167]. The formula and the slip, which is the ratio between the speed of the slip and the speed of the progress in a situation where there is no slip are expressed as in [167] as follows:

$$\begin{cases} F_x = F_z \cdot D \sin(C \cdot \arctan\{B \cdot k - E[Bk - \arctan(\mathrm{Bk})]\}) \\ k = \frac{V_{sx}}{\lvert V_x \rvert} = \frac{r_w \cdot \Omega - V_x}{\lvert r_w \cdot \Omega \rvert} \\ k = \frac{2V_{sx}}{V_{th} + \frac{V_x^2}{V_{th}}} \end{cases} \tag{3.4.5}$$

The third equation within equation (3.4.5) is used or valid at low speeds. Table 3.7 presents the specifications of the tire used for the simulation.

Table 3.7: Tire Specifications [80]

Conditions of Road Surface	**B**	**C**	**D**	**E**
Ice	4	2	0.1	1
Snow	5	2	0.3	1
Wet Tarmac	12	2.3	0.82	1
Dry Tarmac	10	1.9	1	0.97

3.4.3 Simplified Powertrain Development, Optimization, and MATLAB Model

The simplified VW powertrain consists of the Nissan Leaf battery, which provides energy to the system, the PMSM electrical machine, the transmission system, the vehicle dynamics, the sensor, and the controller. The simplified model does not take into account the power electronics components as in the case of the detailed or full-scale model we refer to as a complex model in the context of this dissertation. A closed control loop model was developed on the basis of the GA-PID control strategy to optimize vehicle performance. An energy equivalent model of the electrical machine works based on the electrical losses of the detailed three-phase PMSM drive. Therefore, in this

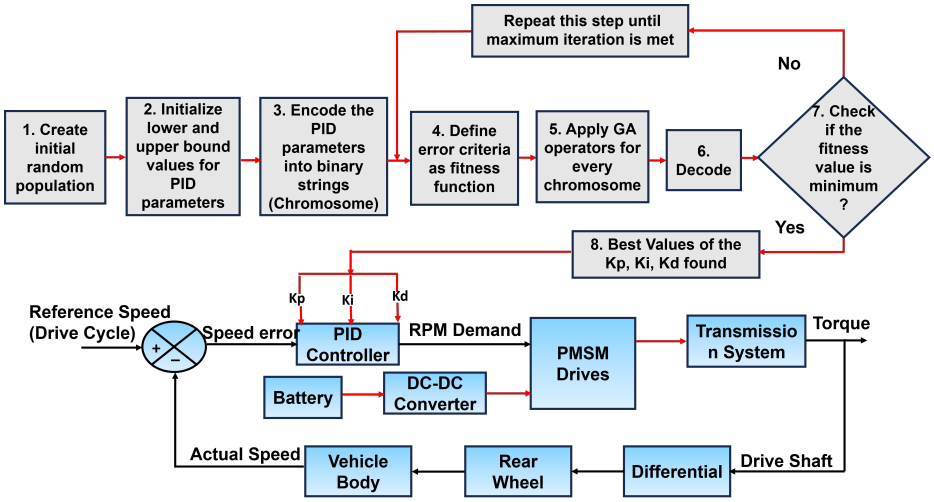

Figure 3.4.3: Simplified e-Crafter based PMSM Control Design

study, we leverage detailed losses to model the simplified model. The detailed model is slower in real-time, and its implementation is quite challenging due to simulation time and the cost of real life. Therefore, to simplify this effect, we model the simplified vehicle model at an abstraction level to predict vehicle behavior in real-world applications. Therefore, in this research, we developed the GA-PID control algorithm to provide optimal torque and speed for optimal energy consumption. PID controllers have been popular for many industrial processes because of their robustness and simple structure. Figures 3.4.3 and 3.4.4 show the general control loop of the pure electric powertrain of the VW Crafter based on the GA-PID controller. The GA procedure described in Figures 3.4.3 and 3.4.4 was adopted from [168].The drive cycle, which is the setpoint (reference), is the crafter's desired speed. Moreover, the error is the input minus the output or the difference between the input and output. Therefore, the optimized gains of the controller were used to provide torque demand to the electrical machine to optimize vehicle consumption. The GA optimization technique inspired by natural selection has been adopted for several optimization problems owing to its ability to handle multi-objective optimization, which is simple and faster in terms of convergence. However, the GA optimizer was implemented based on the eight steps described in Figure 3.4.3 for the powertrain based on the PMSM propulsion or Figure 3.4.4 based on the BLDC propulsion system.

Therefore, the PID controller can be mathematically represented in time-

domain as expressed in [145] as:

$$u(t) = K_p e(t) + K_i \int e(t)dt + K_d \frac{d}{dt} e(t) \tag{3.4.6}$$

Where K_p, K_i, and K_d are the PID gains. Usually, two methods are used to determine these gains: Manual and automatic (using an optimization approach). In this work, these methods have been adopted to tune the PID parameters to optimize them to optimize the performance of the vehicle in terms of fuel consumption and emissions—the meta-heuristic technique, such as the GA, was applied. Although a simple model was developed compared to the full-scaled model, it is pretty nonlinear, and its level of complexity makes it quite challenging to employ the optimizer easily. Therefore, the entire model was estimated, though not precise, using the model linearizer in MATLAB (R2024a), identified as:

$$G(s) = \frac{1}{s^3 + 225.7s^2 + 1.257 \times 10^4 s} \tag{3.4.7}$$

However, the transfer function in equation (3.4.7) is the most simplified model in the frequency domain in the 3×3 matrix, which was simplified and normalized from the complex transfer function model, taking into account the system's dynamics and relative gain. In this case, the precise model is unnecessary since the optimal gains are utilized in the physical model for the optimal fuel consumption. The model with the same dynamics was also identified in the case of the BLDC drive powertrain. This is true because the two physical models have similar configurations at the system level but differ in terms of simulation speed and efficiency. In practice, these electrical machines exhibit identical features with only differences in the shape of their back EMF. Therefore, to implement the GA for the PID controller for the e-Crafter for optimal energy consumption, the steps followed are described in Figures 3.4.3 and 3.4.4 respectively. Moreover, to solve the optimization, an integral time absolute error (ITAE) was used as the objective function to tune the PID gains so that it regulates the vehicle speed to follow the reference trajectory (drive cycle) successfully and, at the same time, provides optimal torque and speed to the electrical machine, and thus minimize the energy consumption. The objective function (ITAE) is expressed mathematically along with other integral errors such as integral absolute error (IAE), integral square error (ISE), and integral time square error (ITSE) as in [145, 151] as follows:

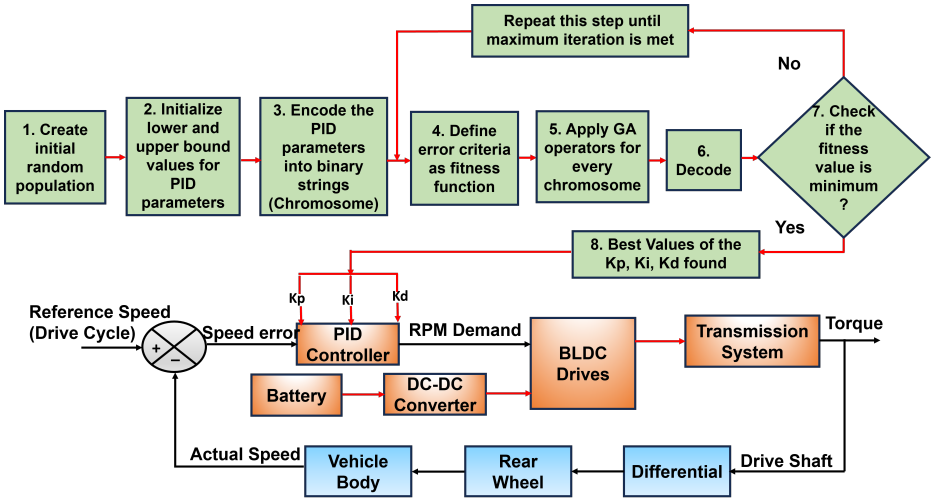

Figure 3.4.4: Simplified e-Crafter based BLDC Drive Control Design

$$\begin{cases} IAE = \int_0^\infty |e(t)|dt \\ ISE = \int_0^\infty |e(t)|^2 dt \\ ITAE = \int_0^\infty t|e(t)|dt \\ ITSE = \int_0^\infty t|e(t)|^2 dt \end{cases} \tag{3.4.8}$$

In this thesis, the optimization problem aims to compute the minimum values of the fitness value (objective function) to find the optimal gains of the PID controller on the basis of GA operators until maximum iterations were met. In other words, the components of the electric vehicle (e-Crafter) were interconnected with the optimization framework of the genetic algorithm to optimize energy consumption. Table 3.8 presents the parameters used for the GA optimization of the two powertrains. Figures 3.4.5 and 3.4.6 show the MATLAB/Simulink/Simscape model of the e-Crafter electric vehicle based on synchronous electrical machines (PMSM and BLDC) propulsion.

3.4.4 Development of Extended Powertrain and MATLAB Model

The difference between the simplified and extended modeling approaches adopted in this thesis is the level of complexity in terms of methodological constraints and technical differences. The complex model takes into account

Table 3.8: GA Parameters for e-Crafter [34]

GA Parameters	Values
Selection Strategy	Random
Fitness Performance	Proportional
Generations	40
Population Size	100
Number of Variables	3
Lower Bound (LB)	[0 0 0]
Upper Bound (UB)	[2000 2000 2000]

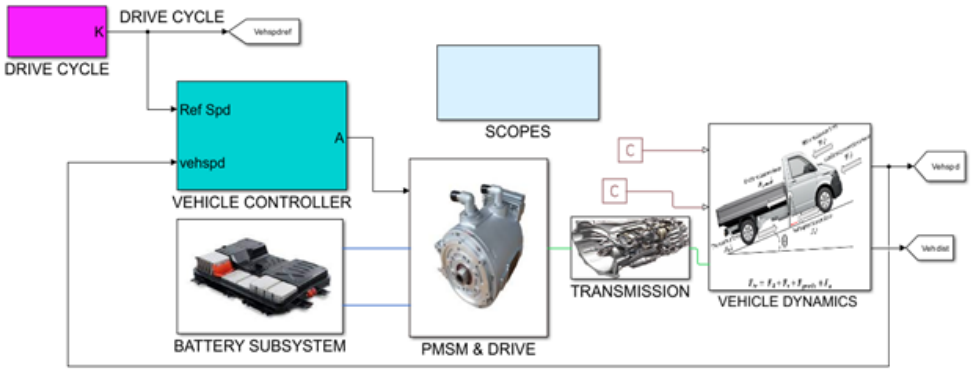

Figure 3.4.5: Simplified e-Crafter based PMSM MATLAB Model

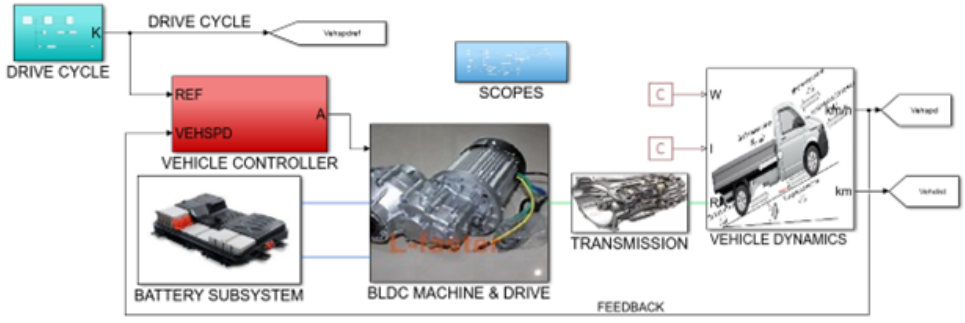

Figure 3.4.6: Simplified e-Crafter based BLDC MATLAB Model

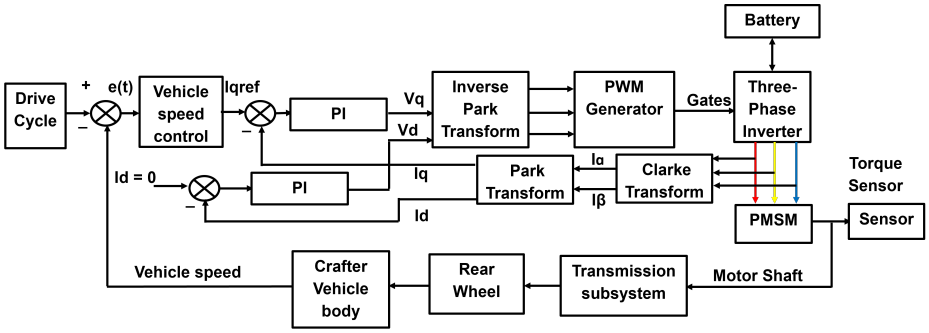

Figure 3.4.7: Extended e-Crafter based PMSM Drive

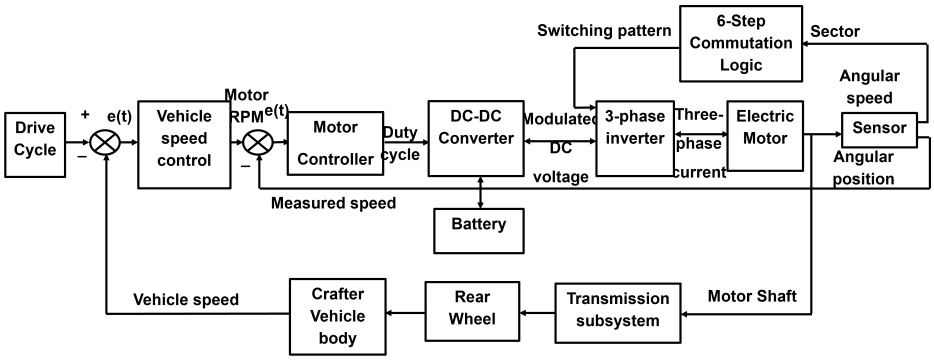

Figure 3.4.8: Extended e-Crafter based BLDC Drive [159]

the battery storage system, the power electronics, the electrical machine, control, transmission, and vehicle dynamics. Just like in the case of the simplified approach, the PMSM and BLDC electrical drives were extended into the full-scaled model to power the vehicle. Therefore, the VW Crafter was developed based on the full-scaled model propelled by the three-phase PMSM electrical machine with an FOC control strategy, as described in this thesis and compared with the same model propelled by the three-phase BLDC electrical drive whose speed optimal path was search PID control algorithm.

Figure 3.4.7 shows the block diagram model of the extended VW Crafter based on the detailed three-phase PMSM electrical drive. On the other hand, Figure 3.4.8 shows the extended model of the vehicle based on the three-phase BLDC electrical drive. In PMSM drive, The electrical machine based on the FOC strategy was used to power the electric vehicle. The drive cycle provides the reference speed. The reference and actual speeds are compared and sent to the vehicle speed controller, which provides I_q demand

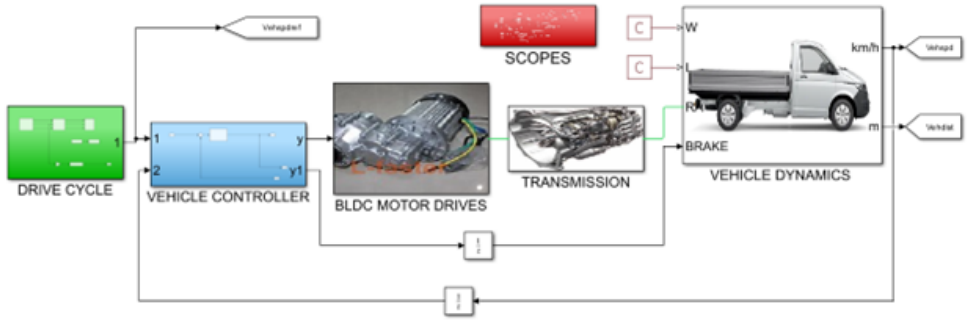

Figure 3.4.9: Extended e-Crafter based BLDC Drive MATLAB Model

to one of the inner loops PI, which provides V_q, together with V_d from the other PI to the inverse park transform block to provide the three-phase voltages to the PWM, producing the pulses to the three-phase inverter for energizing the motor phases. Therefore, the torque from the motor passes through the transmission, which is translated into the vehicle's movement. In BLDC drive, the three-phase BLDC machine was used to power the vehicle. The only difference here is that the pulses required to energize the motor phases are provided by the complex control algorithm known as trapezoidal or commutation control, which is based on switching sequences, as described in the previous section. In this model, the vehicle and motor controllers are replaced by a single controller that receives the difference between the reference and actual speed and provides the motor speed demand. The torque is measured from the sensor to pass to the transmission and then translated into the vehicle's movement. Figures 3.4.9 and 3.4.10 show the MATLAB models of the e-Crafter based on the detailed model of the synchronous electrical machines drives.

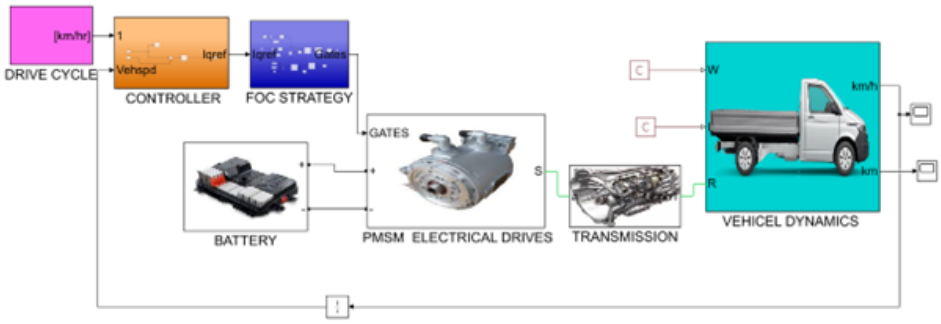

Figure 3.4.10: Extended e-Crafter based PMSM Drive MATLAB Model

3.5 Results and Analysis

The VW Crafter simulated in MATLAB environment based on the two levels of modeling approach demonstrated excellent performance, especially in the case of simplified modeling approaches due to its simplicity, reduced cost, and faster simulation. The adopted reference vehicle of the faculty of engineering is a hybrid powered by diesel and PMSM electrical machines. The main aim of this research is to develop a hybrid vehicle of the faculty of engineering. The simulated and experimental results were compared and analyzed which is given in details in Chapter Five. However, a maximum of 20 km/h is allowed for the vehicle. However, the vehicle was tested under different driving conditions, as the engine was originally capable of high speed, as discussed in the literature (the recent version is up to 90 km/h). Therefore, since this chapter considers the analysis of the vehicle at the simulation level, the NEDC was adopted to investigate its optimal energy consumption. Similar results of this study were published in relevant publications related to this dissertation. Figure 3.5.1 shows the vehicle speed based on the simplified PMSM model using the NEDC drive cycle as a reference input (at 50 km/h) while Table 3.9 presents the optimized PID parameters. The GA-PID has successfully tracked vehicle speed. Figure 3.5.2 shows the battery and electrical machine energy consumption of 0.2053 kWh/1 km and 0.1618 kWh/1 km, respectively, at 200 seconds at the gains of the GA-PID controller [1999.8, 38.6, 41.2], as presented in Table 3.9. This is translated into 20.53 kWh/100 km and 16.18 kWh/100 km for the battery and electrical machine. The values of the cost functions, such as the ISE, ITSE, IAE, and ITAE, were 3.587, 13.92, 6.371, and 49.59, respectively. Since the dynamics of the powertrain are identical

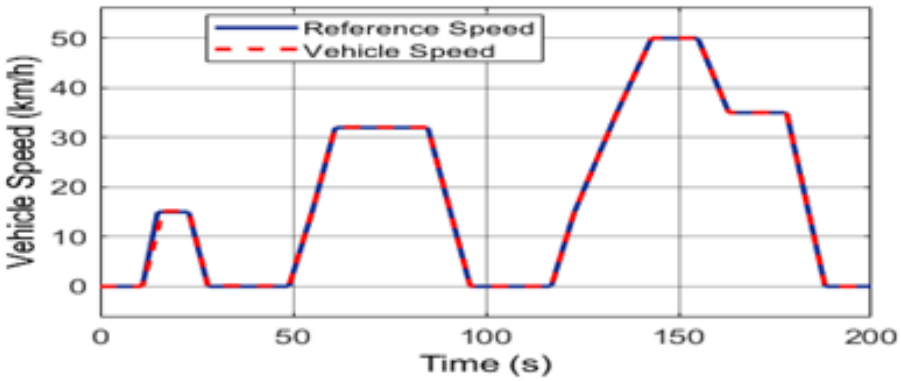

Figure 3.5.1: Simplified Powertrain Speed based PMSM

for both the PMSM and BLDC drives, the same GA parameters were used for the two physical models of the powertrain.

Table 3.9: Optimized PID Parameters

GA-PID Parameters	**Values**
K_p	1999.8
K_i	38.6
K_d	41.2

In addition, Figure 3.5.3 shows the motor torque of 173 Nm, which was the same for both electrical machines. Figure 3.5.4 shows the motor speed. Figure 3.5.5 shows the battery and electrical and motor mechanical power consumed for the PMSM propulsion powertrain. The electrical power consumed was 26.93 kW, and the mechanical power consumed was 24.80 kW, respectively. However, the current of the Nissan battery and the SOC of the PMSM powertrain were 74.5 A and 99.26%, respectively. To calculate the power or energy efficiency of the electrical machine:

$$\begin{cases} \eta_p = \frac{P_m}{P_e} \cdot 100 \\ \eta_e = \frac{E_m}{E_e} \cdot 100 \end{cases} \tag{3.5.1}$$

Where η_p, η_e, P_e, P_m, E_e, and E_m are power efficiency, energy efficiency, electrical power consumed or input power, mechanical power consumed or output power, electrical energy consumed or input energy and mechanical

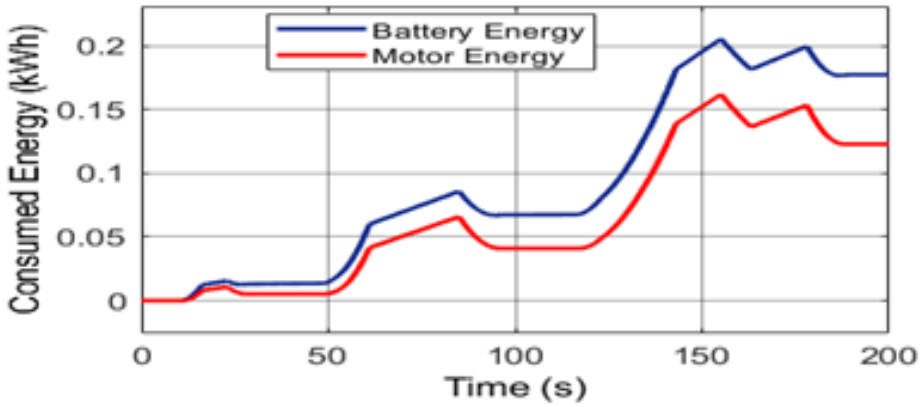

Figure 3.5.2: Simplified Powertrain Energy based PMSM

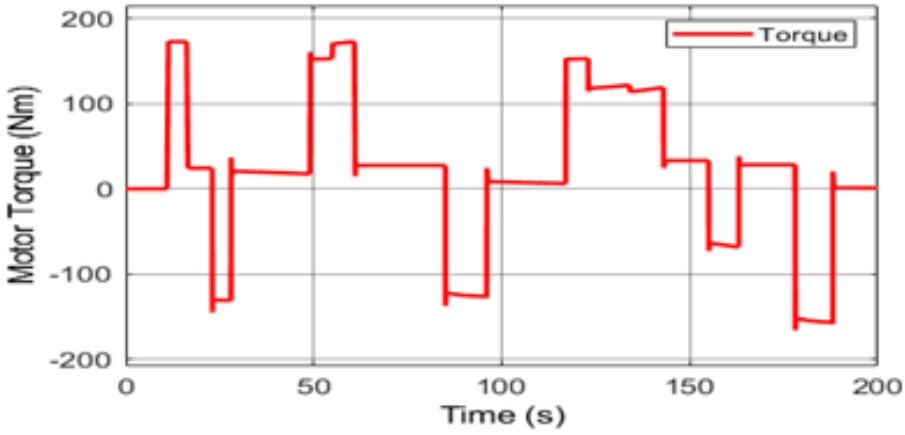

Figure 3.5.3: Simplified Powertrain Torque based PMSM

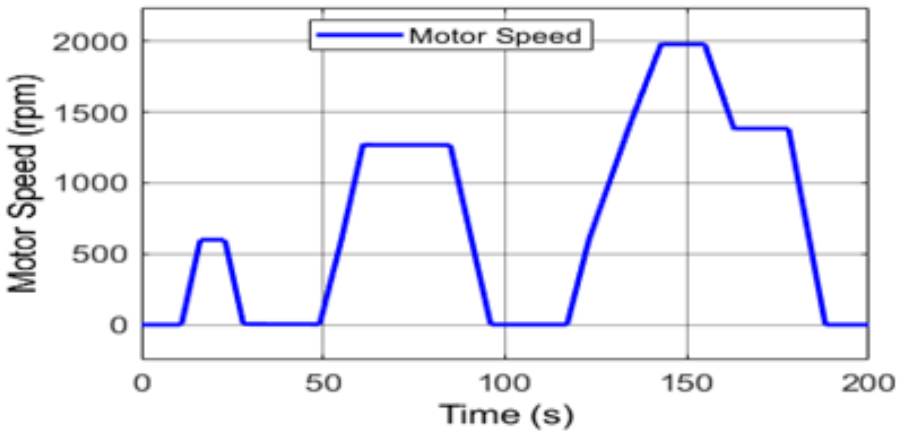

Figure 3.5.4: Simplified Powertrain Speed

energy consumed or output energy, respectively. Therefore, based on equation (3.5.1), the energy efficiency for the simplified powertrain was 78.81% and power efficiency was 92%, respectively. However, Figure 3.5.6 shows the contour plot of the PMSM electrical machine for the simple powertrain. The contour plot or the efficiency map was measured at the maximum torque of the electrical machine and 2000 rpm. It can be seen that this electrical machine was designed to achieve the power efficiency of 96%. The blue area is the area with the lowest efficiency, and the yellow area is the area with the highest efficiency. Therefore, the operating region of the PMSM electrical machine in the simplified powertrain case was up to 92%.

Similarly, in the case of the BLDC, Figure 3.5.7 shows the vehicle speed successfully tracked the reference based on the NEDC drive cycle. We selected the essential results for the BLDC drive since they are similar to the PMSM, and we just mentioned the difference in terms of the performance. The same applies to the extended model of the vehicle. Figures 3.5.8 and 3.5.9 show the energy and power consumption for e-Crafter based on the BLDC drive. At the same controller gains [1999.8, 38.6, 41.2], the electrical energy consumed, or battery energy consumed, was found to be 0.1975 kWh/1 km and mechanical energy consumed or motor energy consumed was found to be 0.1623 kWh/1 km, respectively. This is translated into electrical and mechanical energy consumed to be 19.75 kWh/ 100 km and 16.23 kWh/100 km, respectively. The electrical power consumed was 26.43 kW, and the mechanical power consumed was 24.80 kW. Therefore, the energy and power efficiencies in the case of the BLDC drive were 82.17% and 93.83%. Table

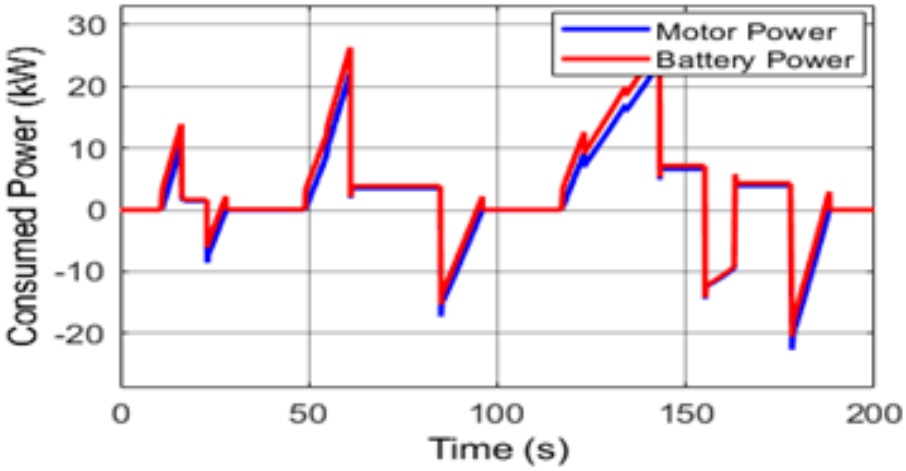

Figure 3.5.5: Simplified Powertrain Power-based PMSM Drive

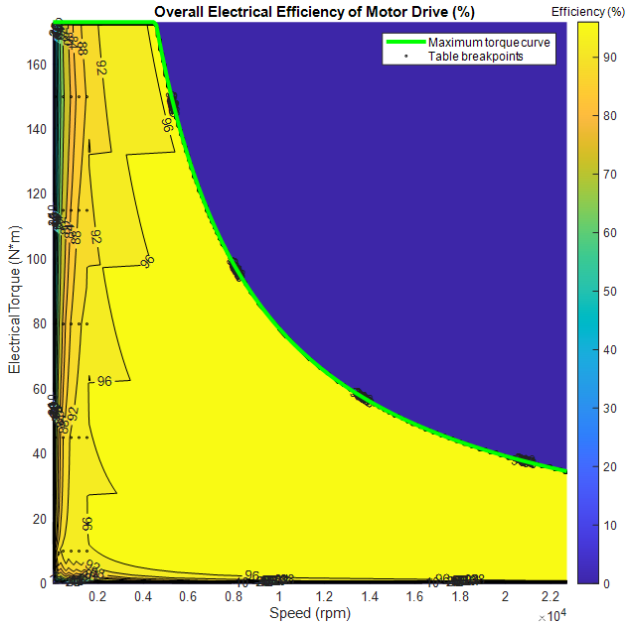

Figure 3.5.6: PMSM Eff. Map based Torque-Speed Characteristics

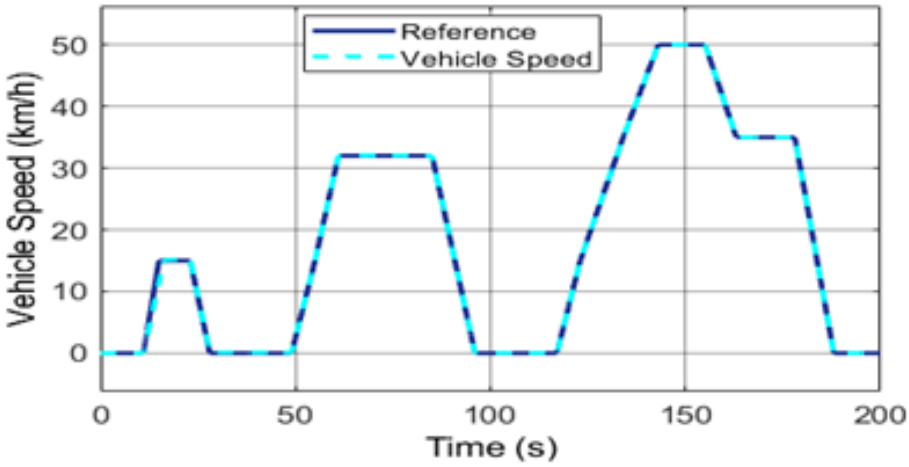

Figure 3.5.7: Vehicle Speed based BLDC Drive

3.10 presents the PID gains for the e-Crafter based on the extended electrical machines model.

Table 3.10: PID Parameters for Exnteded Powertrain

PMSM Drive	**Values**	**BLDC Drive**	**Values**
K_p	200	K_p	40
K_i	60	K_i	10
K_d	5	K_d	0

Figure 3.5.10 shows the efficiency map of the BLDC electrical machine based on the torque-speed characteristics curve. The plot is based on the maximum torque of the electrical machine, just like the case of the PMSM electrical machine. Both plots are identical, with only differences in the operating efficiency of the two electrical machines (92% for the PMSM and approx. 94% for the BLDC). The battery charge for the simple BLDC drive was 65.738 Ah (discharging from 66.2 Ah maximum capacity), the SOC was 99.3% and the current was 73.13 A. However, the motor current was found to be 55.51 A, respectively. However, for the e-Crafter based on the extended electrical machines, the simulation results are shown in Figures 3.5.11–3.5.14. Although the detailed models did not perform satisfactory because of the model complexity, due to high current flow and voltage in both two models,

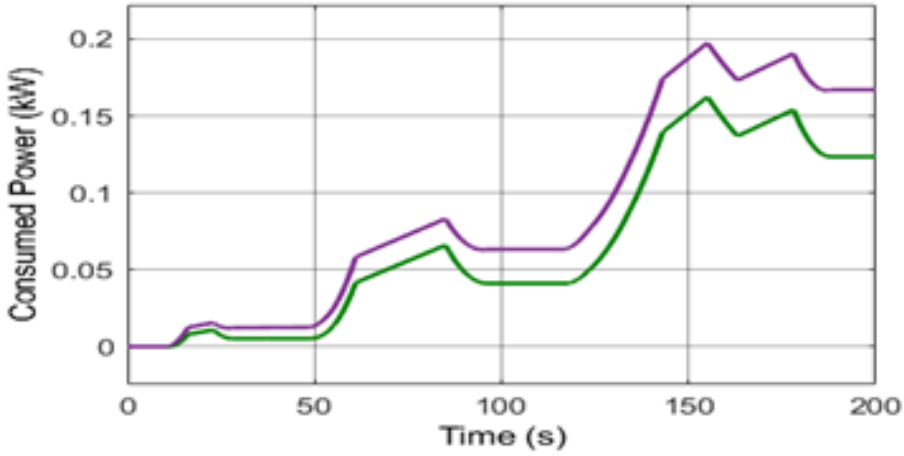

Figure 3.5.8: Energy Consumed based BLDC Drive

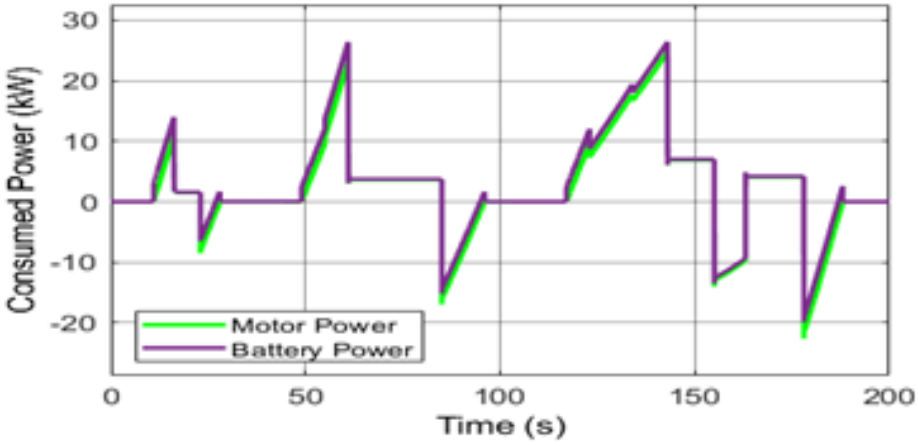

Figure 3.5.9: Power Consumed based BLDC Drive

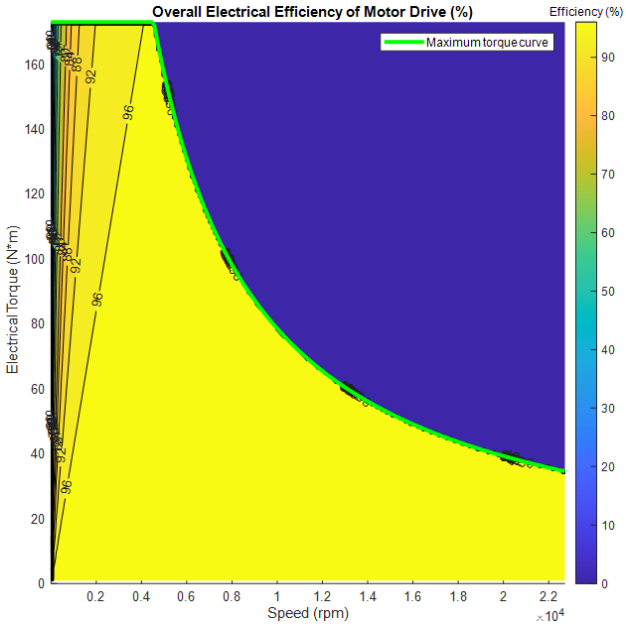

Figure 3.5.10: BLDC Eff. Map based Torque-Speed Characteristics

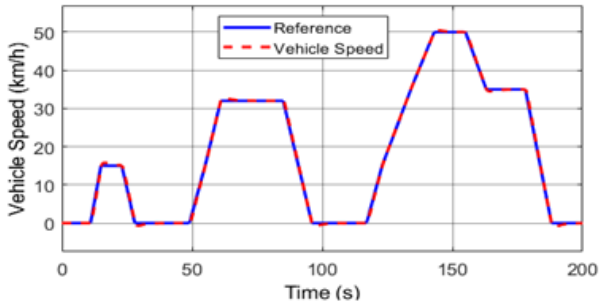

Figure 3.5.11: Vehicle Speed based Detailed PMSM Drive

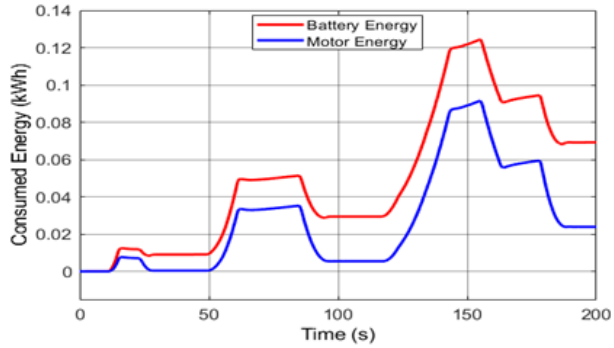

Figure 3.5.12: Energy Consumed based Detailed PMSM Drive

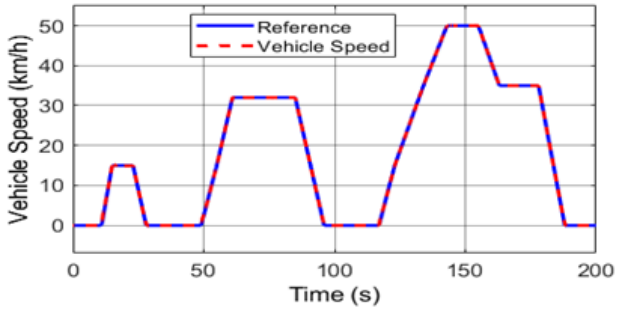

Figure 3.5.13: Vehicle Speed based Detailed BLDC Drive

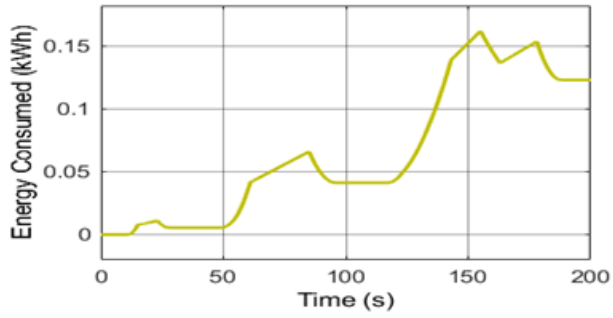

Figure 3.5.14: Energy Consumed based Detailed BLDC Drive

and high recovery energy in the case of BLDC drive. Therefore, we selected these to compare the controller's speed-tracking performance and energy consumption. Figure 3.5.12 shows the extended powertrain's electrical and mechanical energy consumed based on the PMSM drive. The electrical energy consumed was found to be 0.1245 kWh/1 km, and the mechanical energy consumed was 0.09162 kWh/1 km. This is translated to be 12.45 kWh/100 km and 9.162 kWh/100 km, respectively. Therefore, the energy efficiency was calculated to be 73.59%. However, the power efficiency was very low due to the high power of the electrical part. Figure 3.5.13 shows the vehicle speed due to the detailed BLCD drive model. In addition, in the case of this powertrain, the vehicle speed had successfully tracked the drive cycle.

3.5.1 Heat Dissipation in Electrical Machines and Battery

For the complete energy profile, we incorporated the thermal model for both electrical machines and the battery. Therefore, based on this requirement, the following tasks were accomplished to account for the thermal effect

- The battery model in MATLAB was extended to include the heat effect, represented by the thermal mass, which is related to the heat flow, specific heat of the material, mass, temperature, and time. The battery was subjected to an ambient temperature of 25 °C.
- The electrical machine models were extended to include a thermal model with liquid cooling, accounting for heat dissipation within the system.
- For the simplified model, the thermal model is based on the thermal mass. The liquid cooling system was integrated, comprising a pipe, expansion tank, hose inlet and outlet, thermal liquid settings, pump, and radiator. The motor was subjected to an ambient temperature of 25 °C. Figures 3.5.15 and 3.5.16 show the simulation results.
- In the case of the simplified model, a single efficiency setting was chosen instead of tabulating electrical losses to eliminate model error due to the size of the corresponding losses, such as the length of the vector of torques and that of speeds. The solver setting was also changed from the fixed step to variable.

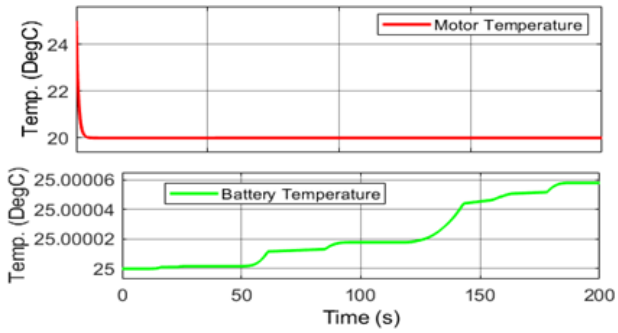

Figure 3.5.15: Simplified Model Temperature

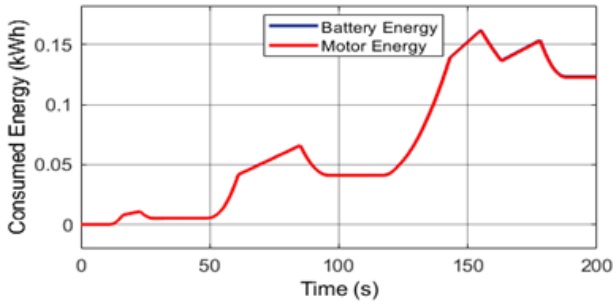

Figure 3.5.16: Energy Consumption due to Temperature effect

- For the complex model, the thermal model was integrated into the three-phase machine windings, including the rotor. The same liquid cooling was applied to the electrical machine and battery to facilitate lowering the temperature beyond the limit that could cause potential damage to the machine windings and battery degradation, thereby affecting the overall energy consumption profile.

The temperature of the electrical machine was reduced to 20 °C due to cooling, as shown in Figure 3.5.15, while the temperature of the battery increased to 25.00006 °C, approximately 25 °C. This means that the battery was operating at approximately ambient temperature. Therefore, the new battery energy consumption was 16.23 kWh / 100 km, while the motor energy was 16.18 kWh/100 km, as shown in Figure 3.5.16. The battery power consumed was 24.90 kW and the power consumed by the electrical machine was 24.80 kW. Moreover, Figure 3.5.17 shows the temperature of the extended or complex model. Despite the cooling method, the temperature rise did not fall below the ambient temperature. Therefore, the temperature

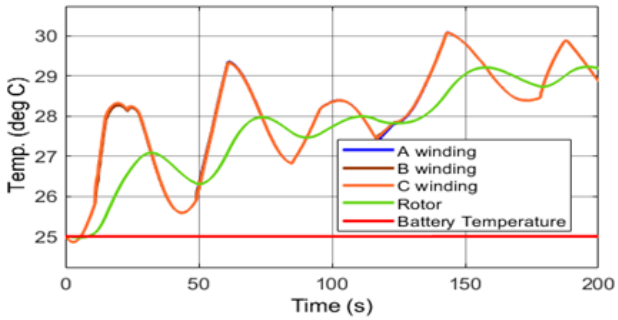

Figure 3.5.17: Complex Model Temperature

for the machine winding was found to be 30.08 °C, each for A, B, and C windings. At the same time, the rotor and the battery were found to be 29.22 °C and 20.002 °C, respectively.

3.6 Discussion

The PMSM and BLDC propulsion based on e-Crafter with rated power of 53.5 kW and peak power of 82.5 kW at different levels of complexity was simulated using MATLAB/Simulink/Simscape environment. The 2011 Nissan Leaf battery of 24 kWh, 360 V rating with over 90 kW output power cooperated with the synchronous electrical machine to provide the traction energy needed to propel the vehicle. After the powertrain, the transmission system consists of a gearbox to distribute the power to the vehicle wheel, facilitating its movement. For the vehicle to move, it must overcome the resistance forces as described in the previous thesis. Therefore, the analysis ensured that the tractive force required to propel the vehicle under a flat surface and inclined was calculated to be within the limit of the rated values of the proposed Parker synchronous electrical machine and the Nissan Leaf battery pack. This research focuses on the transformation of the VW Crafter into an electric vehicle to reduce toxic gas emissions and fuel consumption in the context of current global trends in gas powered vehicles. The first step is to develop electric and conventional powertrains and integrate them to form a hybrid. This chapter considers the development of the pure electric version of the proposed vehicle and studies its energy consumption in standard driving scenarios.

Figures 3.5.1–3.5.6 show some of the simulation results of the VW Crafter based on the PMSM simplified electrified powertrain. Therefore, the success-

ful tracking of the vehicle reference trajectory in Figure 3.5.1 demonstrates the robustness of the proposed GA-PID control strategy carried out in several iterations until minimum errors or maximum iterations were achieved. The vehicle could reach a top speed of 50 km/h according to the reference set-point in 200 seconds. However, the optimal vehicle speed tracking by the controller while allocating optimal torque and speed to the electrical machine impacted the energy consumption, necessitating the need to adjust the controller from the reference speed to steady-state conditions with minimum oscillations. Therefore, we computed and evaluated the energy consumption based on the distance traveled by the vehicle every 1 km and up to 100 km to compare with the real measurement, taking the real measurement as a benchmark to feel the real-world impact of our findings. Figure 3.5.2 shows the battery and electrical machine energy consumption of 0.2053 kWh/1 km and 0.1618 kWh/1 km, at the optimal controller gains of [1999.8, 38.6, 41.2], as presented in Table 3.9. This was the measurement based on the 1 km distance, equivalent to 20.53 kWh/100 km and 16.18 kWh/100 km energy consumption of the vehicle in terms of the battery and electrical machine. The values of the cost functions, such as the ISE, ITSE, IAE, and ITAE, were 3.587, 13.92, 6.371, and 49.59, respectively. In addition, Figure 3.5.5 shows the battery and electrical and motor mechanical power consumed for the simplified PMSM drive. The electrical power consumed was 26.93 kW and the mechanical power consumed was 24.80 kW, respectively. Therefore, the energy efficiency for the simplified powertrain was 78.81% and power efficiency was 92%, respectively.

However, the controller tuning method and test procedure had significantly impacted the performance of the vehicle. Our study in [80] proposed a WLTP drive cycle based on integral cost functions to test this vehicle. A manual tuning technique was applied to stabilize the vehicle system for optimal fuel efficiency. Table 3.11 presents the optimal energy consumed based on enhanced PI control algorithm using the WLTP test procedure. It was observed that the manual tuning technique resulted in fewer errors but had higher consumption despite different test procedures. The electrical and mechanical power consumed was 52 kW and 47.4 kW; therefore, the power efficiency was 91.15%. It can be seen that the vehicle's performance was pretty excellent in terms of power efficiency, which our previous study focused on, making sure that the vehicle operated within the battery-rated capacity limit. However, the energy consumption for the battery decreased as the vehicle was transformed into a hybrid. This is considered in details in the next chapter. Considering the energy consumption of 22.73 kWh/100

km achieved with a conventional manual tuning method fuels the need for the optimizer for the vehicle control system. The conventional technique might not yield optimal performance due to human intuition during manual tuning could constrain the control algorithm to force the dynamics of the vehicle system to deviate from normal or healthy operating conditions. With manual technique, there was less energy efficiency compared to the proposed GA-PID proposed approach (with GA-PID 19.75 kWh/100 km or 20.53 kWh/100 km). Nevertheless, with the manual tuning technique the system was stable despite the higher consumption due to the fewer errors achieved. Therefore, the system was less efficient, especially in the case of the HEV, which aims to reduce CO_2 emissions and fuel consumption. In contrast, the automated tuning technique could effectively find a balance between the objective function and the overall efficiency of the EV and HEV dynamics.

Table 3.11: e-Crafter Energy Consumption [80]

K_p	K_i	**IAE**	**ISE**	**ITAE**	**ITSE**	**[kWh/100 km]**
700	800	0.3753	0.0071	3.6593	0.0670	22.75
700	600	0.4243	0.0090	4.1354	0.0856	22.76
600	500	0.4907	0.0121	4.7829	0.1145	22.77
1000	800	0.3106	0.0048	3.0381	0.0462	22.74
2000	1000	0.1387	0.00096	1.3739	0.0094	22.73

Furthermore, Figure 3.5.3 shows the motor torque due to the interaction of the stator and rotor fields of the electrical machine. The positive and negative torques mean the motoring and generating actions of the electrical machine. When the motor's operation is in the first quadrant; the vehicle accelerates, and the torque and speed are positive. In this way, the machine converts the electrical energy to mechanical energy required to propel the vehicle. However, when the vehicle decelerates, the electrical machine acts as a generator, converting the energy to mechanical again and opposing the vehicle's movement. Then, the nature of the static torque-speed characteristics demonstrated excellent performance in Figure 3.6.1. For this efficiency map, we took 3984.347 rpm and an equivalent torque of 94.56932 Nm, achieving an efficiency of 94.2604%, although MATLAB automatically normalized the scale of its axis to 120 while the useful power was 50 kW and determined the operating point where the electrical machine was performing from its lowest to the highest efficiency. In addition, the contour plot in Figure 3.5.6 based

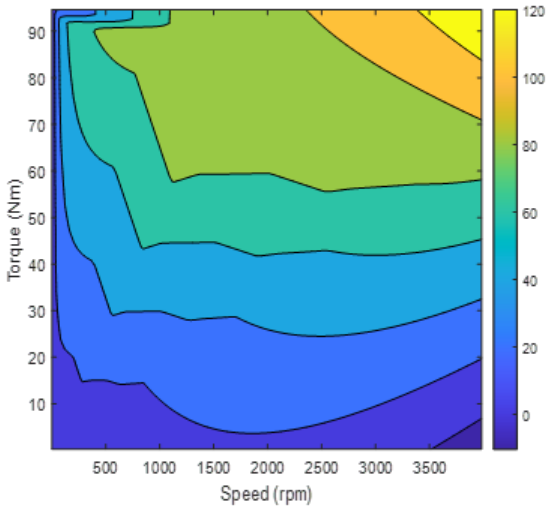

Figure 3.6.1: PMSM Contour Plot at different RPM and Torque [80]

on the electrical torque indicates that the electrical machine performed well in terms of power efficiency.

Furthermore, the electric powertrain-based BLDC drive also demonstrates efficient performance. Just like in the case of the PMSM drive, Figure 3.5.7 indicates the robustness of the proposed GA-PID control strategy due to the successful speed tracking achieved under several iterations until minimum errors or maximum iterations were met despite the nonlinearities of the electric vehicle dynamics. The vehicle could reach a top speed of 50 km/h based on the reference in 200 seconds. Figures 3.5.8 and 3.5.9 show the energy and power consumption for the e-Crafter based on the BLDC drive for the optimal PID gains [1999.8, 38.6, 41.2], the electrical energy consumed, or battery energy consumed and mechanical energy consumed or motor energy consumed were 0.1975 kWh/1 km and 0.1623 kWh/1 km, equivalent to 19.75 kWh/ 100 km and 16.23 kWh/100 km, respectively. The electrical power consumed was 26.43 kW, and the mechanical power consumed was 24.80 kW. Therefore, the energy and power efficiencies in the case of the BLDC drive were 82.17% and 93.83%. Hence, the powertrain based on the BLDC drive demonstrates better efficiency compared to the PMSM drive on the basis of the GA optimization technique.

However, our recent study revealed that the powertrain-based BDCL drive achieved an energy efficiency of approximately 90%, with an energy consumption of 17.34 kWh/100 km. However, the design of the electrical

machine in the study in question was based on the tabulated torque envelope with speed in which the peak torque of 400 Nm was determined by the controller. Therefore, based on this, this torque requirement would enhance the system's performance and decrease energy consumption even better than the current results with the optimizer. Thus, the GA-PID results remain superior due to the higher energy efficiency compared to the conventional technique. Therefore, the BLDC drive design was based on the maximum torque and power to compare its performance with the PMSM drive whose design was already based on the maximum torque and power. Table 3.12 presents the measured energy consumption corrected for based on the battery capacity of the 2011 Nissan Leaf. Although there was no exact information on the vehicle weight at which the original measured data were obtained, the reference data is still valid for our comparison since the reference vehicle is within the standard weight (3500 kg or less) of the VW Crafter group, as presented in Table 2.3 in Chapter Two, with slight decrease due to the transformation to pick-up style. This shows a decrease in energy consumption by 11% compared to the measured data based on our reported results achieved in [159]. However, with thermal and cooling effects, the energy efficiency was 99.07% and the power efficiency was 98.81%, respectively. Based on this, the reduction in energy consumption increased to 16.81%.

Table 3.12: Measured Energy Consumption [158]

Vehicle Model/Year	**Energy Consumed [kWh/100 km]**
VW Crafter 2020	19.51
VW Crafter 2019	14.74
VW Crafter 2018	14.99

For the detailed powertrain, Figure 3.5.12 shows the extended powertrain's electrical and mechanical energy consumed based on the PMSM drive. The electrical and mechanical energy consumed were 0.1245 kWh/1 km and 0.09162 kWh/1 km, equivalent to 12.45 kWh/100 km and 9.162 kWh/100 km, respectively. Therefore, the energy efficiency was calculated to be 73.59%. However, the power efficiency was very low due to the high power of the electrical part. Figure 3.5.13 shows the vehicle speed due to the detailed BLCD drive model. Also, in the case of this powertrain, the vehicle speed had successfully tracked the drive cycle. However, we observed a potential decrease in energy consumption by 36.18% for the extended or advanced

powertrain based on the detailed PMSM model. However, these results cannot be reliable due to the model's complexity, high power losses, and lack of optimized parameters, which might affect its performance. In some cases, especially high-speed applications, like in HEV dynamics, the PMSM drive could outperform the BLDC drive, depending on the driving conditions.

More in-depth justification is required to justify the fuel efficiency gains obtained by integrating the advanced PID controller with the PMAC electrical drive system in the VW Crafter propulsion application. Officially, the Nissan Leaf range is 124-175 km on the NEDC test. This means that for the first three cycles (50 km/h), as proposed in this study, the range can be 124 km for the 24 kWh on a single charge. This is roughly for the Nissan Leaf, which has a gross weight of 1965 kg, much less than the VW Crafter. Therefore, since fuel consumption increases with the vehicle's weight, a lower range than the Nissan Leaf car would be achieved. Hence, for the PMSM electrical drive based on manual tuning (22.73 kWh/100 km), 105.59 km was roughly reached, while for the GA-PID, 117 km was achieved. However, for the BLDC drive (19.75 kWh/100 km), 121.52 km was achieved. On the other hand, PMSM electrical machines have been excellent for traction applications like EVs and HEVs. Although the BLDC machine theoretically performs better in this application at the system level. We could see how the PMSM outperformed it without many issues at the detailed or extended modeling level, though it needs further design and refinement in future studies.

Generally, DC electrical machines are not suitable for real-world traction applications, like EVs, due to their limitations and disadvantages because their angular velocity depends on the input voltage. Therefore, the maximum angular velocity also does if the battery voltage drops due to discharge. The angular velocity of the AC machine depends on the frequency of the AC input voltage. Thus, the inverter can keep the AC frequency constant if the battery voltage drops due to discharge. However, DC machines were still in use 30-40 years ago; due to the limitations of power electronics, MOSFETs were not powerful enough to create vehicle inverters. DC choppers were used for DC machines to control angular velocity. Therefore, old trolleys still use DC machines. Electric forklifts use DC machines, which are simple, reliable, and cheaper than AC machines and inverters. Lead acid batteries can be used as a counterweight.

3.7 Conclusion

The primary reasons for the automotive industry's migration towards EVs are environmental concerns due to pollution, cost, and the quest to attain a cleaner city. Therefore, this thesis is motivated by optimal energy consumption and a desire to meet the mobilty long-range in the vehicle market. Therefore, the energy consumption of the VW Crafter has been presented on the basis of the enhanced PID controller according to the NEDC test procedure. The study presented in this chapter is a journey towards developing the hybrid electrified powertrain of the reference vehicle. The design of the e-Crafter was based on the new gearbox design to connect the electric drive to the rear wheel of the vehicle, which is given in detail in Chapter Five.

The vehicle control strategy was tuned using the GA optimization technique, taking the integral errors as a fitness function to achieve the expected requirements of system robustness and effective tracking capability. However, different electrical drives at varying levels of complexity were developed for the vehicle to investigate energy consumption. The VW Crafter presented in this research powered by permanent magnet synchronous electrical machines with Nissan Leaf battery has achieved energy and power efficiency of 78.8% and 92% for the PMSM drive, and 82.17% and 93.83% for the BLDC drive on the basis of an optimized GA-PID control algorithm. This shows that the proposed GA-PID control algorithm is a valuable and alternative control scheme suitable for optimal energy consumption and efficient performance in electric vehicles. Therefore, the powertrain based on the BLDC drive has slightly demonstrated superior performance compared to the PMSM drive. The simulated pure electric Crafter has reduced the energy consumption by 11.12% in the case of the BLDC drive when the torque requirement of the controller was set to 400 Nm. For complete energy profiling, this study has successfully implemented a heat dissipation model with an appropriate cooling method that further reduced the energy consumption by 16.81%. Moreover, The total required consumption was 21.354 kWh/100 km as presented in Chapter Two, and the actual consumption with thermal control was 16.23 kWh. Therefore, the design in the electric mode achieved 5.124 kWh/100 km energy gain. This means a 24% energy efficiency gain in the electric mode due to good design, functional energy recovery mechanism and optimized energy management system achieved in this study.

Chapter 4

Development of VW Crafter Hybrid Vehicle

4.1 Introduction

Before being transformed into a hybrid, the ICE-powered VW Crafter was attributed to high dependence on fossil fuel and associated dangerous emissions, which are not desirable. Chapter Two (Thesis I) presents the energy storage modeling based on the 2011 Nissan Leaf battery pack. Subsequently, the total tractive force needed, as well as the traction energy required to propel the vehicle, taking into account the factors and forces acting on the vehicle under real-world driving impact, has been presented. Chapter Three (Thesis II) presents the modeling of electrical drive dynamics and the vehicle's powertrain in the electric mode design. Nevertheless, this chapter (Thesis III) presents the complete redesign and investigation of the vehicle's physical assembly from the conventional to the hybrid by integrating the PMSM electrical machine with a 2011 Nissan Leaf battery pack. It is a front wheel drive by a diesel ICE and electric rear wheel drive. It can be operated in three modes: diesel, electric, and hybrid. Therefore, the design of the hybrid vehicle has become popular in the vehicle market due to low energy consumption and CO_2 emissions. It also helps overcome pure EVs' limitations due to charging time, costs, and limited operation range [169].

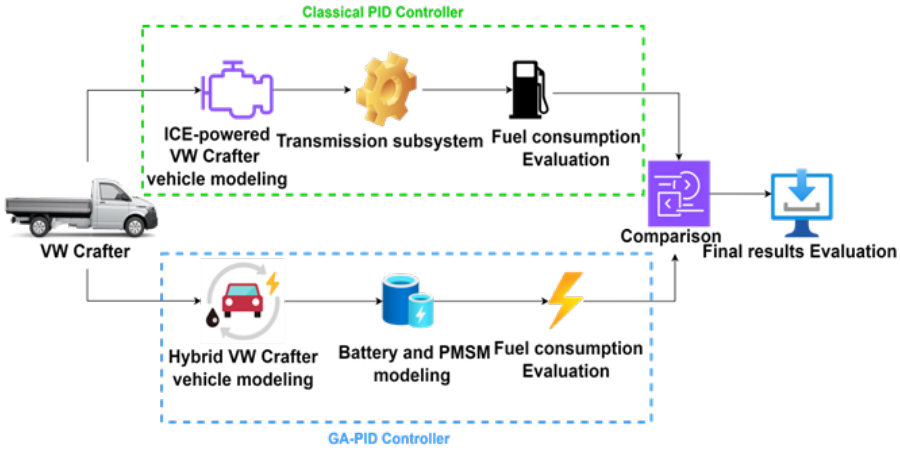

Figure 4.2.1: Hybrid Crafter Workflow [34]

4.2 Hybrid Vehicle Development Workflow

Figure 4.2.1 shows the hybrid vehicle workflow development. The arrow indicates the design process or step, not the system's energy or power flow. The methodology or workflow consists of two main processes or methods: Method 1: In this stage, the MIL method was employed to design the conventional Crafter powered by a 2.0 TDI CR diesel engine incorporated by the six-speed manual transmission. A control loop was created on the basis of the PID classical control technique to investigate the vehicle system's fuel consumption and carbon emissions. This initial design was based on the power and torque requirements discussed in Chapter Two. The results achieved were used as a benchmark for the design, control, and optimization of the hybrid powertrain. Method 2: The hybrid vehicle was developed and analyzed. In this method, the design approach was based on the experimental verification of the developed model. In other words, the design method was based on the experimental data obtained from the measured data. Therefore, an improved PID controller was implemented for the hybrid vehicle to reduce fuel consumption and CO_2 emissions.

The experimental and simulation results were compared to verify and justify the transformation of this vehicle in the field of electric and hybrid cars in general. The contributions related to this section have been published in [80, 34] and other related publications for the VW Crafter. The development of the hybrid powertrain started by determining the tractive force needed for vehicle propulsion. Subsequently, the power and torque required were

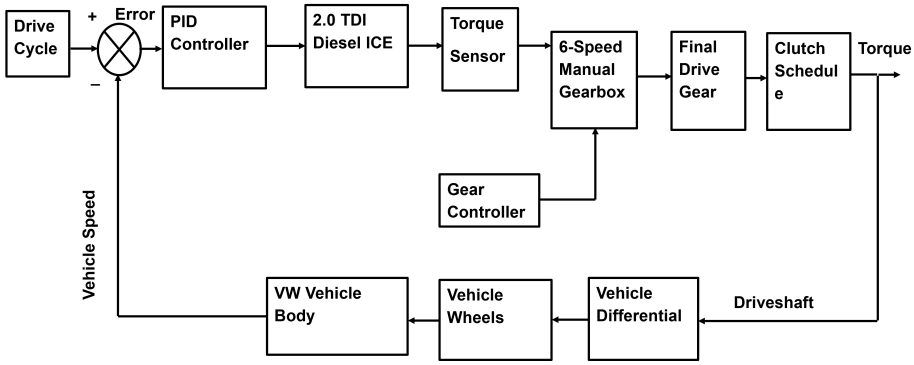

Figure 4.2.2: Conventional VW Vehicle Control Loop

investigated using the dynamical description of the vehicle body and the tire based on the gear's transmission in the gearbox subsystem and the final drive. Therefore, the vehicle's design started by considering the vehicle dynamics mathematical background description as already described in chapter four, and the tire dynamics based on the magic formula.

Figure 4.2.2 shows the control loop of the conventional VW Crafter. This represents the general overview of the traditional powertrain modeling based on the MIL approach. It consists of three essential parts: The powertrain, the drivetrain, and the driveline. The powertrain is made up of the diesel engine, transmission, and driveline components such as axles (front and rear axles), as well as differentials. The drivetrain consists of the transmission and driveline components without the engine. In contrast, the driveline consists of the components mentioned without the transmission. The transmission consists of a six-speed gearbox with its controller as well as six clutch schedules for the gearshift. All this was modeled to form the conventional Crafter in a control loop to analyze fuel consumption and emissions. Then, the hybrid model was built, and the transmission was redesigned into a single speed based on an optimized gear ratio to achieve an optimal system performance.

Figure 4.2.3 shows the control loop of the hybrid powertrain. In addition to some of the components of a conventional Crafter, the electrical drive consists of the DC-DC converter, the electrical machine (PMSM) and the controller. The DC-DC converter was eliminated at the simulation level since the motor model was designed to handle high voltage for the leaf battery. In practice, the presence of the converter prevents the onboard devices from being damaged due to high voltage. Therefore, during the measurement or CAN bus data analysis or even during normal driving, it was necessary to

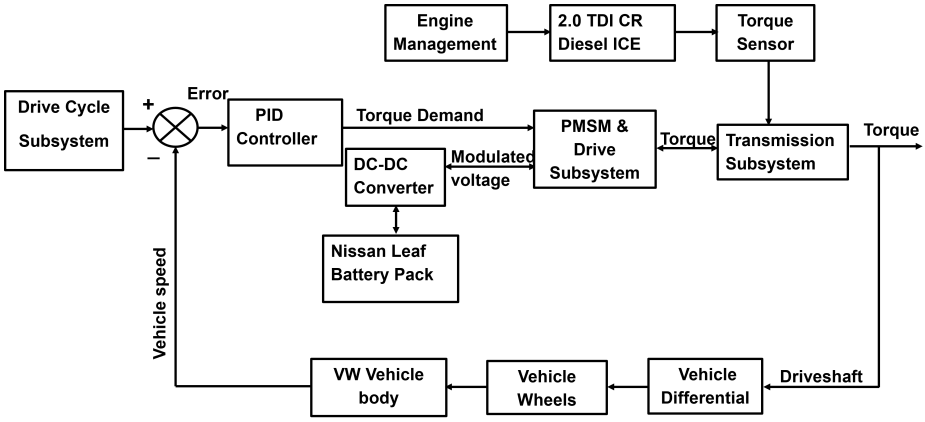

Figure 4.2.3: Hybrid VW Vehicle Control Loop

step down the voltage to 12 V for safe operating conditions on the electrical drive part on the Crafter. The vehicle controller was optimized using the GA technique to compute the fuel consumption of the hybrid powertrain. FOPID and PSO-PI were developed to verify the effectiveness of the proposed PID optimizer, which was used to regulate the vehicle speed and provide the speed and torque demand needed to move the vehicle wheel. An engine management system was developed separately, which provides the speed demand or torque demand combined with the torque of the electrical machine to propel the vehicle.

4.2.1 Dynamic Modeling of the ICE

The generic engine block physical model can be used as a spark ignition or diesel type, depending on the requirements and specific applications. In this research, the engine was used to model our diesel ICE. Therefore, if the $\omega_N(\omega)$, ω, and ω_{PP}, are the normalized engine speed, current engine speed [rpm], and engine speed [rpm] at the maximum power. Moreover, $P(\omega(\omega_N))$, P_P, and p_N are the current power [kW] of the engine, engine maximum power [kW], and normalized power of the engine. Moreover, s_1, s_2, and s_3 are the polynomial constant coefficients as studied in [170]. Therefore, the engine is parametrized based on the third order polynomial as described in [170, 34] as follows:

$$\begin{cases} \omega_N(\omega) \equiv \frac{\omega}{\omega_{PP}} \\ P(\omega(\omega_N)) = P_P p_N(\omega_N) \\ p_N(\omega_N) = s_1\omega_N + s_2\omega_N^2 + s_3\omega_N^3 \end{cases} \tag{4.2.1}$$

For the condition wide open throttle , the ICE torque is described as in [170] as:

$$\begin{cases} T(\omega(\omega_N)) = p_1 + p_2\omega_N + p_3\omega_N^2 \\ p_1 \equiv \frac{s_1 P_P}{\omega_{PP}} \\ p_2 \equiv \frac{s_2 P_P}{\omega_{PP}} \\ p_3 \equiv \frac{s_3 P_P}{\omega_{PP}} \\ \omega_{NPP} = \omega_N(\omega_{NPP}) = 1 \end{cases} \tag{4.2.2}$$

where ω_{NPP} is the ICE normalized speed that aligned with ICE maximum power. Therefore, substituting the normalized speed of the ICE (ω_{NPT}) at the maximum power (P_P) [kW] into p_N and set $p_N((\omega_{PP}))$ to zero [170], we have the following expression:

$$\begin{cases} s_1 + s_2 + s_3 = 1 \\ s_1 + 2s_2 + 3s_3 = 0; p_N = 0 \\ \omega_{NPT} = \omega_N(\omega_{PT}) = \frac{\omega_{PT}}{\omega_{PP}} < 1 \end{cases} \tag{4.2.3}$$

Where the maximum torque speed is less than the maximum power speed, hence, based on the polynomial formulation, the dimensionless normalized torque of the ICE, (τ_N) will be obtained, setting the slope to 0 and solving for s_i as:

$$\begin{cases} \frac{d\tau_N(\omega_{NPT})}{d\omega} = s_2 + 2s_3\omega_{NPT} = 0 \\ s_1 = \frac{3-4\omega_{NPT}}{2(1-\omega_{NPT})} \\ s_2 = -\frac{\omega_{NPT}}{(\omega_{NPT}-1)} \\ s_3 = \frac{1}{2(\omega_{NPT}-1)} \end{cases} \tag{4.2.4}$$

Hence, the torque of the ICE $T(\omega(\omega_N))$, maximum torque (T_P), normalized ICE speed at maximum torque (ω_{NPT}), the speed of the ICE at maximum power (ω_{PP}), and ICE speed at maximum torque (ω_{PT}) have the

following relationship as follows [170]:

$$\begin{cases} T(\omega(\omega_N)) = \frac{2T_P}{3-\omega_{NPT}}(s_1 + s_2\omega_N + s_3\omega_N^2) \\ 2T_P\omega_{PP}^2 - 3P_P\omega_{PP} + P_P\omega_{PT} \\ \omega_{PP} = \frac{3P_P+\sqrt{P_P(9P_P-8T_P\omega_{PT})}}{4T_P} > \omega_{PT} \end{cases} \tag{4.2.5}$$

where $(T_P\omega_{PT})$ should be equivalent to power at maximum torque (P_{PT}), which should always be less than maximum power (P_P) [170]. For the condition of partially opened throttle, we have:

$$\begin{cases} \Pi = max(\Pi_i, \Pi_c) \\ \frac{d\Pi_c}{dx} = \frac{0.5(1-\tanh(4\frac{\omega-\omega_r}{\omega_t}))-\Pi_c}{\tau} \end{cases} \tag{4.2.6}$$

Where Π_c, ω_r, ω, ω_t, Π, and Π_i are the controller throttle, idle reference speed of the engine, speed of the engine, controller threshold's speed, throttle, and input throttle. [34].

In order to calculate other parameters for the engine, like the efficiency of the ICE, fuel flow rate, etc., the formulations described in [171], were applied. Therefore, the torque of the engine $(T(\omega(\omega)$ [Nm] is linked to the power of the engine $(P(\omega(\omega_N)))$ [kW], and the rotational speed ω [rpm] [34]. Therefore, the following equations as expressed in equation (4.2.7) were used:

$$\begin{cases} T(\omega(\omega_N)) = \frac{P(\omega(\omega_N))}{\omega} \\ \eta_f = \frac{1}{Q_{hv}SFC} \\ SFC = \frac{m_f}{P(\omega(\omega_N))} \\ MEP = \frac{P(\omega(\omega_N))n_R}{V_dN} \\ MEP = \eta_f\eta_vQ_{hv}P_{ai}\frac{F}{A} \\ \eta_v = \frac{m_a}{P_{ai}V_d} \end{cases} \tag{4.2.7}$$

Where η_f, Q_{hv}, m_f, n_R, V_d, SFC, N, P_{ai}, m_a , η_v, and $\frac{F}{A}$ are the efficiency of the engine, heating value, flow rate of the fuel, number of crank revolutions for each power stroke per cylinder, displaced volume, engine specific fuel consumption, crankshaft number of revolutions, density of the air-inlet, mass of air, volumetric efficiency of the engine, and air-fuel ratio [34]. Table 4.1 presents the diesel engine general technical specifications.

Table 4.1: ICE Technical Parameters [34]

Parameters	**Values**	**Symbols [Unit]**
Number of Cylinders	4, Inline	-
Fuel Type	Diesel	-
Fuel System	Common Rail (CR)	-
Fuel Density	820–845	ρ_F [g/L]
Engine Displacement	1986	D [cm^3]
Bore × Stroke	0.081 × 0.0955	BxS [m]
Number of Valves	16	-
Compression Ratio	16.2:1	-
Engine Peak Power	103	P_P [kW]
Engine Peak Torque	340	T_P [Nm]
Number of Valves	16	v [-]
Gearbox	6-Speed, Manual	-
After Treatment System	DPF	-
Engine Time Constant	0.4	τ [s]

4.2.1.1 ICE-Mode Design of Gearbox/Gearshift

The transmission system for the VW Crafter is a six-speed manual transmission coupled with a friction disc clutch based on the six switching sequences or schedules for engaging and disengaging the gearbox to facilitate the vehicle's movement. The designed conventional Crafter was developed based on a four-stroke, four-cylinder, 2.0 L diesel ICE. The PID controller was incorporated to control the vehicle speed using WLTP as a test procedure. The gearshift strategy was controlled using MATLAB shift logic, which serves as the gearbox controller. The clutch selection strategy for the six-speed manual gearbox from the first to final drive gear is presented in Table 4.2. The theoretical description of the gearshift strategy and optimization is expressed in [172] as follows:

$$\begin{cases} R_{firstest.} = \frac{r_w m}{T_{eng.}\eta_f}(a_{WLTP} + g\sin\theta_{max}) \\ v = \frac{1000\pi r_w}{30 R_{firstest.}} \\ R_{first} = \frac{r_w}{T_{eng.}\eta_f}[a(m + \frac{I_{Eff}}{r_w^2} + F_A + F_r + F_{grade})] \\ R_{top} = \frac{2\pi r_w N_{engmax.}\eta_f}{60 v_{motorway}} \end{cases} \tag{4.2.8}$$

Therefore, the gear ratio estimated is defined as $R_{firstest.}$ when the first gear ratio is R_{first}. Then, v is the speed of the vehicle calculated at 1000 rpm of the engine's speed. And the rest of the variables and constants, such as $v_{motorway}$, a, m, $T_{eng.}$, r_w, $N_{engmax.}$ are motorway legal speed of the vehicle, the acceleration of the vehicle, mass of the vehicle, engine torque, radius of the tire, effect of the inertia peak engine's speed [172]. The gearbox type is FWD manual compatible with the 2.0 TDI diesel engine. It is an OAX series and the code is TWX. It is a new gearbox constructed in 2020 [173]. The engine code for the TWX gearbox is DAUA, with an output power of 103 kW. However, the gearbox can handle up to 130 kW. The adapted six-speed gear ratios were based on datasheet of the vehicle's manufacturer. This equation-based can be applied when optimizing gear ratios.

Table 4.2: Six-Speed Manual Gearshift and Clutching [34]

GearShifts	**Gear Ratios**	**A**	***B***	**C**	***D***	**E**	***F***
1st Gear	5.06	1	0	0	0	0	0
2nd Gear	2.61	0	1	0	0	0	0
3rd Gear	1.52	0	0	1	0	0	0
4th Gear	1.00	0	0	0	1	0	0
5th Gear	0.79	0	0	0	0	1	0
6th Gear	0.68	0	0	0	0	0	1
Final Drive	3.92	1	1	1	1	1	1

4.2.1.2 Electrical Drive Gearbox Design/Gearshift

A new gearbox was designed for both the MIL design and physical assembly process. The physical process was investigated in [30], and this thesis mainly focuses on the design, optimization and online CAN Bus analysis to perform

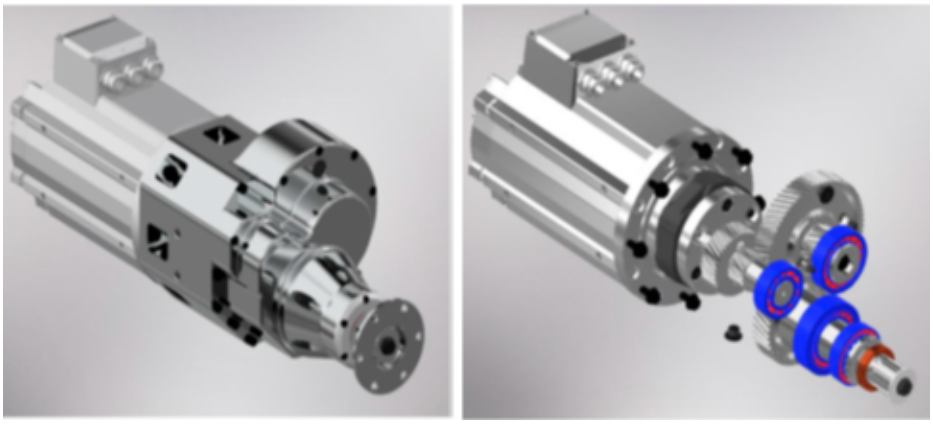

Figure 4.2.4: Gearbox 3D Simulation [30]

Figure 4.2.5: New Designed Gearbox adapted from [30]

an experimental verification of the theoretical findings. Figure 4.2.4 shows the 3-dimensional (3D) simulation of the gearbox from 3D computer aided design (CAD) software as adapted from [30]. The first picture is the enclosed design, and the second picture shows the gear design's inside. This gearbox was incorporated into the rear wheel to facilitate the vehicle movement for electrical drive mode. Table 4.3 presents the gearbox parameters and how they were used to obtain the ratios of the newly designed gearbox in the e-drive mode. The gear ratios based on the initial parameters of the gear were calculated to be 1.54, 3.4, and 2.33, respectively. Figure 4.2.5 shows the position of the new gearbox on the rear wheel of the VW hybrid Crafter responsible for the electric drive as RWD.

Table 4.3: Parameters of the Gearbox [30]

Diameters [mm]	Axial Module [mm]	Teeth Number
d_1	2.25	26
d_2	2.25	40
d_3	2.5	20
d_4	2.5	68
d_5	3	18
d_6	3	42

4.3 Experimental Set-Up for Vehicle Monitoring

The vehicle CAN bus is used for data transmission between the control units. It facilitates communication between the vehicle's components using two data lines. The CAN protocol is utilized to transmit/receive messages between our vehicles' ECUs. The CAN bus is the best standard for vehicular networks used in the automotive industry. This vehicle CAN bus system is developed in the vehicle network systems to monitor vehicle parameters such as the engine speed, fuel consumption, temperature, vehicle, motor speed and so on, from remote areas [126]. In this research, a novel approach on the basis of NetCAN Plus uses an online measurement platform to collect the vehicle for experimental analysis for the electrical drive and VCDS for the engine drive via the vehicle's OBD-II.

4.3.1 Online Measurement using NetCAN Plus 110

Figures 4.3.1 and 4.3.2 show the flowchart of the LabVIEW application on the host PC and the experimental set-up for the online data collection. The measured data which is based on HIL was collected online with the aid of four sets of Net CAN Plus 110 hardware devices implemented for the electrical drive part. The data was collected with the help of the internet protocol (IP) addresses of each NetCAN Plus. The following devices were implemented in a metal box, facilitating online data communication for the vehicle:

- Industrial Box PC from Phoenix Contact
- Power Supply Unit

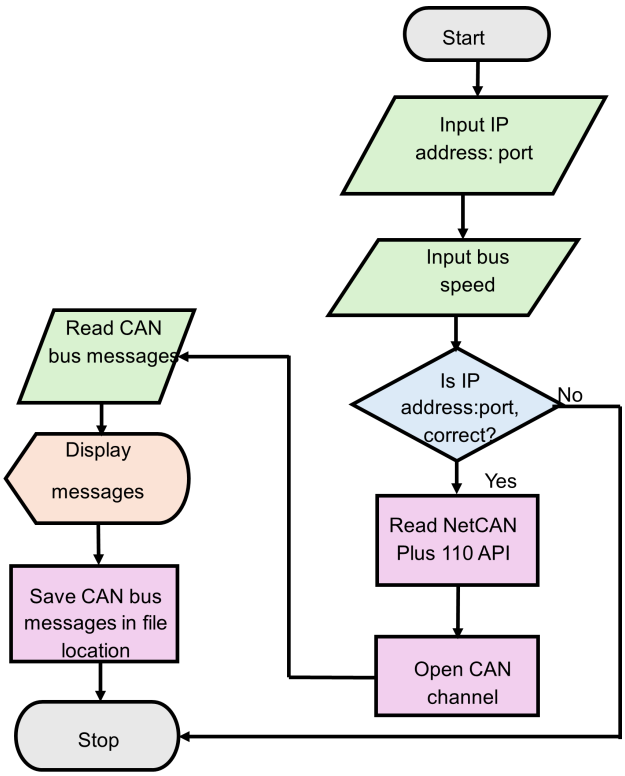

Figure 4.3.1: CAN Bus Message Program Flowchart [174]

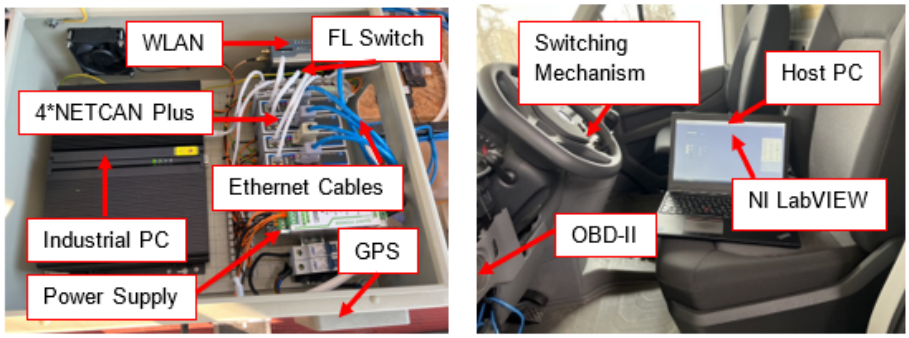

Figure 4.3.2: Experimental Set-up modified from [80]

- Phoenix Contact WLAN 5100
- Vision Systems Net CAN Plus 110
- FL Switch 1000 Wireless Module
- FL Timeserver Network time protocol (NTP)

The Lenovo PC (host PC) was connected to the Phoenix Contact Industrial Box PC remotely via a Local Area Network using an ethernet cable. The LabVIEW software runs on this Lenovo PC to read the CAN Bus Messages from the vehicle through the four (4) NetCAN Plus 110 devices connected to it. The NetCAN plus 110 device with an IP address 192.168.10.13 is used to read the charging data. The NetCAN plus, which has an IP address of 192.168.10.12, is used to read the inverter data. The NetCAN plus with an IP address of 192.168.10.10 is used for reading the temperature data, and the NetCAN plus with an IP address of 192.168.10.11 is used for reading the auxiliary data. The application was implemented on LabVIEW software on the host PC to read the CAN bus data. The application receives IP addresses, the port number of the NetCAN Plus 110 devices, and 500 kbps as input. Then, the open button should be clicked to open the CAN channel to connect it to the NetCAN Plus to read the vehicle's data [80].

The data collected in this form was hexadecimal, which makes it difficult to understand what the CAN message represents. Therefore, a database file was used to decode the raw CAN data into physical values to make sense of the engineering unit's data. The representation of the data collection process, as described in 4.3.2, begins with inputting the IP address for each individual NetCAN Plus to obtain the associated data until the data is saved to the CSV file. The host computer (Lenovo PC) as shown in Figure (4.3.2 b) on the Crafter with LabVIEW program running, which was connected to the NetCAN device set-up as shown in Figure (4.3.2 a) on the electric drive of the vehicle was used to collect the data via the industrial PC.

4.3.2 Data Measurement using VCDS

The VCDS software is used for data collection via the vehicle OBD-II for diagnostics and troubleshooting from the VW group. The data can be collected with the VCDS-compatible cable as an interface between the OBD-II port and a host PC. This collected data can be used to diagnose or optimize vehicle efficiency [34]. Figure 4.3.3 shows the general architecture for the

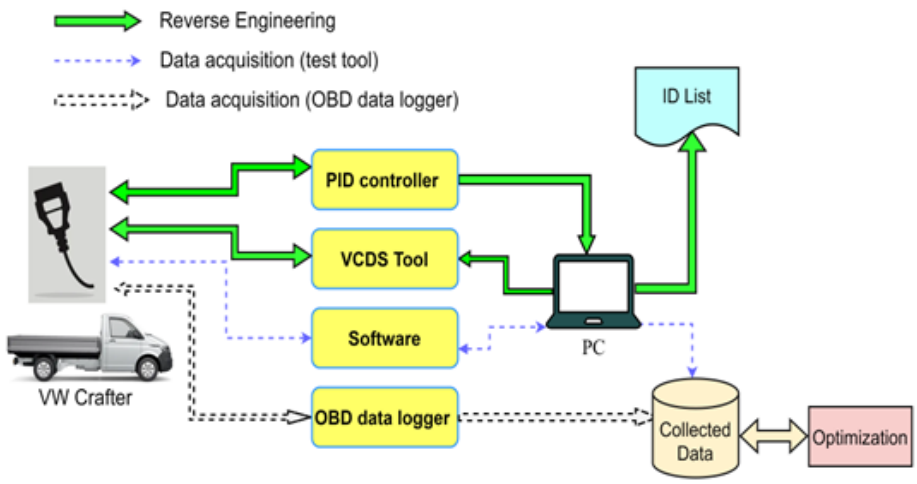

Figure 4.3.3: VCDS Experimental Set-up for Data Collection [34]

data via VCDS tool for the VW Crafter. Therefore, the cable that is VCDS compatible (OBD data logger) is connected to the host computer, and the application running (VCDS software) is on it. The required data to collect are selected and collected as CSV files. The general setup in Figure 4.3.3 represents how the vehicle data collection process is facilitated via ODB2, either for diagnostic or optimization of vehicle consumption. In the context of this research, the data was collected to minimize fuel consumption, maximize efficiency, and reduce CO2 emissions. Therefore, since not all data are sent to the network, only critical ones were sent for the vehicle to operate. The exact data package ID was unknown, so we put the ECU into diagnostic mode via VCDS. ECU does not send all sensor data in broadcast style unless in diagnostic mode.

4.4 Optimization of the PID Controller

After data collection and design of the vehicle, the next was to optimize the vehicle controller to optimize system efficiency. PID control algorithm has been relevant for process control due to its intuition for practical implementation. This is why it is still applicable today in many industrial and commercial mechatronics products. For optimal energy management, the PID parameters such as K_p, K_i, and K_d should be appropriately tuned using either manual technique or optimization techniques. With the manual

method, we could achieve a stable system, but due to human intuition and the highly non-linear nature of the EV dynamics system, there was no proper balance between optimal consumption and tracking performance, which could lead to sub-optimal results. This is why this research used manual and GA techniques and compared the performance when developing the e-Crafter. Therefore, this research proposes the GA-PID controller to serve as an EMS for the HEV control system. Other control algorithms such as PSO-PI and FOPID were proposed to compare performance.

4.4.1 GA-PID Controller

GA is applied to optimization problems and is based on the process of natural selection. The GA has been adopted in many control problems and energy-intensive applications due to its simplicity, faster convergence, and ability to handle multi-objective optimization problems. It has been popularly adopted in electric and hybrid vehicles as an energy management system to ensure optimal fuel consumption and minimize emissions. The primary function of the EMS is to allocate energy from sources such as electrical machines, ICE, and batteries to optimize the system's efficiency. Therefore, in this research, the PID control strategy was optimized based on the GA technique using ITAE as a fitness function to provide optimal torque and speed to the electrical machine, ensure vehicle speed tracking performance, and ensure optimal energy efficiency of the battery, electrical machine, and ICE. Figures 4.4.1 and 4.4.2 show the the hybrid model with optimized PID in the control loop and flowchart of the GA technique applied to tune the gains of the PID controller. The GA procedure described in Figure 4.4.1 was adopted from [168]. The optimization algorithm was repeated using the genetic parameters until the gains of the control algorithm iteratively converged to optimal solutions or minimum values of the proposed fitness function were determined.

The vehicle controller generated the controlled signal needed to provide the torque or speed command to the electrical drive. The engine control system was implemented to provide the regulated speed required for the diesel engine for optimal torque, which would be combined with the electrical drive torque to propel the vehicle. The reference speed is the drive cycle in km/h, and the actual speed is the vehicle in km/h. The error signal determines the controller action, increasing or decreasing the output or desired vehicle speed. Therefore, the electrical and engine drive systems together with the vehicle dynamics, were integrated into the framework of the proposed optimization

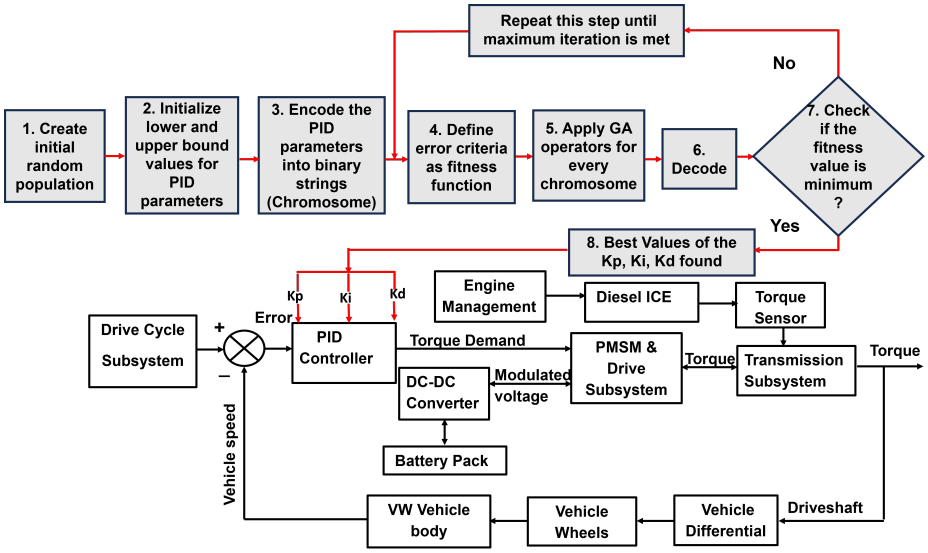

Figure 4.4.1: HEV with GA-PID in the Control Loop

problem for optimal operation of the vehicle system to optimize fuel and energy consumption. Tables 4.4 presents the parameters for the control optimization. The same parameters were adopted for the pure EV since we selected enough search space for the algorithm to choose the best values in each case. This is possible since the dynamics of each plant is different.

Table 4.4: GA Parameters for Hybrid [34]

Name of Parameters	**Values**
Selection Strategy	Random
Fitness Performance	Proportional
Generations	40
Population Size	100
Number of Variables	3
Lower Bound (LB)	[0 0 0]
Upper Bound (UB)	[2000 2000 2000]

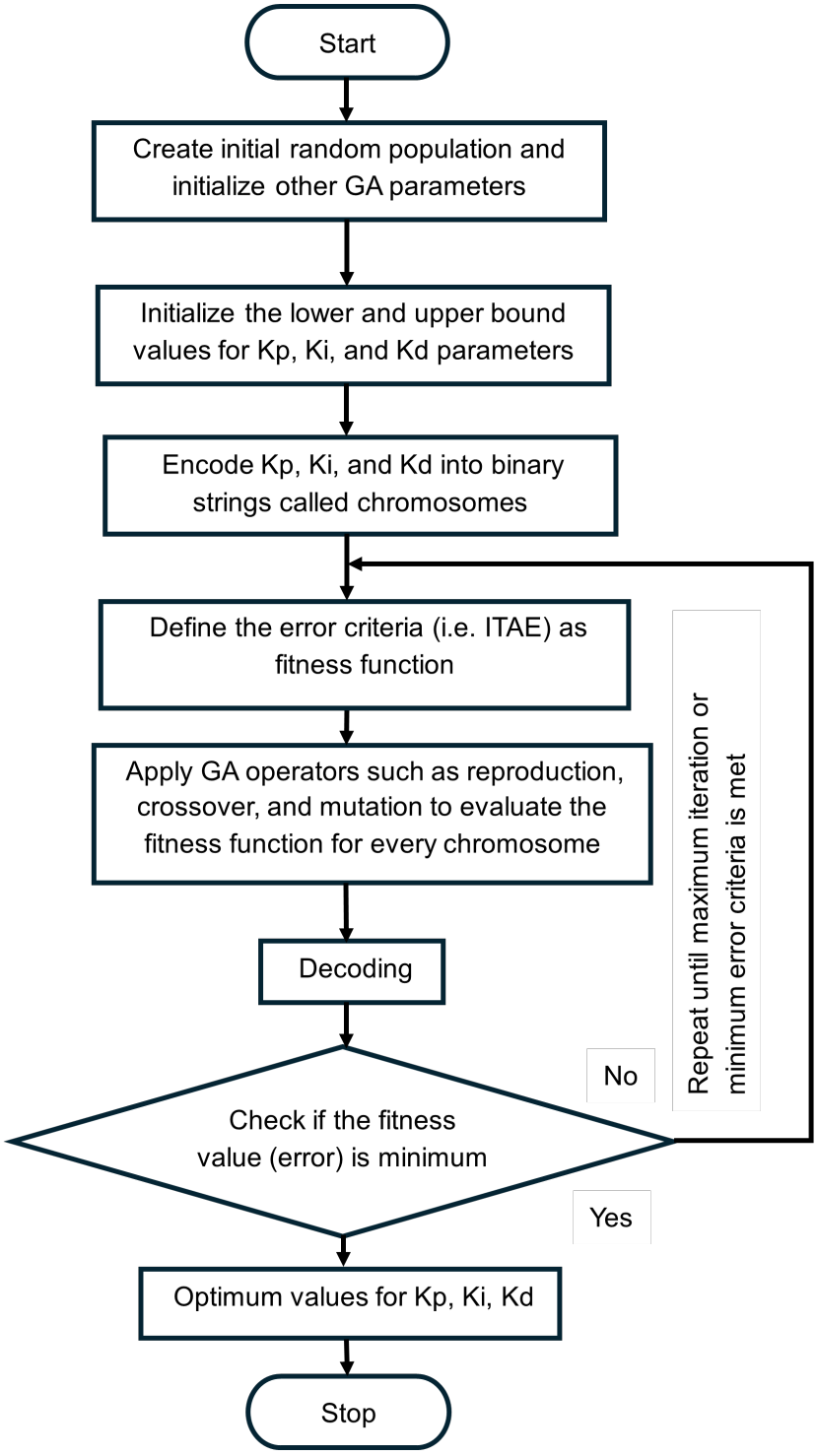

Figure 4.4.2: Flowchart of GA Technique [168]

4.4.2 PSO-PI Controller

The PSO is an optimization method inspired by the basis of the social behavior of some animals, like birds. This optimization technique is meant to simulate social behavior on the population. For the PSO optimization problem, each particle in the population keeps searching for the best position in the multidimensional space. Based on the position of the neighboring particles, the particle that is flying changes its position based on the experience from the position of the neighboring particles. Therefore, during the change of this positioning process, the individual particles would have undergone the position changes, which were influenced by the experience of the flying particles and their neghboring particles [175]. Hence, the position and velocity of the particles are updated as described in [175] as:

$$\begin{cases} V_i^{k+1} = w \cdot V_i^k + C_1 \cdot \mathrm{rad}_1 \cdot (P^{\mathrm{lbest}} - P_i^k) + C_2 \cdot \mathrm{rad}_2 \cdot (P^{\mathrm{gbest}} - P_i^k) \\ P_i^{k+1} = P_i^k + V_i^{k+1} \end{cases} \tag{4.4.1}$$

"Where P_i^k, V_i^k, C_1, C_2, w, P^{lbest}, P^{gbest} are particle's position, velocity, acceleration coefficients, inertia weight, local best position, global best position, and $rand_1$ and $rand_2$ are the random number between 0 and 1" [175]. Figure 4.4.3 shows the procedure for implementing the PSO for the vehicle controller and Table 4.5 presents the parameters used for the hybrid VW Crafter.

Table 4.5: PSO Parameters for Hybrid [34]

Name of Parameters	**Values**
Number of Particles	100
Number of Iterations	300
Number of Variables	2
Lower Bound [LB]	0
Upper Bound [UB]	6000
Cognitive Coefficient (c)	1.9
Inertia Weight (w)	0.09

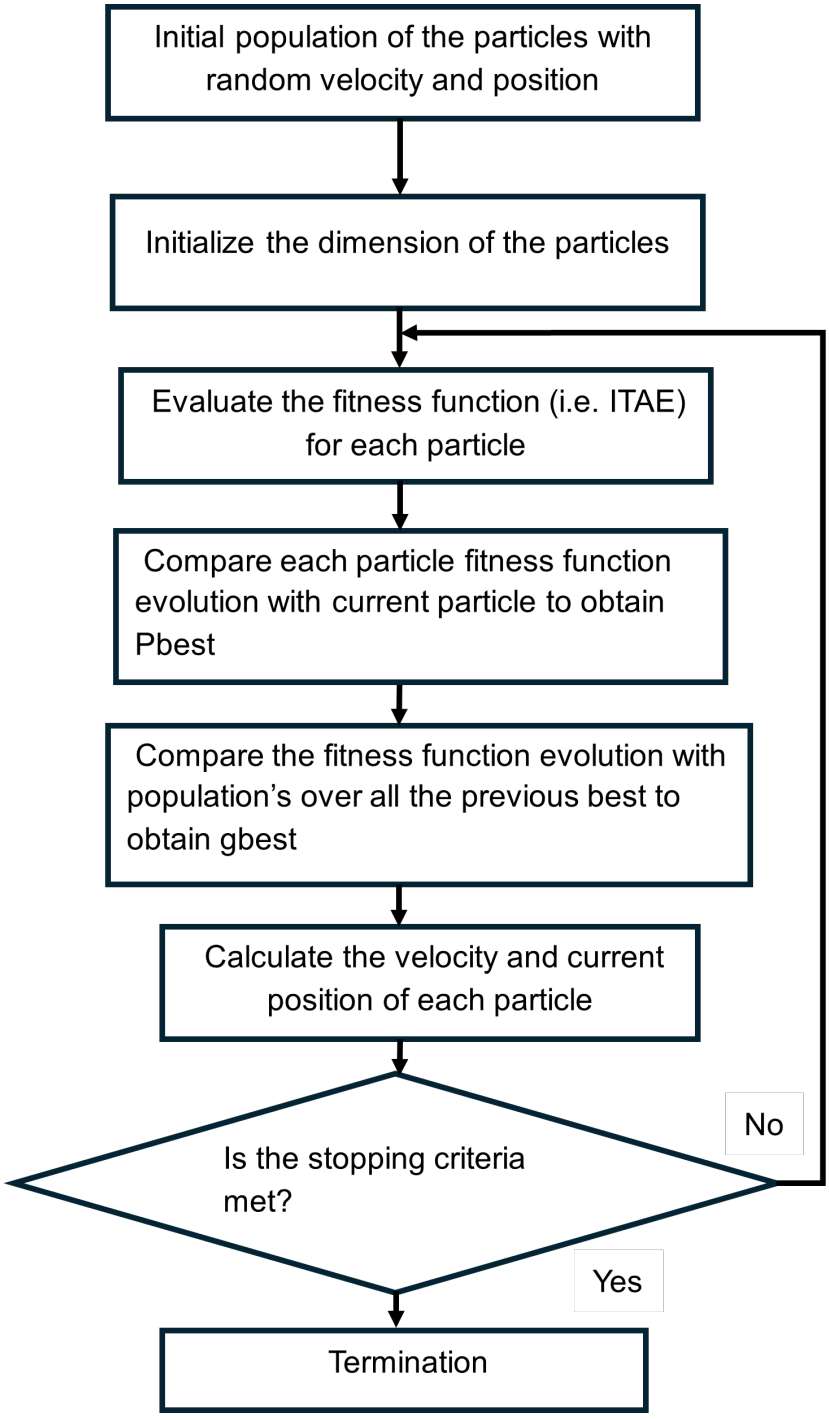

Figure 4.4.3: Flowchart of PSO Technique [176]

4.4.3 Fractional Order Controller

Fractional calculus has been popular in the fields of science and engineering in recent years since its inception 3000 years ago. Fractional calculus is the generalization of integral calculus and classical integer order differential calculus to the non-integer order. Therefore, using the concept of fractional calculus, the classical PID controller has been extended and improved with two more control parameters to form the FOPID controller [34]. The design of the FOPID from the famous PID can be done by modifying the traditional transfer function of the controller, and it can be expressed as in [177] as follows:

$$G(s) = K_p + \frac{K_i}{s^\lambda} + K_d s^\mu \tag{4.4.2}$$

"where $\frac{1}{s^\lambda}$ is the operator of the fractional integrator and s^μ is the operator of the fractional differentiator" [177].

4.5 MATLAB Models

The models for both the conventional and hybrid vehicles were developed in MATLAB/Simulink/Simscape environment which is the MIL approach. The conventional powertrain is made up of the engine, torque and speed sensor, six-speed gearbox, tire and vehicle dynamics, and vehicle controller subsystems. Moreover,the proposed 2.0 TDI engine is characterized by its efficient performance compared to the older versions due to its high torque output, better fuel economy and minimum emissions. It has 1968 cm^3 displacement and can cover up to 8—900 km distance. It has a 70 L capacity of the diesel tank. The WLTP drive cycle was utilized as a test procedure to investigate the vehicle's fuel economy. The conventional drivetrain results of the fuel consumed and CO_2 emissions were used as references to examine the consumption of the hybrid drivetrain [34]. The hybrid powertrain was developed to reduce fuel consumption and emissions and improve performance. The controller enhanced on the basis of the proposed meta-heuristic technique was applied as the energy management system for the optimal consumption and reduction of the CO_2 emissions. Figures 4.5.1 and 4.6.1 show the MATLAB models of the hybrid and conventional VW Crafter.

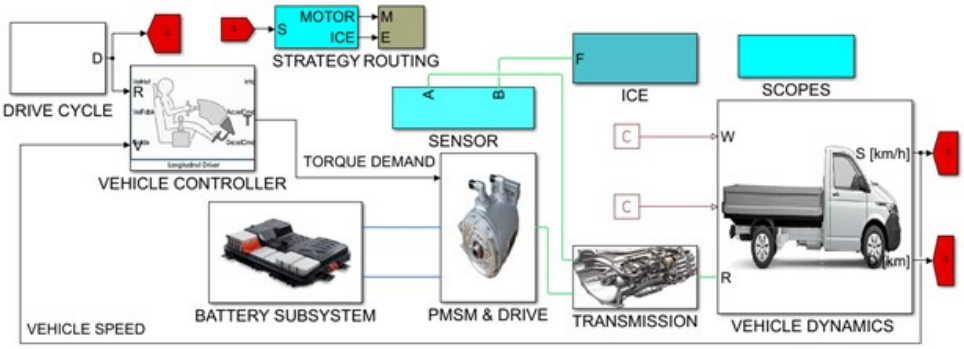

Figure 4.5.1: Hybrid Vehicle MATLAB Model [34]

4.6 Results and Analysis

The Simulink and Simcape toolboxes have been integrated using Simulink physical to Simulink and Simulink physical converters to facilitate the modeling process. Just like in the case of the electric vehicle, the development of the optimization technique directly on the physical model is difficult due to the system's nonlinear nature, and therefore, solving the equation by MATLAB takes longer than expected. Since the enhanced controller does not rely solely on the accurate or precise model of the system, we employed a system identification idea to estimate the mathematical dynamics of the vehicle model in the frequency domain, which is a more straightforward technique for applying the optimization problem. The results of the optimized gains were then applied to the Simcape model and the optimal performance was easily realized. Therefore, the entire model was estimated, though not precise, using the model linearizer in MATLAB (R2024a), identified as:

$$G(s) = \frac{1}{s^3 + 230s^2 + 130s} \tag{4.6.1}$$

Therefore, the transfer function in equation (4.6.1) is the most simplified model in the frequency domain in the 3×3 matrix, which was simplified and normalized from the complex transfer function model, taking into account the system's dynamics and relative gain. In this case, the precise model is unnecessary since the optimal gains are utilized in the physical model for the optimal fuel economy and reduction of the CO_2 emissions. Table 4.6 presents optimized parameters of the classical PID, the GA-PID, and PSO-PI on the basis of the ITAE fitness value. For the proposed energy management strategy (GA-PID), the optimized gains of the controller [K_p,

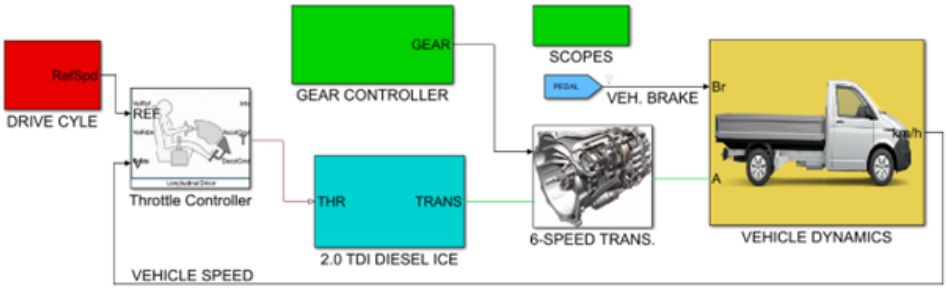

Figure 4.6.1: Conventional MATLAB Model [34]

K_i, K_d] were iteratively computed and found as [70.6657, 0.3339, 72.4406]. However, for the PSO-PI energy management strategy, the optimized gains of the controller [K_p, K_i] were iteratively found to be [1243.1, 1.3453]. While Table 4.7 presents the gains of the FOPID control technique, respectively [34].

Table 4.6: Classical PID, GA-PID, and PSO-PI Gains [34]

PID Parameters	**Classical PID**	**GA-PID**	**PSO-PI**
K_p	60	70.6657	1243.1
K_i	10	0.3339	1.3453
K_d	60	72.4406	-

WLTP was proposed for vehicle testing since it represents the standard real-world driving scenario to determine the CO_2 levels of emissions and fuel consumption for ICE and hybrid vehicles. Figure 4.6.2 shows reference speed successfully tracked by the vehicle speed-based GA-PID control algorithm for the hybrid powertrain. The proposed GA-PID was found to have a more efficient performance than the FOPID and PSO-PI controllers regarding power and energy consumption. Figure 4.6.3 shows the speed of the conventional VW Crafter due to the WLTP drive cycle. The vehicle speed successfully tracked the reference. It can be observed in the case of the ICE vehicle the level of tracking performance was better than that of the hybrid of the hybrid. This is due to the complexity and nonlinear nature of the hybrid powertrain. We tested the conventional VW Crafter with only one control

Table 4.7: FOPID Control Gains [34]

FOPID Parameters	Values of Gain
K_p	1000
K_i	20
K_d	0.05
$lamda$ $[\lambda]$	0.5
mu $[\mu]$	0.02

algorithm since that the aim was only to study its fuel consumption and how well it is justified when transformed into a hybrid; reducing the fuel consumption, CO_2 emissions, and improving the overall system efficiency. The derivative controller of the PID did not provide satisfactory performance in the case of the PSO optimization, which prevented it from reaching the desired optimal solution. This is why we proposed PSO-PI and FOPID to verify the effectiveness of the GA-PID control strategy. Figures 4.6.4 and 4.6.5 show the electrical and mechanical power and energy consumed by the electrical machine and the battery. The electrical and mechanical energy consumed by the battery and the electrical machine was 0.1295 kWh / km and 0.1162 kWh / km, which is equivalent to 11.62 kWh/100 km and 12.95 kWh/100 km for the optimized gains of GA-PID strategy [70.6657, 0.3339, 72.4406]. The electrical and mechanical power consumed by the electrical machine and the battery was 44.94 kW and 50.80 kW, respectively. It should be noted noted that the conversion factor from the rpm to rad/s was approximated as report in [34], and therefore, the model was revised and updated the motor power and energy consumptions. The updated energy consumed by the motor was 12.12 kWh/100 km and its power consumption was 46.85 kW for the GA-PID control strategy.

Therefore, based on these updated consumptions, the power and energy efficiency would be 92.22% and 93.59%, respectively. In the mechanical energy consumption of the electrical machine, we observed a negative recovery energy during the machine's motoring and generating action [34]. The positive and negative portion representing the energy consumption and recovery concept was studied in [178]. The difference between the electrical and mechanical energy is due to the energy loss during transmission from the battery to the electrical machine.

At the same time, the difference between the electrical and mechanical

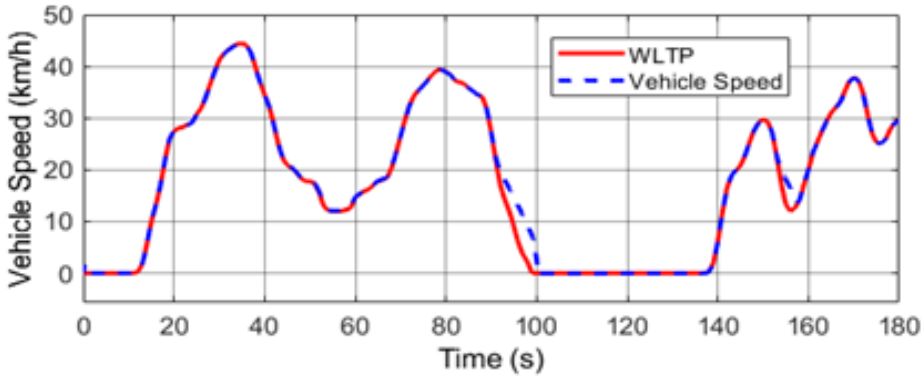

Figure 4.6.2: Hybrid Vehicle Speed [34]

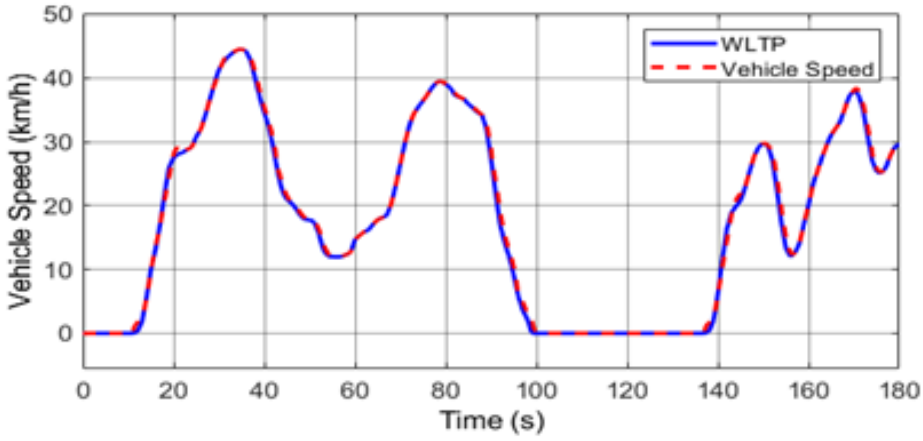

Figure 4.6.3: Conventional Vehicle Speed

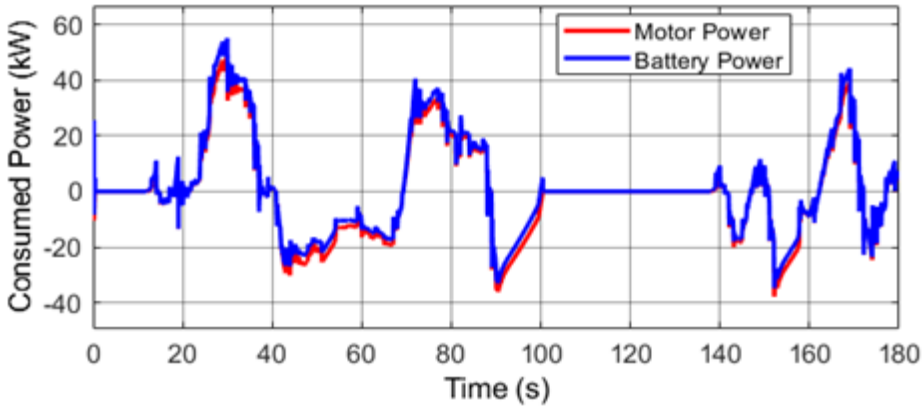

Figure 4.6.4: Electrical and Mechanical Power [34]

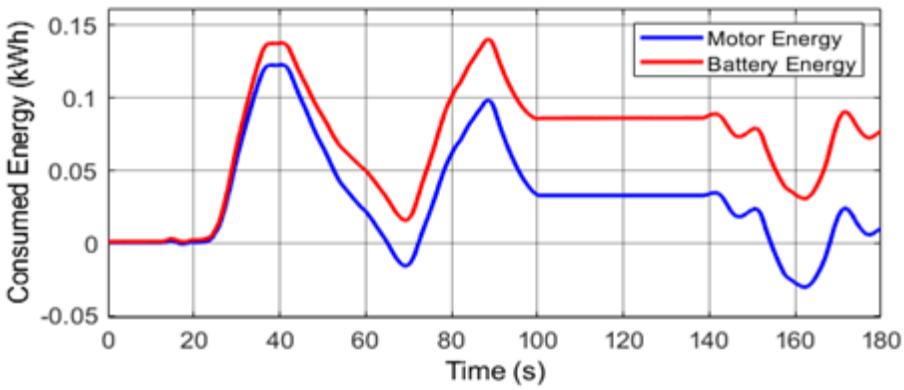

Figure 4.6.5: Electrical and Mechanical Energy [34]

power is the power loss from the battery to the electrical machine. However, the PSO-PI control strategy gains were 1243.1 and 1.3453, respectively. The electrical and mechanical energy consumed was 0.1403 kWh/km and 0.1228 kWh/1km, which is equivalent to 14.03 kWh/100 km and 12.28 kWh/100 km for the PSO-PI controller. The electrical and mechanical consumed power was 55.06 kW and 48.61 kW, respectively. Therefore, the updated power and energy consumptions for the electrical machine would be 50.68 kW and 12.81 kWh/100 km, respectively. Hence, the energy efficiency would be 91.30% and the power efficiency would be 92.04%. At the same time, electrical and mechanical power and energy were 54.99 kW, 50.62 kW, 14 kWh/100 km, and 12.80 kWh/100 km for the FOPID control strategy. Therefore, the energy efficiency would be 91.43% and power efficiency would be 92.05%.

The discharge of the Nissan Leaf battery or battery current capacity in ampere-hours (Ah) based on the drive cycle during the 180 seconds was simulated. The peak current capacity or initial capacity of the battery was 66.2 Ah. Therefore, the capacity consumed was 65.85 Ah, which was finally steady or charged to 66.02 Ah when the motor acted as a generator, and the battery drew current from the system. Therefore, the Nissan Leaf SOC at this charge is shown in Figure 4.6.6 and was 99.80% for the drive cycle test procedure. The engine speed for the hybrid vehicle was measured as 3662 rpm. This torque was managed by the developed ICE management for fuel efficiency, unlike the conventional Crafter, in which the engine was running at high speed, which is not safe for a diesel engine. Figures 4.6.7 and 4.6.8 show the simulated flow of the hybrid and conventional Crafter. The fuel flow for the conventional Crafter was 3.781 g/s, which cumulatively stands at 9.379 L/100 km, and for the hybrid was 2 g/s, which cumulatively stands at

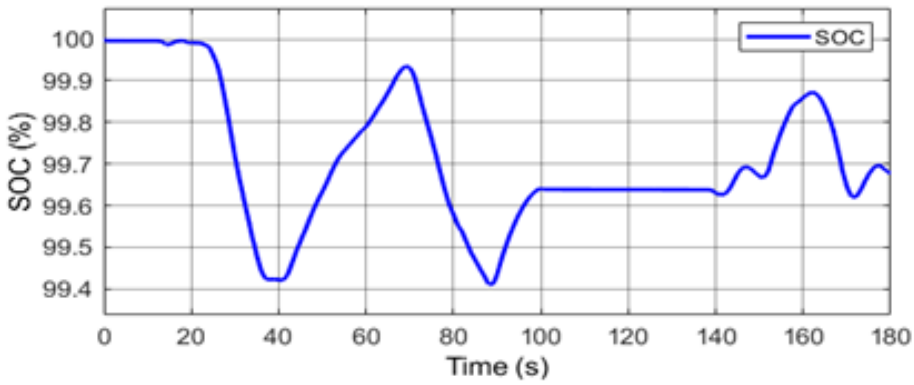

Figure 4.6.6: Nissan Leaf Battery SOC [34]

3.069 L/100 km, respectively. However, Figure 4.6.9 shows the engine power of 31.6 kW for the conventional Crafter and the motor power of 44.94 kW (46.85 kW, updated) for the hybrid vehicle.

When the vehicle accelerated, the operating torque was 67.12 Nm; when decelerated, the operating torque was −67.12 Nm, respectively. When based on the rough estimate, we can analyze the wheel torque. For the conventional drivetrain, this is translated to wheel torque of 1,198.205 Nm when the first gear ratio and the final drive ratio were 5.06 and 3.92, respectively, which is much less than 7727.186 Nm maximum or 6,069.572 Nm theoritical torque which is approximately close to the calculated torque of 1118.384 Nm when the speed was 20 km/h. The torque requirement for the hybrid powertrain was reduced to 430.105 Nm for the engine drive on a single-speed transmission with an optimized gear ratio of 7.12. This torque would be higher when considering the electrical drive torque.

The combined torque requirement for the simulated hybrid drivetrain would, therefore, be 1,538.689 Nm. Therefore, this shows that the vehicle would not slip due to the safe design. The tractive force was reasonably necessary to ensure safety and optimal performance. Based on this analysis, it can be observed that high torque is critical for the vehicle when climbing uphill and when carrying heavy cargo. Therefore, torque increase improves the performance of the vehicle dynamics when fast acceleration is required [34]. However, the experimental analysis of the vehicle was conducted based on an actual driving scenario, which was compared with the simulation results. The experimental data collected and electrical and engine drive types were used as basis for the simulation analysis. Then, the simulation and experimental and experimental results were analyzed and compared. The

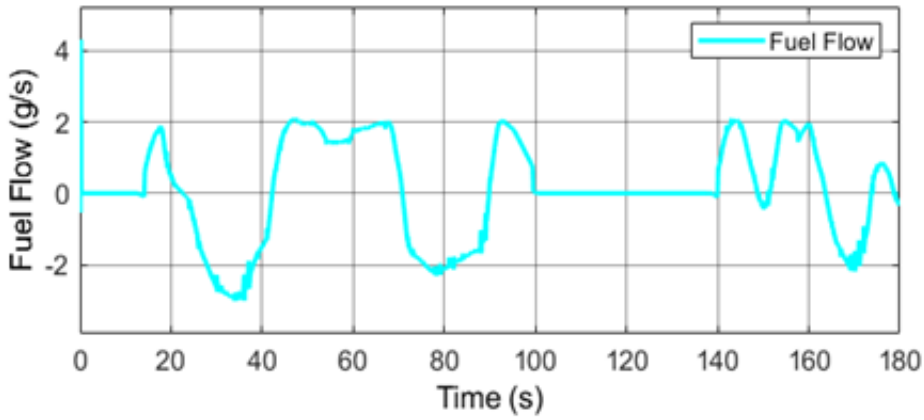

Figure 4.6.7: Hybrid Simulated Fuel Flow [34]

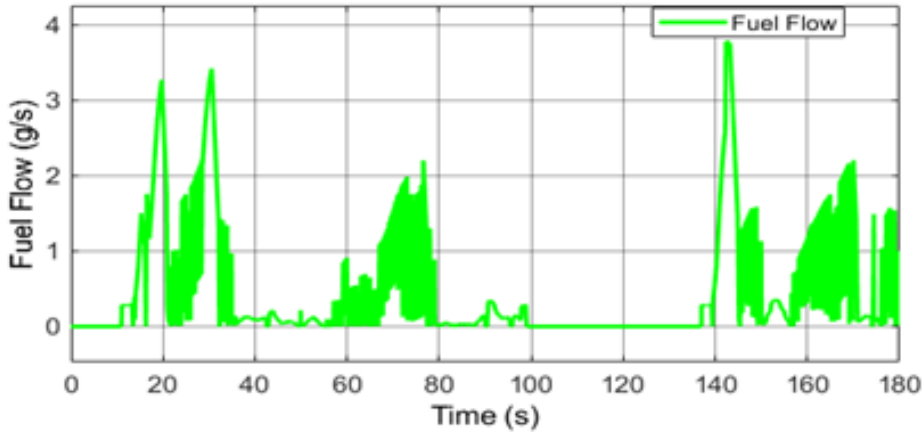

Figure 4.6.8: Conventional Simulated Fuel Flow [34]

since vehicle is not permitted above 20 km/h, the simulation speed was taken to be 13 km/h out of the 20 km/h from the experimental or measured speed. Figures 4.6.10, 4.6.11, and 4.6.12 show the simulation and experimental results. Figures 4.6.13–4.6.15 show the experimental results collected using the VCDS.

Figure 4.6.13 shows the vehicle speed in km/h, the mass air flow (MAF) measured in milligrams per stroke (mg/str), and the engine rpm. The MAF's peak value was 1138 mg/str at the engine speed of 2743 rpm. This shows a significant fuel flow at this speed. Therefore, at 180 seconds, the steady state MAF was measured to be 490 mg/str at an engine speed of 2310 rpm, while the vehicle speed was 108 km/h. Therefore, this is translated to an MAF

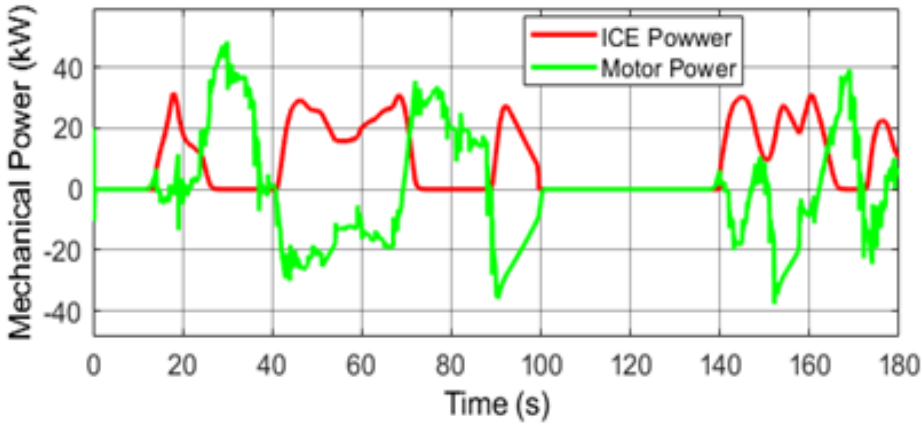

Figure 4.6.9: ICE and Motor Power [34]

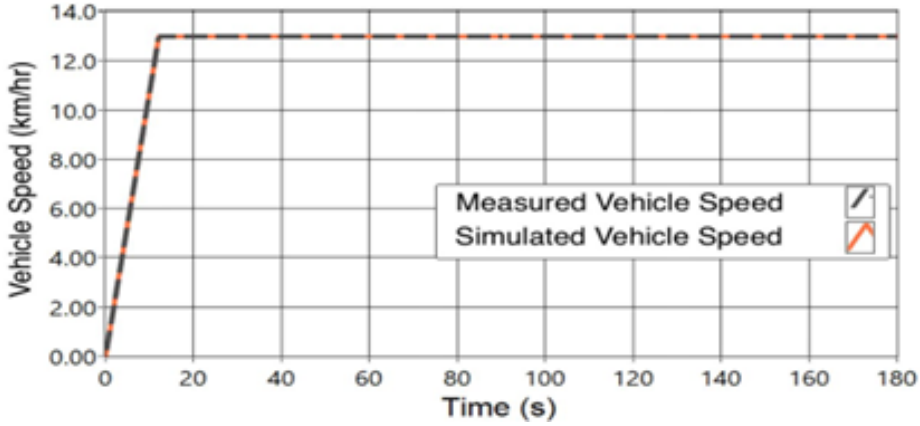

Figure 4.6.10: Experimental and Measured Speed [34]

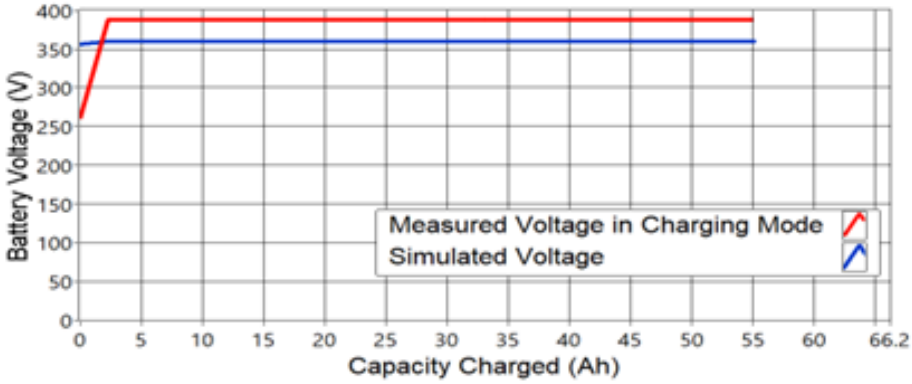

Figure 4.6.11: Experimental and Measured Voltage [34]

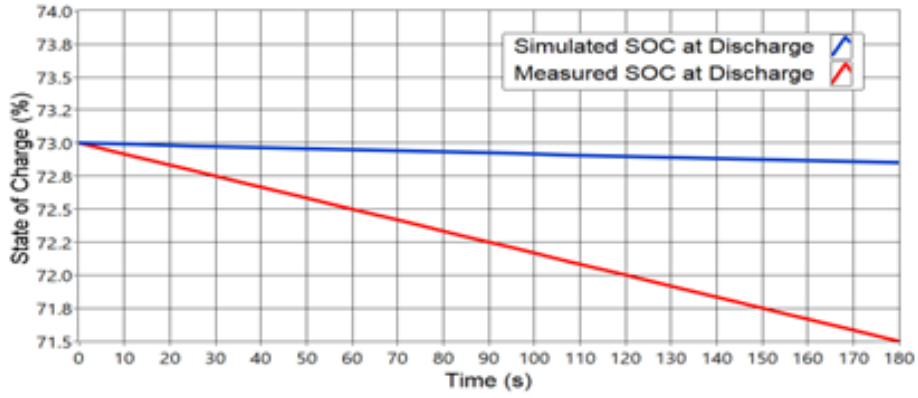

Figure 4.6.12: Experimental battery Capacity [34]

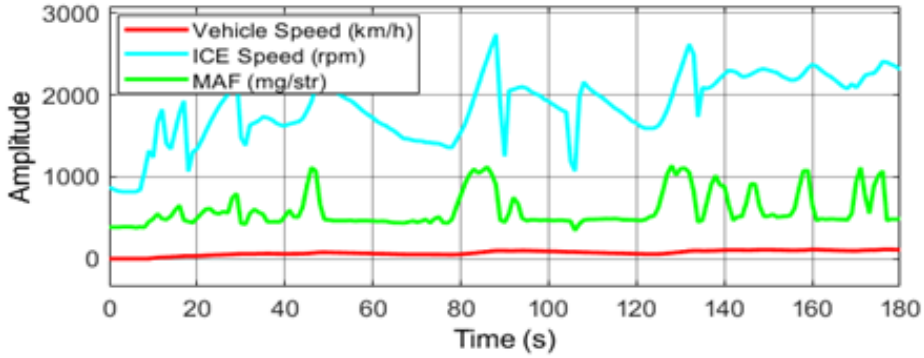

Figure 4.6.13: Mass Air Flow [34]

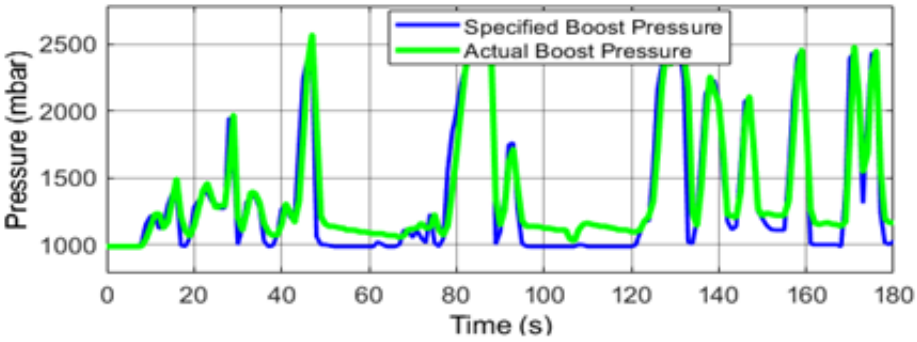

Figure 4.6.14: Pressure [34]

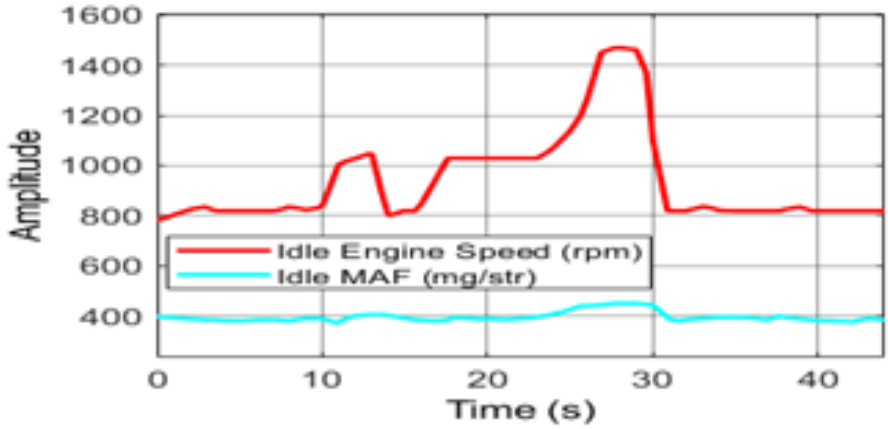

Figure 4.6.15: Ideal MAF and ICE Speed [34]

of 56.5905 g/s. Moreover, assuming the engine air-fuel ratio (AFR) is 14.5, then the mass fuel flow (MFF) was calculated to be 3.9 g/s. The volume flow rate was found to be 17.1342 L/h, which was converted to 15.5766 L/100 km at the vehicle speed of 108 km/h, given the diesel density of 820 g/L. Hence, the estimated fuel consumption of the VW Crafter was found to be 6.4181 L/100 km. The specified pressure and actual boost pressure were measured to be 1.0275 bar and 1.1645 bar when the speed of the engine was 2310 rpm at 180 seconds and rose to 2.466 bar (peak) when the engine increased to 2743 rpm, as shown in Figure 4.6.14. In an ideal situation, the MAF and engine rpm were 385 mg/str and 450 rpm, respectively, as shown in Figure 4.6.15. Tables 4.8 and 4.9 present the comparison for the fuel and energy consumption for different control strategies and the fuel consumption and CO_2 emissions for the conventional and hybrid vehicles.

Table 4.8: Fuel and Energy Consumption for Different Controls [34]

Controls	**L/100 km**	**MPG**	**km/L**	**kWh/100 km**	**[g/km]**
GA-PID	3.069	32.59	76.65	12.95	74.79
PSO-PI	2.203	45.39	106.8	14.03	53.58
FOPID	2.229	44.86	105.5	14	54.1743

The fuel consumption of 3.069 L/100 km with 74.79 gCO_2/km was achieved for the GA-PID controller. However, the PSO-PI energy management strategy achieved 2.203 L / 100 km fuel consumption or fuel economy of

Table 4.9: Fuel Consumption and CO_2 Emissions comparison [34]

Powertrains	**L/100 km**	**MPG**	**km/L**	**TFU [L]**	**[g/km]**
Conventional	9.739	10.27	24.15	0.09566	255.4122
Hybrid	3.069	32.59	76.65	0.02801	74.79

45.39 km/L with emissions of 53.58 gCO_2/km. Furthermore, FOPID reduced fuel consumed to 2.229 L/100 km or achieved 44.86 km/L with the reduction of emissions by 54.1743 gCO_2/km. While 12.95, 14.03, and 14 kWh/100 km were the energy consumption for the three energy management strategies, respectively. The diesel ICE-powered vehicle achieved fuel consumption of 9.739 L/100 km with emissions of 255.4122 gCO_2/km, while 3.069 L/100 km for the hybrid and reduced emissions to 74.79 gCO_2/km. [34].

4.6.1 Motor Thermal Stress and Battery Aging

Figures 4.6.16 and 4.6.17 show the simulation results for the temperature and cooling effect, as well as the thermal stress, plotted against time. The thermal model was incorporated into the electrical machine and the battery under the ambient temperature of 25 °C, like in Chapter Four. The liquid cooling was incorporated, which reduced the temperature to 20 °C and the battery temperature was increased to 25.25 °C. In all cases, no cooling was applied to the battery due to small temperature increases, which are within the acceptable limit. Therefore, too much cooling would do more harm than good to the battery system. The thermal stress was 1.013×10^5 Pa, which is approximately equal to the atmospheric pressure with a slight increase. According to the ideal gas law, this stress should increase with an increase in temperature and vice versa. However, the slight increase here when the temperature decreases would be due to the nonlinear nature of the HEV dynamic and other factors that might affect it.

Therefore, under the thermal with liquid cooling, new results were obtained for the vehicle. For the GA-PID, the battery energy consumed was 12.16 kWh / 100 km while the energy of the electrical machine was 12.06 kWh / 100 km, which translates to 99.17% energy efficiency. However, electrical power was found to be 47.39 kW, and mechanical power was 46.87 kW, translating to 98.90% power efficiency. While the fuel consumption and economy were 3.056 L/100 km, 32.72 km/L, 76.97 MPG, and the TFU was 0.02789 L.

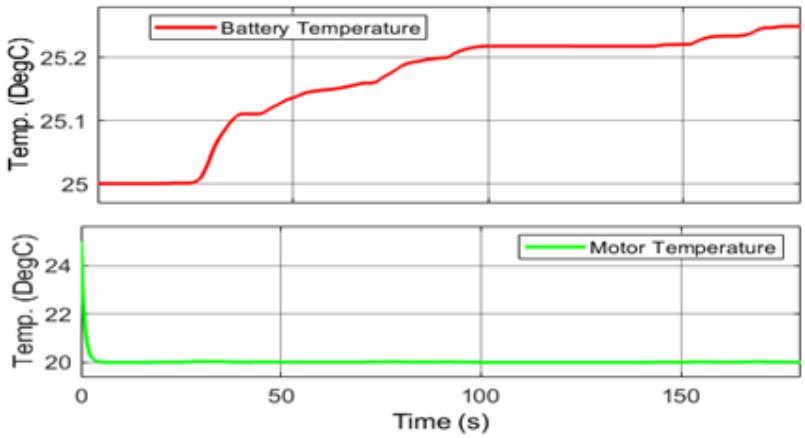

Figure 4.6.16: Motor and Battery Temperature

For PSO-PI, the energy efficiency was 99.07% when the energy consumed by electrical or battery and mechanical or electrical machine energy was 12.86 and 12.74 kWh/100 km, respectively. The electrical and mechanical power was 51.29 kW and 50.68 kW, translating to 98.81% power efficiency. While the fuel consumption and economy were 2.198 L/100 km, 45.51 km/L, 107 MPG, and the TFU was 0.02002 L.

However, due to the cooling effect and based on the results of the battery temperature, the ageing effect on the battery is negligible. Under these conditions, we do not expect an increase in resistance; therefore, the impact of degradation has been mitigated by the appropriate thermal control system and enhanced energy management strategies.

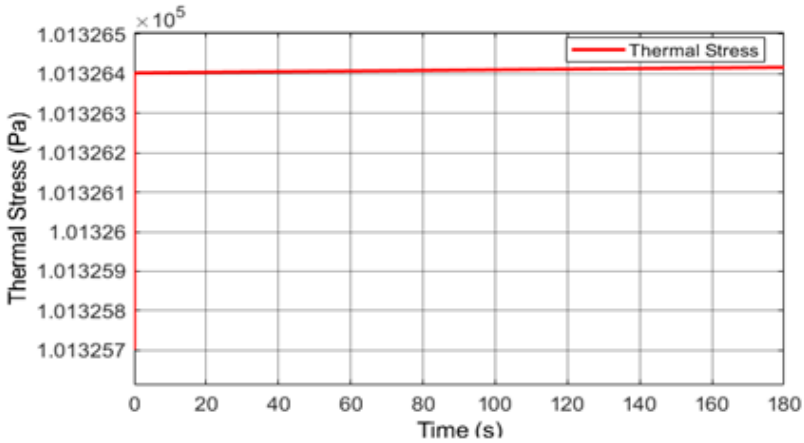

Figure 4.6.17: Thermal Stress

4.7 Discussion

The VW Crafter was successfully transformed from conventional to hybrid, significantly reducing fuel consumption, energy consumption, and CO_2 emissions. An energy management strategy using GA-PID was proposed to realize fuel economy and optimize overall hybrid powertrain performance. Hybrid and conventional powertrains consumed 3.069 L/100 km or fuel economy of 32.59 km/L and 9.739 L/100 km or 10.27 km/L fuel economy, which translated into a 68.49% reduction in fuel consumed. On the other hand, with the PSO-PI controller, we achieved a reduction in the fuel consumed by 77.38% when the consumption was 2.203 L/100 km. Furthermore, for energy consumed based on the GA-PID control strategy, the electrical and mechanical energy consumption was 12.95 kWh/100 and 12.12 kWh/100 while the electrical and mechanical power consumption was 50.80 kW and 46.85 kW, respectively. Therefore, the energy and power efficiencies would be 93.59% and 92.22%. The battery pack would be extended from the range of 128.75 km to 185.3281 km. For CO_2 emissions, there was a significant reduction in the conversion of the traditional diesel ICE-powered vehicle to a hybrid vehicle. Although, according to the datasheet of the vehicle manufacturer, the emissions range from 223 gCO_2/km to 232 gCO_2/km on the basis of the WLTP test. Hence, the simulated VW Crafter emitted 255.4122 gCO_2/km into the atmosphere which was reduced to 74.79 gCO_2/km when hybridized according to the proposed energy management strategy.

Furthermore, for the PSO-PI-based energy management strategy, the energy consumption for the battery and the electrical machine was 14.03

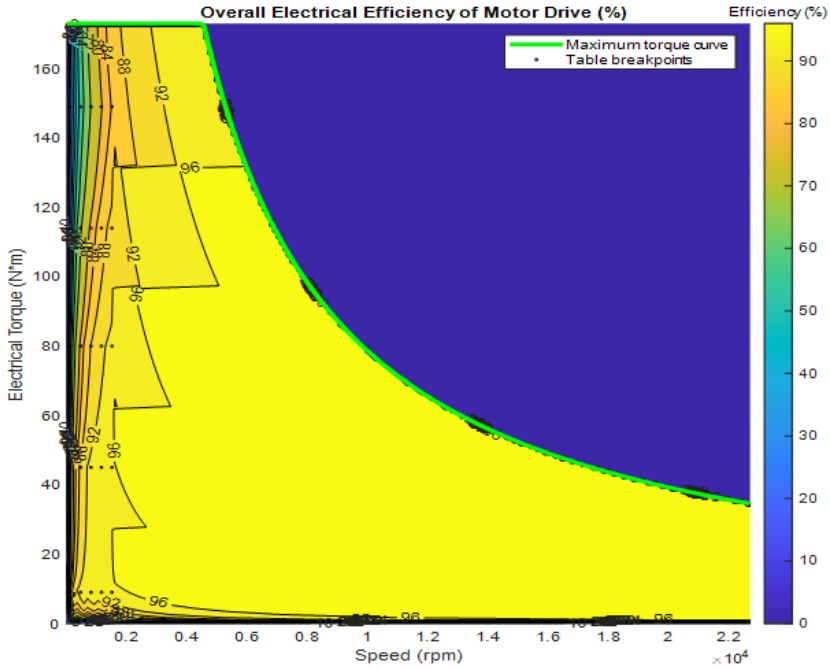

Figure 4.7.1: Eff. Map-based Torque-Speed Characteristics

kWh/100 km and 12.81 kWh/100 km while the power consumption was 55.06 kW and 50.68 kW. Hence, the efficiencies were 91.30% and 92.04%, respectively. For FOPID, power consumption for the battery and electrical machine was 54.99 kW and 50.62 kW and energy consumed for the battery and electrical machine was 14 kWh/100 km and 12.80 kWh/100 km, respectively. Then, the efficiencies were 91.43% and 92.05%, respectively. Therefore, it could be observed that the three developed energy management strategies realized efficient performance for the HEV. However, the proposed energy management (GA-PID) performed better, giving a wider km battery range and energy consumption compared to PSO-PI and FOPID. In addition, there was less energy loss, translating to better efficiency. Figure 4.7.1 shows the contour plot of the PMSM electrical machine based on the static torque-speed characteristics for the hybrid vehicle.

In terms of energy efficiency, the e-Crafter has achieved an energy consumption of 20.53 kWh/100 km, while the hybrid has achieved 12.95 kWh/100 km, which means a 7.58 kWh/100 km reduction in the energy consumption of the battery as well as reduction of 4.06 kWh/100 km in the energy consumption for the PMSM electrical machine. This means that there was a 36.922% reduction in electrical energy consumed and a 25.093% reduction in

mechanical energy. However, when comparing the manual and automated tuning processes, there was a significant improvement in the latter, such as applying the GA optimizer. We therefore adopted the results of our research reported in [80] to make this comparison. The energy consumption was recorded according to the change in the driver behavior. Table 4.10 presents the results computed based on the integral objective functions.

Table 4.10: e-Crafter Energy Consumption [80]

K_p	K_i	**IAE**	**ISE**	**ITAE**	**ITSE**	**[kWh/100 km]**
1500	2000	0.0887	0.000394	0.8553	0.0037	22.07
2000	2000	0.0780	0.000304	0.7670	0.0029	22.08
2000	1500	0.0574	0.0000165	0.5669	0.0016	22.07

In the case of manual tuning, the hybrid vehicle achieved energy consumption of approximately 22.07 kWh/100 km. This proved the significance of applying an optimization algorithm for optimal fuel consumption and improved performance in EVs and HEVs applications.

The experimental OBD-II dataset was measured from the same engine type of VW group having almost similar configurations like fuel system, fuel type, etc. Hence, the exact fuel consumption may not be realized, but we used it as a benchmark to estimate the fuel consumed of the reference vehicle. This is because the onboard computer data can not be realistic, which may not provide exact data. The computational approach is used for accurate results [48]. Therefore, if the MAF is the air mass flow [g/s], AFR is the actual air fuel ratio [14.5 in our case], FD is the fuel density [g/L], then knowing the MAF, engine rpm and vehicle speed, the following formulations in equation (4.7.1) can be used to calculate the fuel economy as expressed in [179] as follows:

$$\begin{cases} \text{Fuel Consumption [L/100 km]} = \frac{\text{Fuel Flow [L/h]}}{\text{Vehicle Speed [km/h]}} \cdot 100 \\ \text{Instant. Fuel Consumption [L/km]} = \frac{\text{Fuel Flow [L]}}{\text{Vehicle Distance [km]}} \\ \text{Fuel Fow [L/h]} = \frac{\text{MAF} \cdot 3600}{\text{AFR} \cdot \text{FD}} \end{cases} \tag{4.7.1}$$

However, if MFF [g/s] or MAF [g/s] is available, we can determine the fuel consumed. Based on the measured data, the MAF was found to be 56.5905

g/s when the MFF was 3.9 g/s. Hence, the volume flow rate was calculated to be 17.1342 L/h, which is equivalent to 15.5766 L/100 km. Therefore, the estimated fuel consumption for the Crafter would be 6.4181 L/100 km. This result was as expected, taking into account the operating conditions and the vehicle speed. The average fuel consumption for the VW Crafter of the same engine type was measured to be 10.582 L/100 km while the same version manufactured in 2020 had a fuel consumption of 8.8 to 10 L/100 km on the basis of WLTP drive cycle. The mass flow of the simulated VW Crafter was 3.781 g/s which is equivalent to 9.739 L/100 km cumulatively. Therefore, this shows that we have achieved good design with classical PID controller. While in the the hybrid, we have achieved 3.069 L/100 km for the GA-PID at [70.6657, 0.3339, 72.4406] control gains. Although, we proposed only ITAE as the objective function, the GA-PID could yield another optimal gains if we considered all the four sets of fitness values computed in Table 4.11. With thermal control, the fuel consumption was reduced by 68.62% while the CO_2 emission was reduced to 74.46 gCO_2/km, translating to a 70.84% reduction for the proposed strategy.

Table 4.11: GA-PID Gains According to Four Different Fitness Values [80]

Parameters	**PID**	**IAE**	**ISE**	**ITAE**	**ITSE**
K_p	60	179.0359	87.6310	100.9146	37.2668
K_i	10	0.0060	0.5625	0.0255	0
K_d	60	251.2025	164.3265	160.2977	4.3553

The MAF and engine speed were measured in an idle situation. Under idle conditions, the vehicle was stationary, i.e. at 0 km/h. The speed of the engine was measured to be 819 rpm when the peak speed was 1470 rpm to keep the flow of the fuel. Therefore, the MAF and MFF were 15.7644 g/s and 1.0872 g/s at this speed. The simulated fuel flow (MFF) was 1.062 g/s when the simulated engine idle speed was 800 rpm. Then, the simulated MAF would be 15.399 g/s. This shows the vehicle was performing in almost the same condition under idle conditions. Moreover, the engine's speed and pressure, i.e., specified pressure and actual boost pressure, are factors affecting the engine's performance. The specified pressure and actual boost pressure were measured to be 1.0275 bar and 1.1645 bar when the speed of the engine was 2310 rpm at 180 seconds. The turbocharger spun faster as the engine speed increased to 2743 rpm, generating more boost pressure and rising to

2.466 bar. Therefore, under this condition, the specified boost pressure is less than the actual boost pressure, which would decrease the engine efficiency and cause other damage to the engine. Hence, it is essential to monitor the boost pressure and adjust its regulator as required to keep the specified boost pressure. Further, engine management should be implemented to control the speed of the engine for the conventional Crafter to avoid potential damage due to the high rpm. Diesel ICEs should not run at high speed [34].

The experimental measurements were used as the basis for the design and development of the simulated vehicle. However, not all the measured data was used for that purpose because not all of them were available. Therefore, since we know the hybrid vehicle components and their specifications from the manufacturer, we adopted the fixed parameters to design and develop the vehicle at the simulation level. This may not always provide accurate results. Therefore, we implemented an enhanced PID control strategy for energy management to realize the vehicle's optimal performance based on the standard real-world driving scenario. Hence, after we determined the measured results, we tested the simulated vehicle's performance under the same conditions as the experiment. In other words, we designed the simulation model from some of the available experimental data. This gives the basis for the comparison between the simulated and experimental results. The online DAQ approach was based on HIL and implemented on the vehicle's electrical drive was used for the vehicle's CAN bus analysis. The DAQ system was implemented using the standard CAN frame protocol, J1939, with a novel approach that interconnected four sets of Net CAN Plus 110 hardware. Consequently, all NetCAN Pluses and GPS modules ran their own HTTP server. To establish a connection, the host PC's static IP address was configured, and an Ethernet cable linked the PC to the devices' network. Since the network used a mixed configuration, we specified the MAC addresses of the devices and assigned static IP addresses provided by the DHCP server. Therefore, each device on the network was assigned the IP address as explained in subsection 4.3.1.

The vehicle was tested at 13 km/h speed for the electrical drive test, and this measured value was compared with the simulated speed. The vehicle control strategy controlled the vehicle speed using MATLAB. When the vehicle was parked and charged, the measured voltage was 388 V. This means it is 15.20 V to reach its maximum. This measured value was obtained due to the charging condition when it was increased from the initial voltage of 260 V (we assumed minimum safe discharged voltage). The peak voltage of the Nissan Leaf voltage is 403.2 V, and the nominal voltage is 360 V. The

simulated voltage was measured and steady at 360 V. Based on the WLTP drive cycle, the Nissan Leaf voltage was measured to be 362. 6 V maximum and a minimum of 355.8 V. The measured battery capacity was 55 Ah at 388 V. This means it is 11.2 Ah less to reach its maximum. These measured physical results were decoded using the database (CAN DBC) file from the raw values of CAN messages and identified through the CAN ID. One of the difficulties was identifying all the messages across the CAN network due to error frames. However, it was easy to identify CAN bus messages for the measurement from the battery, which was used as the basis of our analysis in both the simulation and experiment aspects.

During the discharging mode, the measured initial SOC of the battery 73%, as noted from the onboard computer for the electrical drive, and therefore, we set the initial SOC for the simulation to compare the performance. Hence, 71.5% and 72.5% at 180 s were obtained as the measured and simulated SOC. The Nissan Leaf current was measured to be 180 A based on the decoded message from the raw CAN message, and therefore, each cell can be 90 A. In addition, the battery's current capacity was measured to be 53.5 Ah when the initial capacity was 55 Ah. Therefore, the remaining battery capacity would be 23.34 kWh when the total capacity of the Nissan Leaf battery is 24 kWh. This means that even if we cannot identify the battery capacity over the CAN network, it was calculated based on the measured data from the current capacity. The mathematical formulations for this have been explained in Chapter Three. The initial current capacity was also set to 55 Ah to compare with the experiment, and the final capacity was 54.7 Ah. Hence, we applied the same method for the experiment, and the remaining capacity was 23.87 kWh. Therefore, the simulated and measured battery capacity was 23.34 kWh and 23.87 kWh out of the 24–kWh rated capacity.

One of the main objectives of this research was to employ the appropriate control algorithm to manage the power and energy at an optimal level to give a broader range of kilometers covered by the vehicle. Although it was seen that the proposed controller is better than other controllers, such as the PSO-PI and FOPID, in terms of the energy consumption and efficiency of the vehicle, we proposed a statistical method based on Wilcoxon signed rank test to justify how effective the proposed control algorithm is compared to others on the basis of ITAE fitness function. Table 4.12 presents the Wilcoxon signed rank test for the objective functions for GA-PID and PSO-PI controllers. Therefore, to use the Wilcoxon test method, we assumed that the data is not normally distributed (for non-parametric technique) and that the research hypothesis is one-sided. Let W be the Wilcoxon ranks which is called a

critical value read from a table; W^+ be the sum of the positive ranks; W^- be the sum of the negative ranks. Therefore, according to Table 4.12, we have $W^+ = 0$ and $W^- = 7 + 6 + 5 + 2 + 4 + 3 + 1 = 28$. Hence, the test statistics, W is as expressed in [34] as follows:

$$W = min(W^+, W^-) = min(0, 28) = 0 \tag{4.7.2}$$

Let the sample size (n) be $n = 7$ based on the number of samples from the Table. Therefore, $W = 4$ from the standard Table. Let the null hypothesis be (H_0) and the research hypothesis (H_1). The critical value or Wilcoxon ranks is such that it either supports the research hypothesis or the null hypothesis. In other words, we reject the null hypothesis H_0 if $W \leq 4$. Hence, the research is true since $0 \leq 4$. This means that there was a significant increase in the fit value from the GA technique to PSO, proving that the system was more stable based on the proposed control strategy. Therefore, the GA-PID outperformed the other control techniques, taking into account all the performance measures.

Table 4.12: Wilcoxon Signed Rank Test for Fitness Values [80]

n	**GA-PID**	**PSO-PI**	**Difference**	**Ranks**	**Singed Ranks**
1	18.50	136.24	−117.74	7	−7
2	18.13	113.48	−95.35	6	−6
3	18.63	94.77	−76.14	5	−5
4	31.04	86.19	−55.15	2	−2
5	18.37	85.37	−67	4	−4
6	19.02	83.44	−64.42	3	−3
7	31.48	83.33	−51.85	1	−1

4.8 Conclusion

In this research, the development of a VW Crafter hybrid powertrain with a novel DAQ system has been presented for the first time. The control strategy proposed as an energy management strategy demonstrates robust performance, realizing optimal fuel consumption and reduced CO_2 emissions. The 2011 Nissan Leaf battery pack with a rated capacity of 24 kWh and

more than 90 kW output power was integrated with a 2.0 TDI engine with higher output torque and better fuel economy that had replaced an older 2.5 L TDI engine characterized by turbo failure, leading to its redesign in 2010.

The proposed control strategy reduced the fuel consumption of 9.739 L/100 km for the mechanical diesel powertrain to 3.069 L/100 km when transformed to the electrified hybrid powertrain, and this means a reduction in vehicle fuel consumption by 68.488% based on the WLTP test procedure and a reduction of 7.58 kWh/100 km in energy consumption. This means 36.92% reduction in transforming from electric to hybrid. Moreover, the CO_2 emissions was reduced by 70.718%. However, with thermal control, the fuel and energy consumption were reduced to 3.056 L/100 km and 12.16 kWh/100 km, translating to 68.62% and 25.08%, respectively. While the CO_2 emission was reduced to 74.46 gCO_2/km, translating to a 70.84% reduction for the proposed strategy. The GA-PID control outperformed the PSO-PI and FOPID control strategies, achieving better efficiency and battery range extension. In addition, this research demonstrates an excellent efficiency gain due to the energy recovery during the generating action of the electrical machine in terms of the tractive energy computed in kWh/100 km in Chapter Two required for the vehicle. The total consumption was 21.354 kWh/100 km, and the actual consumption with thermal control was 12.16 kWh. Therefore, the design in the hybrid mode achieved 9.194 kWh/100 km energy gain. This means a 43.06% energy efficiency gain mode due to good design, functional energy recovery mechanism and optimized energy management system achieved in this study.

The proposed energy management was applied to optimize the vehicle's efficiency and robustness, reduce the development cost, improve safety, and extend range, taking into account nonlinear effects that may be present and affect vehicle performance. Hence, the simulation results show that the control algorithm could serve as a valuable and alternative control scheme for the robust performance of the designed vehicle in terms of optimal fuel economy and minimized CO_2 emissions. Therefore, this indicates that the proposed controller is a valuable and alternative control scheme from the aspect of optimal consumption to the CO_2 emissions for electric and hybrid vehicle applications. Moreover, the online vehicle monitoring system based on NetCAN Plus 110 hardware is a relatively new and innovative approach that facilitates data collection for the vehicle MIL design and control implementation in the simulation environment. This methodology can help monitor the vehicle even remotely to ensure safe driving conditions.

Chapter 5

Summary, Conclusion, and Recommendations for Future Development

This chapter presents the summary of theses, contributions, and the conclusion of the dissertation.

5.1 Summary

5.1.1 Thesis I: Energy Storage Modeling and Traction Analysis

The contribution of this thesis is that it presents the modeling of the 2011 Nissan Battery pack. The complex battery pack simulation provides a detailed simulation of each cell and module. Therefore, to reduce the complexity of the entire pack due to low simulation time and to make the system faster, the detailed model is compressed into a system-level model that replicates the detailed model behavior in real-time and provides an effective simulation environment for the battery management system. The battery has been simulated over a realistic current profile. The battery's thermal performance and capacity fade (degradation) over time and number of life cycles have been investigated. The simulated battery could deliver over 90 kW and operate at a safe temperature of 29.30 °C. The simulated results have been validated with real test data. The simulated battery still maintains 60.3% remaining capacity in its first life with 56% fading rate per 1000 cycles.

Another contribution is that it provides a detailed analysis of the tractive force required to propel the vehicle. The excess tractive force for the VW Crafter has been presented on the basis of Taylor series. The excess force has been formulated in the frequency domain on the basis of the Laplace transformation. The traction force depends on the resistance forces acting on the vehicle, such as:

- Wind resistance force.
- Rolling resistance force.
- Grade resistance.
- Acceleration resistance force.

The analysis of these forces gives rise to the investigation of the power and energy required to propel the vehicle on the basis of the dynamics of the vehicle, along with the factors affecting the power and energy demand, such as the vehicle size, mass, frontal area, battery and engine size, and so on. Therefore, this thesis provided an idea for the design of the conventional, electric, and hybrid VW Crafter. The tractive powers based on the resistance forces have been analyzed:

- The tractive power required to overcome the wind resistance force.
- The tractive power needed to overcome the rolling resistance force.
- The tractive power required to overcome the grade resistance.
- The tractive power needed to overcome the acceleration resistance force.

This thesis analyzed the traction required based on the total tractive power necessary for level and sloppy road conditions. The total traction torque was also investigated on the basis of the vehicle's gear ratios and tire radius. Based on this analysis, this thesis demonstrates a safe vehicle design without slipping. The total traction energy has been analyzed per distance covered under a real-world driving trajectory. In summary, for the first time, this thesis has investigated the optimal design of the VW Crafter as a trade-off between vehicle size, battery size, engine, vehicle mass, driving range and consumption. A comprehensive sensitivity analysis, based on a Tornado chart, has been presented to investigate how changes in key parameters, such as vehicle mass, affect energy consumption at higher speeds, including those

based on the WLTP, thereby extending the applicability and relevance of our model to real-world tasks. Moreover, the modeling approaches adopted related to the dynamics of the proposed vehicle have been compared using a SWOT analysis to confirm the reliability and understanding of our chosen methods. Therefore, the analysis of the exact power source of the proposed vehicle has been presented as a prerequisite condition that ensures the safety of the vehicle, driver, and cargo. In nutshell, the main contributions of thesis I are as follows:

1. The thermal performance and capacity fade (degradation) of the 2011 Nissan Leaf battery over time and number of life cycles have been investigated in its first and second life cycles, using a realistic current profile at a 5 C-rate. The simulated battery still maintains 60.3% remaining capacity in its first life with a 56% fading rate per 1000 cycles at 29.30 °C operating temperature.

2. For the first time, this thesis investigates the optimal design of the VW Crafter as a trade-off between vehicle size, battery size, engine, vehicle mass, driving range and consumption.

5.1.2 Thesis II: Electric Drives Dynamics and e-Crafter Simulation

This thesis has presented the dynamical modeling of electrical drives based on PMSM and BLDC electrical machines and the simulation of the VW Crafter pure electric version for the first time in the literature. The dynamic model of the electrical drives based on the two different levels model has been developed. These models are as follows.

- Simplified model-based PMSM and BLDC drives.
- Detailed or complex model-based PMSM and BLDC drives.

An FOC complex control strategy was proposed to regulate the detailed PMSM drive, while a six-step commutation logic or trapezoidal complex control was proposed to regulate the BLDC drive. Meanwhile, the simplified model was based on the torque-speed envelope. The outer loop control strategy was used to control the speed of the vehicle and provide the load demand to the power source. Therefore, these drives were used to model the VW Crafter at two different modeling levels:

- Simplified e-Crafter-based simplified PMSM and BLDC drives.
- Extended e-Crafter-based detailed or complex PMSM and BLDC drives.

The traction battery and the electrical machines were extended to include the heat effect with control only for the electrical machine (liquid cooling), represented by the thermal mass, which is related to the heat flow, specific heat of the material, mass, temperature, and time and subjected to an ambient temperature of 25 ℃. Both results with thermal and control (liquid cooling) and without thermal effect were compared. This thesis showcases the importance of simplifying a complex engineering concept to an abstract level. With this innovative approach, the efficiency of the EV has been improved. Energy loss has been minimized, and the cost of implementation in real life would have been reduced. The energy and fuel consumption for the e-Crafter has been optimally realized, which is close to real-world consumption compared to a full-scale model in a complex domain. Therefore, this thesis has made the following significant contributions:

1. Thesis II designs different physical models of the VW Crafter (simplified and extended) levels, considering technical differences and complexity levels. The simplified model accounts for the transmission losses and the computational burden of the analytical approaches adopted in the existing literature. This method enables a more effective and accurate investigation of the optimal fuel economy of the proposed vehicle. The extended model takes into account a full-scale model of the components of electric vehicles.

2. An energy efficiency of over 90% has been achieved, reducing the energy consumption by 16.81% for the electric mode compared to the measured data, which exceeds many existing studies.

5.1.3 Thesis III: Development of VW Crafter Hybrid Vehicle

This thesis presents the final stage of the development of the hybrid powertrain using the model-based approach (MIL method) transition and physical assembly process of the VW Crafter from the conventional diesel-powered drivetrain to hybrid, introducing a novel methodology of CAN bus analysis of experimental vehicles acquired through NetCAN Plus hardware devices (HIL method). This new approach formed the basis for vehicle transformation

for optimal consumption and reduction of CO_2 emissions. The physical assembly process of the VW Crafter started from construction to assembly, as investigated and led by a research group of the Faculty of Engineering in [30]. The engineering faculty unveiled the real transformation of this vehicle within the framework of the TKP project funding scheme. The vehicle is allowed a maximum speed of 20 km/h. Therefore, the hybrid vehicle was tested in the range of 0-20 km/h (precisely 13 km/h). However, we tested the simulated vehicle at different inputs based on standard road profiles, such as NEDC in the case of pure electric (at 50 km/h) and WLTP in the case of hybrid (at 45 km/h), to investigate its performance under standard real-world impact. The WLPT was proposed in the case of the hybrid because it is closer to the real-world driving scenario, hence the comparison with the real-world measured data. In summary:

- In thesis III, the mechanical powertrain of the conventional VW Crafter was developed. The vehicle was powered by a 2.0 L TDI diesel engine with a maximum power of 103 kW (DAUA engine code). A 6-speed manual gearbox was incorporated, with disc friction clutch along with the gearbox controller. A classical PID controller was used to control the speed of the vehicle and compute fuel consumption and CO_2 emissions.

- The measured data from the engine drive unit, such as mass airflow, speed, engine rpm, etc., were collected with the VCDS-compatible cable as an interface between the OBD-II port and a host PC. The data collected was used as the basis to compute the optimal consumption of the vehicle's engine drive.

- The hybrid vehicle was developed with an optimal energy management system. An enhanced PID controller was implemented for the vehicle to reduce fuel consumption and CO_2 emissions. The experimental and simulation results were compared to verify and justify the transformation of this vehicle in the field of electric and hybrid cars, in general.

- The online DAQ system implemented via standard CAN frame protocol such as J1939, using a novel approach of interconnecting four sets of NetCAN Plus 110 hardware, WLAN, FL switch, and GPS device was used for the data collection. Thus, all the Net CAN pluses and GPS modules ran on their HTTP server. Hence, the static IP address of the host PC was set, and was connected to the devices network with

an Ethernet cable. Since the network used a mixed configuration, we specified the MAC addresses of the devices and assigned static IP addresses provided by the DHCP server. Therefore, each device in the network was assigned an IP address. The raw CAN data were acquired using an application developed in LabVIEW software on the host PC, saved in a CSV file, and decoded using the DBC file into physical values.

- The energy management strategy was developed on the basis of a PID-based GA optimization problem to enhance the efficiency of the system, calculate optimal fuel consumption and reduce CO_2 emissions for the VW Crafter. The GA was proposed due to its global search capability, ability to solve multi-objective optimization problems, and fast convergence. Furthermore, FOPID and PSO-PI were developed to verify the efficacy of the proposed energy management strategy. The function of the proposed energy management is to allocate the load demand to the power sources.

- The traction battery and the electrical machines were extended to include the effect due to thermal stress with control only for the electrical machine (liquid cooling), represented by the thermal mass, which is related to the heat flow, specific heat of the material, mass, temperature, and time and subjected to an ambient temperature of 25 ℃. Both results with thermal stress and control (liquid cooling) and without thermal effect were compared. Therefore, without the thermal model, the proposed energy management strategy reduces fuel consumption, CO_2 emissions, and energy consumption by 68.488%, 70.718%, and 36.92%, respectively. With the thermal model (employing liquid cooling to control heat), the energy management strategy reduces fuel consumption, CO_2 emissions, and energy consumption by 68.620%, 70.840%, and 25.080%, respectively.

Therefore, this thesis has made the following significant contributions:

1. This thesis demonstrates a successful transformation of the VW Crafter for the first time from conventional to hybrid electrified powertrain, focusing on the realization of optimal tracking performance and robustness.

2. Although the VW Crafter has been considered in [30], it was based on the physical transformation and assembly process of the vehicle.

This thesis proposes an improved PID controller to optimize system efficiency for optimal fuel economy and reduced CO_2 emissions. Thus, this research reduces fuel consumption by 68.620%, CO_2 emissions by 70.840%, and energy consumption by 25.080%.

3. Compared to the required traction of 21.354 kWh/100 km, this thesis has achieved an energy gain of 5.124 kWh/100 km and 9.194 kWh/100 km based on the enhanced PID controller, translating to a 24% and 43.06% efficiency gain for the electric and hybrid modes.

4. Contrary to the existing literature, for example [54], [55], [56], [48], [57], [58], [59], [60], this thesis uses LabVIEW software in the framework of a new methodology to establish online vehicle CAN bus data analysis facilitated by NetCAN plus 110 hardware based on a standard frame J1939 CAN protocol.

5.2 Conclusion

This dissertation has presented the development of a hybrid powertrain for VW Crafter for the first time. The research has applied a novel data collection approach facilitated by NetCAN Plus hardware to decode the CAN bus message, which is based on the HIL method, to investigate the vehicle performance by leveraging the acquired experimental results to design the vehicle on the basis of the MIL method, creating the control loop in the MATLAB/Simulink/Simscape simulation environment using an enhanced PID control algorithm (GA-PID) as an energy management strategy. Despite the complexity and nonlinear effects of the EV and HEV dynamics, the proposed energy management demonstrated robust performance. In addition to this control strategy, PSO-PI and FOPID were applied to compare performance. The results obtained proved the superiority of the proposed control algorithm as a valuable and alternative control scheme in transportation electrification.

In addition, this research presented a tractive force analysis of the proposed study, of which there are only a few similar studies. The conventional, pure electric, and hybrid versions of the vehicle were designed for the first time. The practicality of the PID control motivated its adoption as a control candidate in this research. Therefore, applying a popular metaheuristic technique, GA, to optimize its gains for efficient energy management for the first time is a valuable contribution that has yielded novel solutions in hybrid vehicle applications.

Investigating the 2011 Nissan Leaf battery temperature and its degradation or capacity fading over time and number of life cycles at the system level, with validation of the real data analysis adapted, is another viable contribution to existing studies. In general, fuel efficiency has been investigated and compared with and without thermal effects. Therefore, designing electrical machines and traction batteries for industrial vehicle size with effective thermal control is an alternative approach to efficient transportation electrification, including other traction purposes.

5.3 Recommendations for Future Development

This dissertation has applied a novel data collection approach facilitated by Net CAN Plus hardware to collect the vehicle CAN bus data, which is based on the HIL method, to investigate the vehicle performance by leveraging the acquired experimental results to design the vehicle on the basis of MIL method, creating the control loop in MATLAB/Simulink/Simscape simulation environment using an enhanced PID control algorithm (GA-PID) as an energy management strategy, reducing the fuel consumption and CO_2 emissions. The traction requirement was investigated, and the vehicle's electric, conventional, and hybrid powertrains were developed. The following recommendations are made for the future development:

1. The online vehicle monitoring system was implemented for the proposed vehicle (VW Crafter 35 EIKA MR103, 2020 manufactured). The measured data mainly focused on the electrical drive via the novel Net CAN Plus approach. Since different control units are equipped with various sensors and actuators, all control units are connected via CAN bus. However, the CAN gateway, which manages the data packages, acts like a firewall on a network where multiple CAN buses are distributed. Therefore, not all data are sent to the network; only critical ones were sent for the vehicle to operate. The exact data package ID was unknown, so we put the ECU into diagnostic mode via VCDS. ECU does not send all sensor data in broadcast style if not in diagnostic mode. Therefore, data measurement for the engine drive via the Net CAN interface deserves critical attention in future studies.

2. The vehicle monitoring via NetCAN Plus was only possible when the host computer was inside the Crafter. Thus, extending the DAQ

process to enable the vehicle CAN bus analysis remotely while driving the Crafter is a promising area for future research both in present and future electric cars.

3. The integer order PID controller has been adopted as the vehicle controller due to its intuition for practical use, making it a suitable control candidate for the Crafter. This dissertation considered three variants of PID control strategies as energy management for optimal fuel economy and CO_2 emissions. Other variants can be proposed to compare performance, such as sigmoid PID (SPID), neuro-endocrine PID (NPID), nonlinear PID, and adaptive PID.

4. The simplified BLDC electrical drive performed well in terms of system efficiency without the thermal model but slower when the thermal model was incorporated which needs further investigation. In addition, the detailed model of the BLDC drive needs further improvement. There could be a more significant energy recovery during the generating action of the electrical machine, which made the battery draw a high current and thus give negative energy, and this is possible which could be due to either one of the following:

    - Regenerative braking effect. In this case, the interpretation of energy consumption is the absolute quantity of consumed energy.
    - The battery system level model is not suitable for the complex BLDC drive. Therefore, the detailed model of the VW Crafter based on the BLDC drive with a detailed 2011 Nissan Leaf pack is another promising research direction to achieve the optimal performance of the electrical machine with the appropriate battery model in all its cycles of operation (four quadrant operation) as summarized in [159].

5. In this research, a traditional HEV powertrain with ICE was considered, but it still emits toxic gases into the environment. Therefore, other energy sources, such as fuel cells, super-capacitors, superconducting magnetic energy storage, solar photovoltaics, etc., can be combined with the Nissan Leaf battery pack to power the vehicle without the need for the ICE. This is popularly known as a fuel cell hybrid electric vehicle (FCHEV), a crucial research area that has recently gained global attention.

6. Although this research was not aimed at optimizing the mechanical powertrain of the conventional Crafter, an engine management strategy is necessary to keep the diesel ICE of the vehicle at an appropriate or desired rpm. In addition, electronics boost controllers can be implemented to regulate the actual boost pressure to ensure consistent pressure difference for optimal performance, and this deserves a special attention as a promising future research direction.

References

[1] European Commission. *https://climate.ec.europa.eu/eu-action/transport-decarbonisation/road-transport/light-duty-vehicles$_e$n*. EIB Climate Survey, (accessed on 23 May 2025), 2023.

[2] Xiao Yu et al. "Decarbonization potential of future sustainable propulsion—A review of road transportation". In: *Energy Science & Engineering* 12.2 (2024), pp. 438–455. DOI: https://doi.org/10.1002/ese3.1434.

[3] Uwe Tietge Jan Dornoff Victor Valverde Morales. *On the way to 'real-world' CO2 values? The European passenger car market after 5 years of WLTP*. Tech. rep. European Environmental Agency (EEA) and spritmonitor.de, 2024.

[4] Pengfei Fan et al. "Fuel consumption estimation in heavy-duty trucks: Integrating vehicle weight into deep-learning frameworks". In: *Transportation Research Part D: Transport and Environment* 130 (2024), p. 104157. DOI: https://doi.org/10.1016/j.trd.2024.104157.

[5] Wawrzyniec Golebiewski et al. "Reducing the fuel consumption of an hybrid electric vehicle with the use of model predictive control-case study". In: *IEEE Transactions on Vehicular Technology* 72.9 (2023), pp. 11458–11468. DOI: https://doi.org/10.1109/TVT.2023.3266829.

[6] AM Ţıţu et al. "Mathematical Modeling of the Normal Fuel Consumption of Certain Vehicles". In: *IOP Conference Series: Materials Science and Engineering*. Vol. 1303. 1. IOP Publishing. 2024, p. 012051. DOI: 10.1088/1757-899X/1303/1/012051.

[7] C Minzatu et al. "Research concerning the autonomy of the electric vehicles, simulated and measured, in the case of driving at the low and the medium speed, specific to the WLTC test." In: *IOP Conference Se-*

ries: Materials Science and Engineering. Vol. 1303. 1. IOP Publishing. 2024, p. 012003. DOI: 10.1088/1757-899X/1303/1/012003.

[8] Crownoil.co.uk. *https://www.crownoil.co.uk/guides/euro-6-emissions-standards/*. Crown Oil, (accessed on 19 June 2025).

[9] Jozsef Menyhart. "Overview of Sustainable Mobility: The Role of Electric Vehicles in Energy Communities". In: *World Electric Vehicle Journal* 15.6 (2024), p. 275. DOI: https://doi.org/10.3390/wevj15060275.

[10] Muhammad Candra Saputra and Erna Andajani. "Analysis of Factors Influencing Intention to Adopt Battery Electric Vehicle in Indonesia". In: *ADI Journal on Recent Innovation* 5.2 (2024), pp. 100–109. DOI: https://doi.org/10.34306/ajri.v5i2.993.

[11] Ruixue Liu et al. "A cross-scale framework for evaluating flexibility values of battery and fuel cell electric vehicles". In: *Nature communications* 15.1 (2024), p. 280. DOI: https://doi.org/10.1038/s41467-023-43884-x.

[12] Fabian Rücker et al. "Battery Electric Vehicles in Commercial Fleets: Use profiles, battery aging, and open-access data". In: *Journal of Energy Storage* 86 (2024), p. 111030. DOI: https://doi.org/10.1016/j.est.2024.111030.

[13] Turki Alsuwian et al. "A Review of Expert Hybrid and Co-Estimation Techniques for SOH and RUL Estimation in Battery Management System with Electric Vehicle Application". In: *Expert Systems with Applications* (2024), p. 123123. DOI: https://doi.org/10.1016/j.eswa.2023.123123.

[14] R Punyavathi et al. "Sustainable power management in light electric vehicles with hybrid energy storage and machine learning control". In: *Scientific Reports* 14.1 (2024), p. 5661. DOI: https://doi.org/10.1038/s41598-024-55988-5.

[15] Achikkulath Prasanthi et al. "Optimal Sizing and Dynamic Energy Source Characteristics of Hybrid Electric Vehicles: A Comprehensive Review and Future Directions". In: *IEEE Access* (2024). DOI: https://doi.org/10.1109/ACCESS.2024.3380464.

[16] Husam A Neamah et al. “Development of a Volkswagen Jetta MK5 Hybrid Vehicle for Optimized System Efficiency Based on a Genetic Algorithm”. In: *Energies* 17.5 (2024), p. 1116. DOI: https://doi.org/10.3390/en17051116.

[17] VĂSCAN Iulia and SZABÓ Loránd. “A Brief History of Electric Vehicles.” In: *Journal of Computer Science & Control Systems* 15.1 (2022).

[18] Murat Ferhat Dogdu and Iskender Atilla Reyhancan. “The comparison of gasoline powered vehicle and serial hybrid vehicle on emissions”. In: *Heliyon* (2024). DOI: https://doi.org/10.1016/j.heliyon.2024.e28532.

[19] Eng Irina-Ioana PICIOROAGĂ. “PH. D. THESIS SUMMARY”. PhD thesis. University Politehnica of Bucharest, 2020.

[20] Teng Liu et al. “Driving conditions-driven energy management strategies for hybrid electric vehicles: A review”. In: *Renewable and Sustainable Energy Reviews* 151 (2021), p. 111521. DOI: https://doi.org/10.1016/j.rser.2021.111521.

[21] Mohsen Moghimi, Mohammad Mahdi Teymoori, and Iman Chitsaz. “New vehicle control strategy for fuel consumption and battery state of health improvement in a series hybrid vehicle utilizing fuzzy logic”. In: *Journal of the Brazilian Society of Mechanical Sciences and Engineering* 46.5 (2024), pp. 1–20. DOI: https://doi.org/10.1007/s40430-024-04851-9.

[22] Patrick Phlips. *Simple Hybrid Electric Vehicle Operating and Fuel Consumption Model*. Tech. rep. SAE Technical Paper, 2024. DOI: https://doi.org/10.4271/2024-01-2153.

[23] Fazel Mohammadi and Mehrdad Saif. “A comprehensive overview of electric vehicle batteries market”. In: *e-Prime-Advances in Electrical Engineering, Electronics and Energy* 3 (2023), p. 100127. DOI: https://doi.org/10.1016/j.prime.2023.100127.

[24] Likang Fan et al. “Real-Time Energy Management Strategy with Dynamically Updating Equivalence Factor for Through-The-Road (TTR) Hybrid Vehicles”. In: *Energy* (2024), p. 131343. DOI: https://doi.org/10.1016/j.energy.2024.131343.

[25] Nikiforos Zacharof et al. “A simulation model of the real-world fuel and energy consumption of light-duty vehicles”. In: *Frontiers in Future Transportation* 5 (2024), p. 1334651. DOI: https://doi.org/10.3389/ffutr.2024.1334651.

[26] Naila Ben Halima et al. “Fuel consumption comparative optimization for parallel hybrid electric vehicle based on PSO and DIRECT algorithms”. In: *Proceedings of the Institution of Mechanical Engineers, Part D: Journal of Automobile Engineering* (2024), p. 09544070241233797. DOI: https://doi.org/10.1177/09544070241233797.

[27] Mingi Choi, Junepyo Cha, and Jingeun Song. “Analysis of fuel economy reduction factors of hybrid electric vehicles in winter using on-road driving data”. In: *Energy* 289 (2024), p. 129977. DOI: https://doi.org/10.1016/j.energy.2023.129977.

[28] Roberto HQ Filho et al. “Development of a Genetic Algorithm-Based Control Strategy for Fuel Consumption Optimization in a Mild Hybrid Electrified Vehicle’s Electrified Propulsion System”. In: *Energies* 17.9 (2024), p. 2015. DOI: https://doi.org/10.3390/en17092015.

[29] European Investiment Bank. *https://www.eib.org/en/press/all/2022-043-when-shopping-for-a-new-car-the-vast-majority-of-hungarians-say-they-will-opt-for-a-hybrid-or-electric-vehicle*. EIB Climate Survey, (accessed on 1 May 2024), 2022.

[30] Sándor Bodzás et al. “Redesign of a Volkswagen Crafter vehicle to a hybrid vehicle having e-motor and diesel engine”. In: *IOP Conference Series: Materials Science and Engineering*. Vol. 1237. 1. IOP Publishing. 2022, p. 012008. DOI: 10.1088/1757-899X/1237/1/012008.

[31] Sprit Monitor. *https://www.spritmonitor.de/en/detail/764168.html*. Fisch und Fischl GmbH, (accessed on 23 May 2024).

[32] Sprit Monitor. *https://www.spritmonitor.de/en/detail/635135.html*. Fisch und Fischl GmbH, (accessed on 23 May 2024).

[33] Volkswagen e-Crafter Review. *https://motoreu.com/volkswagen-e-crafter-mpg-fuel-consumption-technical-specifications-177251*. VW, (accessed on 23 May 2024).

[34] Aminu Babangida et al. “Development of Meta-Heuristic Optimization Based Control of Redesigned VW Crafter Hybrid Vehicle”. In: *2024 IEEE 21st International Power Electronics and Motion Control Conference (PEMC)*. IEEE. 2024, pp. 1–6. DOI: https://doi.org/10.1109/PEMC61721.2024.10726405.

[35] Debalina De, Uttara Das, and Champa Nandi. “A comprehensive approach of evolving electric vehicles (EVs) to attribute “green self-generation”–a review”. In: *Energy Harvesting and Systems* 11.1 (2024), p. 20230023. DOI: https://doi.org/10.1515/ehs-2023-0023.

[36] Sarvesh Babu RG et al. “Techno-economic assessment of distribution system considering different types of electric vehicles and distributed generators”. In: *IET Generation, Transmission & Distribution* (2024). DOI: https://doi.org/10.1049/gtd2.13158.

[37] Julio A Sanguesa et al. “A review on electric vehicles: Technologies and challenges”. In: *Smart Cities* 4.1 (2021), pp. 372–404. DOI: https://doi.org/10.3390/smartcities4010022.

[38] Apurva Pamidimukkala et al. “Barriers and motivators to the adoption of electric vehicles: a global review”. In: *Green Energy and Intelligent Transportation* (2024), p. 100153. DOI: https://doi.org/10.1016/j.geits.2024.100153.

[39] Tigran Parikyan. “Efficient modeling of engine parts and design analysis tasks in simulation of powertrain dynamics: an overview”. In: *Advances in Engine and Powertrain Research and Technology: Design Simulation Testing Manufacturing* (2022), pp. 3–33. DOI: 10.1007/978-3-031-45705-0_98.

[40] Mehrdad Ehsani et al. *Modern electric, hybrid electric, and fuel cell vehicles*. CRC press, 2018. DOI: https://doi.org/10.1201/9780429504884.

[41] Loay M Mubarak and Ahmed Al-Samari. “Investigation of driving behavior on performance and fuel consumption of light-duty vehicle”. In: *Diyala Journal of Engineering Sciences* (2020), pp. 102–113. DOI: http://dx.doi.org/10.24237/djes.2020.13412.

[42] Daniel Briggs. *https://www.motorfinity.uk/blog/fwd-vs-rwd/*. Motor Finity, (accessed on 23 May 2024).

[43] Volkswagen. *https://www.vwpress.co.uk/assets/documents/original/19821-117257vwcv.doc*. Volkswagen Commercial Vehicles, (accessed on 23 May 2024).

[44] E Crafter. *https://www.autokostencheck.de/VW/VW-Crafter/Crafter/e-crafter-kombi-sym1e$_4$7106.html*. Autokostencheck, (accessed on 23 May 2025).

[45] electrive. *https://www.electrive.com/2020/02/10/france-chronopost-orders-420-volkswagen-e-crafter/*. France: Chronopost orders 420 Volkswagen e-Crafter, (accessed on 23 May 2024).

[46] Vaibhav V Jadhav and Prasad B Warule. *Comparative Analysis of P2 and P3 HEV Architectures for Different Vehicle Segments*. Tech. rep. SAE Technical Paper, 2024. DOI: https://doi.org/10.4271/2024-26-0284.

[47] Zhenpo Wang. "Parallel Hybrid Electric Vehicles". In: *Annual Report on the Big Data of New Energy Vehicle in China (2022)*. Springer, 2023, pp. 307–335. DOI: http://dx.doi.org/10.1007/978-981-99-6411-6_8.

[48] Özgün Balcı et al. "Numerical and experimental investigation of fuel consumption and CO2 emission performance for a parallel hybrid vehicle". In: *Alexandria Engineering Journal* 60.4 (2021), pp. 3649–3667. DOI: 10.1016/j.aej.2021.02.025.

[49] Zar Ni Lin and V Sidorov. "Study of the parameters for a parallel hybrid electric vehicle". In: *E3S Web of Conferences*. Vol. 402. EDP Sciences. 2023, p. 04014. DOI: https://doi.org/10.1051/e3sconf/202340204014.

[50] Jamal Wilson et al. "Powertrain Design For Small Scale Parallel Hybrid-Electric Test Bench". In: *Journal of Physics: Conference Series*. Vol. 2716. 1. IOP Publishing. 2024, p. 012019. DOI: 10.1088/1742-6596/2716/1/012019.

[51] Latif Kasım Uysal and Necmi Altın. "Modelling and fuzzy logic based control scheme for a series hybrid electric vehicle". In: *Journal of Energy Systems* 7.1 (2023), pp. 106–120. DOI: https://doi.org/10.30521/jes.1107190.

[52] Liuquan Yang et al. “Time-delay-aware power coordinated control approach for series hybrid electric vehicles”. In: *Energy* 294 (2024), p. 130934. DOI: https://doi.org/10.1016/j.energy.2024.130934.

[53] Turner Cotterman et al. “The transition to electrified vehicles: Evaluating the labor demand of manufacturing conventional versus battery electric vehicle powertrains”. In: *Energy Policy* 188 (2024), p. 114064. DOI: https://doi.org/10.1016/j.enpol.2024.114064.

[54] Karto Iskandar et al. “Mobile-Based Car Diagnostic Application Using Onboard Diagnostic-II Scanner”. In: *ComTech: Computer, Mathematics and Engineering Applications* 14.2 (2023), pp. 129–141.

[55] Pruthvish Rajput and Rutu Parekh. “On-Board diagnostics based remote emission test for light motor vehicles”. In: *2020 IEEE International Conference on Electronics, Computing and Communication Technologies (CONECCT)*. IEEE. 2020, pp. 1–6. DOI: https://doi.org/10.1109/CONECCT50063.2020.9198374.

[56] Dimitrios Rimpas, Andreas Papadakis, and Maria Samarakou. “OBD-II sensor diagnostics for monitoring vehicle operation and consumption”. In: *Energy Reports* 6 (2020), pp. 55–63. DOI: https://doi.org/10.1016/j.egyr.2019.10.018.

[57] Howell Li et al. “Extraction of Vehicle CAN Bus Data for Roadway Condition Monitoring”. In: (2020). DOI: 10.5703/1288284317212.

[58] Michele Mattetti et al. “Outlining the mission profile of agricultural tractors through CAN-BUS data analytics”. In: *Computers and Electronics in Agriculture* 184 (2021), p. 106078. DOI: https://doi.org/10.1016/j.compag.2021.106078.

[59] Francesco Mocera. “A model-based design approach for a parallel hybrid electric tractor energy management strategy using hardware in the loop technique”. In: *Vehicles* 3.1 (2020), pp. 1–19. DOI: https://doi.org/10.3390/vehicles3010001.

[60] Pedro Aguilar-Álvarez et al. “Instrumentation and Dynamic Characterization of a Commercial Electric Vehicle for Rural Public Transport”. In: *IEEE Access* 11 (2023), pp. 12640–12648. DOI: https://doi.org/10.1109/ACCESS.2023.3242206.

[61] Umberto Previti et al. “Influence of energy management system control strategies on the battery state of health in hybrid electric vehicles”. In: *Sustainability* 14.19 (2022), p. 12411. DOI: https://doi.org/10.3390/su141912411.

[62] V Prasanna Moorthy et al. “A hybrid technique based energy management in hybrid electric vehicle system”. In: *International journal of energy research* 46.11 (2022), pp. 15499–15520. DOI: https://doi.org/10.1002/er.8248.

[63] Yunfei Cao, Ming Yao, and Xiaodong Sun. “An overview of modelling and energy management strategies for hybrid electric vehicles”. In: *Applied Sciences* 13.10 (2023), p. 5947. DOI: https://doi.org/10.3390/app13105947.

[64] N Ding, K Prasad, and TT Lie. “Design of a hybrid energy management system using designed rule-based control strategy and genetic algorithm for the series-parallel plug-in hybrid electric vehicle”. In: *International Journal of Energy Research* 45.2 (2021), pp. 1627–1644. DOI: https://doi.org/10.1002/er.5808.

[65] Yavuz Eray Altun and Osman Akın Kutlar. “Energy Management Systems’ Modeling and Optimization in Hybrid Electric Vehicles”. In: *Energies* 17.7 (2024), p. 1696. DOI: https://doi.org/10.3390/en17071696.

[66] Pengli Yu et al. “Fuel cell hybrid electric vehicles: A review of topologies and energy management strategies”. In: *World Electric Vehicle Journal* 13.9 (2022), p. 172. DOI: https://doi.org/10.3390/wevj13090172.

[67] Arash Khalatbarisoltani et al. “Energy management strategies for fuel cell vehicles: A comprehensive review of the latest progress in modeling, strategies, and future prospects”. In: *IEEE Transactions on Intelligent Transportation Systems* 25.1 (2023), pp. 14–32.

[68] Mehrdad Ehsani et al. “State of the art and trends in electric and hybrid electric vehicles”. In: *Proceedings of the IEEE* 109.6 (2021), pp. 967–984. DOI: 10.1109/JPROC.2021.3072788.

[69] Z Chen et al. “A survey on key techniques and development perspectives of equivalent consumption minimisation strategy for hybrid electric vehicles”. In: *Renewable and Sustainable Energy Reviews* 151 (2021), p. 111607. DOI: 10.1016/j.rser.2021.111607.

[70] Federico Millo et al. “Development of a neural network-based energy management system for a plug-in hybrid electric vehicle”. In: *Transportation Engineering* 11 (2023), p. 100156. DOI: https://doi.org/10.1016/j.treng.2022.100156.

[71] Fengqi Zhang et al. “Energy management strategies for hybrid electric vehicles: Review, classification, comparison, and outlook”. In: *Energies* 13.13 (2020), p. 3352. DOI: https://doi.org/10.3390/en13133352.

[72] Hailu Abebe Debella, Samson Mekbib Atnaw, and Venkata Ramayya Ancha. “A Comprehensive Review on Hybrid and Electric Vehicle Energy Control and Management Strategies”. In: *The Dynamics of Vehicles-Basics, Simulation and Autonomous Systems* (2023). DOI: 10.5772/intechopen.111421.

[73] Julakha Jahan Jui et al. “Optimal energy management strategies for hybrid electric vehicles: A recent survey of machine learning approaches”. In: *Journal of Engineering Research* 12.3 (2024), pp. 454–467. DOI: https://doi.org/10.1016/j.jer.2024.01.016.

[74] Q Xue et al. *A comprehensive review on classification, energy management Strategy, and control algorithm for hybrid electric vehicles. Energies 2020; 13: 5355*. DOI: https://doi.org/10.3390/en13205355.

[75] Hari Maghfiroh, Oyas Wahyunggoro, and Adha Imam Cahyadi. “Energy Management in Hybrid Electric and Hybrid Energy Storage System Vehicles: A Fuzzy Logic Controller Review”. In: *IEEE Access* (2024). DOI: https://doi.org/10.1109/ACCESS.2024.3390436.

[76] Luigi Tresca et al. “Development of a deep Q-learning energy management system for a hybrid electric vehicle”. In: *Transportation Engineering* 16 (2024), p. 100241. DOI: https://doi.org/10.1016/j.treng.2024.100241.

[77] HS Das et al. *A comprehensive review on power conditioning units and control techniques in fuel cell hybrid systems. Energy Reports, 8, 14236–14258*. 2022. DOI: https://doi.org/10.1016/j.egyr.2022.10.407.

[78] Abrar Ahmed, Palaksh Yelamali, and R Udayakumar. “Modelling and simulation of hybrid technology in vehicles”. In: *Energy Reports* 6 (2020), pp. 589–594. DOI: https://doi.org/10.1016/j.egyr.2019.11.123.

[79] Henrique de Carvalho Pinheiro, Massimiliana Carello, and Elisabetta Punta. “Torque vectoring control strategies comparison for hybrid vehicles with two rear electric motors”. In: *Applied Sciences* 13.14 (2023), p. 8109. DOI: https://doi.org/10.3390/app13148109.

[80] Aminu Babangida, Chiedozie Maduakolam Light Odazie, and Péter Tamás Szemes. “Optimal Control Design and Online Controller-Area-Network Bus Data Analysis for a Light Commercial Hybrid Electric Vehicle”. In: *Mathematics* 11.15 (2023), p. 3436. DOI: https://doi.org/10.3390/math11153436.

[81] Adlan Pradana, Mejbaul Haque, and Mithulanathan Nadarajah. “Control strategies of electric vehicles participating in ancillary services: a comprehensive review”. In: *Energies* 16.4 (2023), p. 1782. DOI: https://doi.org/10.3390/en16041782.

[82] Arkan A Jassim, Ekhlas H Karam, and Mohammed Moanes E Ali. “Design of Optimal PID Controller for Electric Vehicle Based on Particle Swarm and Multi-Verse Optimization algorithms”. In: *Engineering and Technology Journal* 41.2 (2023), pp. 446–455. DOI: http://doi.org/10.30684/etj.2023.135587.1279.

[83] Eddy Lybrech Talakua, Erwin Dhaniswara, and Simson Simson. “Performance Comparison Between Differential Evolution and Bat Algorithm in PID Tuning for Optimization of Speed Control on Parallel Hybrid Electric Vehicle”. In: *Fidelity: Jurnal Teknik Elektro* 6.1 (2024), pp. 64–74. DOI: https://doi.org/10.52005/fidelity.v6i1.202.

[84] Yitong Niu and Vugar Abdullayev. “Design and performance analysis of hybrid electric vehicles using Matlab/Simulink”. In: *Wasit Journal of Computer and Mathematics Science* 2.2 (2023), pp. 60–71. DOI: https://doi.org/10.31185/wjcms.149.

[85] Md Shahin Munsi and Hicham Chaoui. “Energy Management Systems for Electric Vehicles: A Comprehensive Review of Technologies and Trends”. In: *IEEE Access* (2024). DOI: https://doi.org/10.1109/ACCESS.2024.3371483.

[86] Enrico Galvagno et al. “Hybrid Electric Vehicle Platoon Control and Optimal Energy Management System for Fuel Economy, Safety, and Dynamic Performance”. In: *IFToMM World Congress on Mechanism and Machine Science*. Springer. 2023, pp. 980–991. DOI: https://doi.org/10.1007/978-3-031-45705-0_95.

[87] Fan Wu et al. “Fractional-order sliding mode attitude coordinated control for spacecraft formation flying with unreliable wireless communication”. In: *IET Control Theory & Applications* 17.4 (2023), pp. 368–380. DOI: https://doi.org/10.1049/cth2.12360.

[88] Nahida Naji Kadhim, Layla H Abood, and Yousra Abd Mohammed. “Design an Optimal Fractional Order PID Controller for Speed Control of Electric Vehicle.” In: *Journal Européen des Systèmes Automatisés* 56.5 (2023), pp. 735–741. DOI: https://doi.org/10.18280/jesa.560503.

[89] Kanendra Naidu et al. “Enhancing Hybrid Electric Vehicle Speed Controller based on Fractional Order PID using Jaya Optimization Algorithm”. In: *2024 IEEE 4th International Conference in Power Engineering Applications (ICPEA)*. IEEE. 2024, pp. 74–79. DOI: https://doi.org/10.1109/ICPEA60617.2024.10498786.

[90] Gaurav Singhal, Shujaat Husain, and Haroon Ashfaq. “Electric Vehicle EMS with FOPID”. In: *Intelligent Systems and Smart Infrastructure*. CRC Press, 2023, pp. 586–598. ISBN: 9781003357346.

[91] Ke Li and Thanh Vo-Duy. “IEEE VTS Motor Vehicles Challenge 2024-Energy and Powertrain Losses Management of an e-Racing Vehicle”. In: *2023 IEEE Vehicle Power and Propulsion Conference (VPPC)*. IEEE. 2023, pp. 1–6. DOI: https://doi.org/10.1109/VPPC60535.2023.10403256.

[92] Carlos Reusser et al. “Novel Energy Management Scheme for a Permanent Magnet Electric Drive-Based Hybrid Vehicle Using Model Predictive Control”. In: *Machines* 12.1 (2023), p. 3. DOI: https://doi.org/10.3390/machines12010003.

[93] Shabab Saleem et al. “Artificial intelligence based robust nonlinear controllers optimized by improved gray wolf optimization algorithm for plug-in hybrid electric vehicles in grid to vehicle applications”. In: *Journal of Energy Storage* 75 (2024), p. 109332. DOI: https://doi.org/10.1016/j.est.2023.109332.

[94] Sameh Abd-Elhaleem, Walaa Shoeib, and Abdel Azim Sobaih. “Improved Power Management Under Uncertain Driving Conditions for Plug-In Hybrid Electric Vehicles via Intelligent Controller”. In: *IEEE Transactions on Intelligent Transportation Systems* (2023). DOI: https://doi.org/10.1109/TITS.2023.3308509.

[95] Mojgan Fayyazi et al. “Artificial intelligence/machine learning in energy management systems, control, and optimization of hydrogen fuel cell vehicles”. In: *Sustainability* 15.6 (2023), p. 5249. DOI: https://doi.org/10.3390/su15065249.

[96] Hamid Khayyam et al. “Artificial intelligence and internet of things for autonomous vehicles”. In: *Nonlinear approaches in engineering applications: Automotive Applications of engineering problems* (2020), pp. 39–68. DOI: https://doi.org/10.1007/978-3-030-18963-1_2.

[97] Jinglai Wu et al. “A robust online energy management strategy for fuel cell/battery hybrid electric vehicles”. In: *International Journal of Hydrogen Energy* 45.27 (2020), pp. 14093–14107. DOI: https://doi.org/10.1016/j.ijhydene.2020.03.091.

[98] Anılcan Özkan, S Davoud S Garmroodi, and Senem Kurşun. “Energy Management in Power-Split Hybrid Electric Vehicles Using Fuzzy Logic Controller”. In: *Decision Making Using AI in Energy and Sustainability: Methods and Models for Policy and Practice*. Springer, 2023, pp. 301–312. DOI: https://doi.org/10.1007/978-3-031-38387-8_18.

[99] Basima Taresh Dawood, Yasser Ahmad, and Amjed Alwan Kadhim. “Coordination of hybrid vehicles strategies to improve fuel consumption and reduce the economic cost”. In: *International Journal of Power Electronics and Drive Systems (IJPEDS)* 15.2 (2024), pp. 725–732. DOI: 10.11591/ijpeds.v15.i2.pp725-732.

[100] Sundeep Siddula. “Optimizing Electric Vehicle Energy Consumption with Fuzzy based Energy Management System”. In: *2024 IEEE International Conference for Women in Innovation, Technology & Entrepreneurship (ICWITE)*. IEEE. 2024, pp. 631–636. DOI: https://doi.org/10.1109/ICWITE59797.2024.10503375.

[101] Chinju Saju, Prawin Angel Michael, and T Jarin. “Modeling and control of a hybrid electric vehicle to optimize system performance for fuel efficiency”. In: *Sustainable Energy Technologies and Assessments* 52 (2022), p. 102087. DOI: https://doi.org/10.1016/j.seta.2022.102087.

[102] Yılmaz Seryar Arıkuşu, Nevra Bayhan, and Hasan Tiryaki. “Determination of Energy Savings via Fuel Consumption Estimation with Machine Learning Methods and Rule-Based Control Methods Devel-

oped for Experimental Data of Hybrid Electric Vehicles". In: *Energies* 16.24 (2023), p. 7970. DOI: https://doi.org/10.3390/en16247970.

[103] Matheus HR Miranda et al. "Electric vehicle powertrain and fuzzy controller optimization using a planar dynamics simulation based on a real-world driving cycle". In: *Energy* 238 (2022), p. 121979. DOI: https://doi.org/10.1016/j.energy.2021.121979.

[104] Jony Javorski Eckert et al. "Energy management and gear shifting control for a hybridized vehicle to minimize gas emissions, energy consumption and battery aging". In: *Energy Conversion and Management* 240 (2021), p. 114222. DOI: https://doi.org/10.1016/j.enconman.2021.114222.

[105] Naila Ben Halima et al. "Energy management of parallel hybrid electric vehicle based on fuzzy logic control strategies". In: *Journal of Circuits, Systems and Computers* 32.01 (2023), p. 2350007. DOI: https://doi.org/10.1142/S021812662350007X.

[106] Ahtisham Urooj and Ali Nasir. "Review of intelligent energy management techniques for hybrid electric vehicles". In: *Journal of Energy Storage* 92 (2024), p. 112132. DOI: https://doi.org/10.1016/j.est.2024.112132.

[107] Quan Zhou and Changqing Du. "A quantitative analysis of model predictive control as energy management strategy for hybrid electric vehicles: A review". In: *Energy Reports* 7 (2021), pp. 6733–6755. DOI: https://doi.org/10.1016/j.egyr.2021.09.119.

[108] Laiwei Lu et al. "MPC-ECMS Energy Management of Extended-Range Vehicles Based on LSTM Multi-Signal Speed Prediction". In: *Electronics* 12.12 (2023), p. 2642. DOI: https://doi.org/10.3390/electronics12122642.

[109] Yuanhang Chen et al. "A new hybrid model predictive controller design for adaptive cruise of autonomous electric vehicles". In: *Journal of Advanced Transportation* 2021 (2021), pp. 1–25. DOI: https://doi.org/10.1155/2021/6626243.

[110] Jan Glos et al. "Hybrid model predictive control for fully electric vehicle thermal management system optimal mode selection". In: *IECON 2020 The 46th Annual Conference of the IEEE Industrial Electronics Society*. IEEE. 2020, pp. 2036–2043. DOI: https://doi.org/10.1109/IECON43393.2020.9254286.

[111] Xiaosong Hu et al. “Model predictive control of hybrid electric vehicles for fuel economy, emission reductions, and inter-vehicle safety in car-following scenarios”. In: *Energy* 196 (2020), p. 117101. DOI: https://doi.org/10.1016/j.energy.2020.117101.

[112] Trieu Minh Vu et al. “Parallel hybrid electric vehicle modelling and model predictive control”. In: *Applied Sciences* 11.22 (2021), p. 10668. DOI: https://doi.org/10.3390/app112210668.

[113] Massimo De Mauri et al. “Real-time model predictive control for a parallel hybrid electric vehicle using outer approximation and semi-convex cut generation”. In: *2020 IEEE 16th International Workshop on Advanced Motion Control (AMC)*. IEEE. 2020, pp. 198–203. DOI: https://doi.org/10.1109/AMC44022.2020.9244369.

[114] Sebastian East and Mark Cannon. “Scenario model predictive control for data-based energy management in plug-in hybrid electric vehicles”. In: *IEEE Transactions on Control Systems Technology* 30.6 (2022), pp. 2522–2533. DOI: https://doi.org/10.1109/TCST.2022.3154155.

[115] Benxiang Lin et al. “A Predictive Energy Management Strategy for Heavy Hybrid Electric Vehicles Based on Adaptive Network-Based Fuzzy Inference System-Optimized Time Horizon”. In: *Energies* 17.10 (2024), p. 2288. DOI: https://doi.org/10.3390/en17102288.

[116] Ying Yao et al. “Vehicle fuel consumption prediction method based on driving behavior data collected from smartphones”. In: *Journal of Advanced Transportation* 2020 (2020), pp. 1–11. DOI: https://doi.org/10.1155/2020/9263605.

[117] Young-Rong Kim, Min Jung, and Jun-Bum Park. “Development of a fuel consumption prediction model based on machine learning using ship in-service data”. In: *Journal of Marine Science and Engineering* 9.2 (2021), p. 137. DOI: https://doi.org/10.3390/jmse9020137.

[118] Erkan Türker et al. “Estimation of Energy Management Strategy Using Neural-Network-Based Surrogate Model for Range Extended Vehicle”. In: *Applied Sciences* 12.24 (2022), p. 12935. DOI: https://doi.org/10.3390/app122412935.

[119] Ziwang Lu et al. “Neural network energy management strategy with optimal input features for plug-in hybrid electric vehicles”. In: *Energy* 285 (2023), p. 129399. DOI: https://doi.org/10.1016/j.energy.2023.129399.

[120] Mohammadali Kargar, Chen Zhang, and Xingyong Song. "Integrated optimization of powertrain energy management and vehicle motion control for autonomous hybrid electric vehicles". In: *IEEE Transactions on Vehicular Technology* (2023). DOI: https://doi.org/10.1109/TVT.2023.3270127.

[121] S Titus, S Rajalakshmi, and G Gabriel Santhosh Kumar. "Optimal Sliding Mode Converter with Energy Management System for Hybrid Electric Vehicle". In: *2021 International Conference on Advances in Electrical, Computing, Communication and Sustainable Technologies (ICAECT)*. IEEE. 2021, pp. 1–12. DOI: https://doi.org/10.1109/ICAECT49130.2021.9392466.

[122] Min Hua et al. "Energy management of multi-mode plug-in hybrid electric vehicle using multi-agent deep reinforcement learning". In: *Applied Energy* 348 (2023), p. 121526. DOI: https://doi.org/10.1016/j.apenergy.2023.121526.

[123] Sangjoon Kim, Sung Hoon Yu, and Hyeongcheol Lee. "Traction control using a disturbance observer for hybrid electric vehicles". In: *International Journal of Automotive Technology* 22 (2021), pp. 1485–1494. DOI: https://doi.org/10.1007/s12239-021-0128-x.

[124] Kornél Katona, Husam A Neamah, and Péter Korondi. "Obstacle avoidance and path planning methods for autonomous navigation of mobile robot". In: *Sensors* 24.11 (2024), p. 3573. DOI: https://doi.org/10.3390/s24113573.

[125] Ivan Lopez-Sanchez and Javier Moreno-Valenzuela. "PID control of quadrotor UAVs: A survey". In: *Annual Reviews in Control* 56 (2023), p. 100900. DOI: https://doi.org/10.1016/j.arcontrol.2023.100900.

[126] J Mohan and C Kishore. "Smart vehicle monitoring for detecting anomalies on CAN bus". In: *2021 IEEE International Conference on Electronics, Computing and Communication Technologies (CONECCT)*. IEEE. 2021, pp. 1–6. DOI: https://doi.org/10.1109/CONECCT52877.2021.9622628.

[127] *https://www.csselectronics.com/pages/can-bus-simple-intro-tutorial*. CSS ELECTRONICS, (Accesssed, 10 January, 2023).

[128] Michele Ruta et al. “A mobile knowledge-based system for on-board diagnostics and car driving assistance”. In: *4th International Conference on Mobile Ubiquitous Computing, Systems, Services and Technologies (UBICOMM)*. 2010, pp. 91–96.

[129] OBD2 Frame Format and Message Structure. *https://www.rfwireless-world.com/terminology/obd2-frame-format-message-structure*. RF Wireless World, (accessed on 23 May 2024).

[130] Bogdan Anton and Adriana Florescu. “Design and development of series-hybrid automotive powertrains”. In: *IEEE Access* 8 (2020), pp. 226026–226041. DOI: https://doi.org/10.1109/ACCESS.2020.3044500.

[131] Fredy Rosero et al. “Real-world fuel efficiency and emissions from an urban diesel bus engine under transient operating conditions”. In: *Applied energy* 261 (2020), p. 114442. DOI: https://doi.org/10.1016/j.apenergy.2019.114442.

[132] Hamidreza Abediasl et al. “Real-time vehicular fuel consumption estimation using machine learning and on-board diagnostics data”. In: *Proceedings of the Institution of Mechanical Engineers, Part D: Journal of Automobile Engineering* (2023), p. 09544070231185609. DOI: https://doi.org/10.1177/09544070231185609.

[133] Garrett Whitmore et al. *A data driven approach for real-world vehicle energy consumption prediction*. Tech. rep. SAE Technical Paper, 2024. DOI: https://doi.org/10.4271/2024-01-2870.

[134] Mozhgan Nasr Azadani and Azzedine Boukerche. “Performance evaluation of driving behavior identification models through can-bus data”. In: *2020 IEEE Wireless Communications and Networking Conference (WCNC)*. IEEE. 2020, pp. 1–6. DOI: https://doi.org/10.1109/WCNC45663.2020.9120734.

[135] Matthew Bunting, Rahul Bhadani, and Jonathan Sprinkle. “Libpanda: A high performance library for vehicle data collection”. In: *Proceedings of the Workshop on Data-Driven and Intelligent Cyber-Physical Systems*. 2021, pp. 32–40. DOI: https://doi.org/10.1145/3459609.3460529.

[136] Satish S Salunkhe et al. “Energy optimization for CAN bus and media controls in electric vehicles using deep learning algorithms”. In: *The Journal of Supercomputing* (2022), pp. 1–16. DOI: https://doi.org/10.1007/s11227-021-04186-5.

[137] MIT Admin. *https://milestone.ac.in/blog-mit/what-is-data-acquisition/*. Milestone Institute of Technology, (accessed on 23 May 2025).

[138] CAN Bus Errors. *https://www.autopi.io/blog/what-are-can-bus-errors/*. Auto PI, (accessed on 10 June 2025).

[139] Aiguo Zhou, Zhenyu Li, and Yong Shen. "Anomaly detection of CAN bus messages using a deep neural network for autonomous vehicles". In: *Applied Sciences* 9.15 (2019), p. 3174. DOI: https://doi.org/10.3390/app9153174.

[140] Jie Liu et al. "Review of thermal coupled battery models and parameter identification for lithium-ion battery heat generation in EV battery thermal management system". In: *International Journal of Heat and Mass Transfer* 218 (2024), p. 124748. DOI: https://doi.org/10.1016/j.ijheatmasstransfer.2023.124748.

[141] Zhijie Yang, Haibo Huang, and Feng Lin. "Sustainable electric vehicle batteries for a sustainable world: perspectives on battery cathodes, environment, supply chain, manufacturing, life cycle, and policy". In: *Advanced Energy Materials* 12.26 (2022), p. 2200383. DOI: https://doi.org/10.1002/aenm.202200383.

[142] Yusheng Zheng et al. "Thermal state monitoring of lithium-ion batteries: Progress, challenges, and opportunities". In: *Progress in Energy and Combustion Science* 100 (2024), p. 101120. DOI: https://doi.org/10.1016/j.pecs.2023.101120.

[143] John G Hayes and G Abas Goodarzi. "Electric powertrain: energy systems, power electronics and drives for hybrid, electric and fuel cell vehicles". In: (2018).

[144] Wei Liu, Tobias Placke, and KT Chau. "Overview of batteries and battery management for electric vehicles". In: *Energy Reports* 8 (2022), pp. 4058–4084. DOI: https://doi.org/10.1016/j.egyr.2022.03.016.

[145] Aminu Babangida and Péter Tamás Szemes. "Electric vehicle modelling and simulation of a light commercial vehicle using pmsm propulsion". In: *Hungarian Journal of Industry and Chemistry* 49.1 (2021), pp. 37–46. DOI: https://doi.org/10.33927/hjic-2021-06.

[146] Simon EJ O'Kane et al. "Lithium-ion battery degradation: how to model it". In: *Physical Chemistry Chemical Physics* 24.13 (2022), pp. 7909–7922. DOI: https://doi.org/10.1039/D2CP00417H.

[147] Engineeringonline.com. *https://www.evengineeringonline.com/how-does-ambient-temperature-affect-ev-batteries/*. EV Engineering Infrastructure, (accessed on 23 May 2025).

[148] Wei Gao et al. "Evaluation of the second-life potential of the first-generation Nissan Leaf battery packs in energy storage systems". In: *ETransportation* 20 (2024), p. 100313. DOI: https://doi.org/10.1016/j.etran.2024.100313.

[149] PK Prathibha and Elizabeth Rita Samuel. "Performance analysis of electric car based on drag coefficients and road angles". In: *2022 2nd International Conference on Power Electronics & IoT Applications in Renewable Energy and its Control (PARC)*. IEEE. 2022, pp. 1–6. DOI: https://doi.org/10.1109/PARC52418.2022.9726686.

[150] Adeel Saleem et al. "Modelling of an electric vehicle for tractive force calculation along with factors affecting the total tractive power and energy demand". In: *2020 3rd International Conference on Computing, Mathematics and Engineering Technologies (iCoMET)*. IEEE. 2020, pp. 1–5. DOI: https://doi.org/10.1109/iCoMET48670.2020.9073845.

[151] Aminu Babangida and Péter Tamás Szemes. "Electric Vehicle Modeling and Simulation of Volkswagen Crafter with 2.0 TDI CR Diesel Engine". In: *Recent Innovations In Mechatronics* (2021). DOI: https://doi.org/10.17667/riim.2021.1/1..

[152] Crafter. *https://www.waterloovans.co.uk/cars/volkswagen/crafter/2.0-tdi-cr35-trendline/1461065/*. (accessed on 10 June 2025).

[153] Volkwagen Crafter. *https://en.wikipedia.org/wiki/Volkswagen_Crafter*. Wikipedia, (accessed on 23 May 2025).

[154] Sándor Guba et al. "Laboratory Measurement of Rolling Resistance Coefficient under Different Conditions". In: *Hungarian Journal of Industry and Chemistry* 51.1 (2023), pp. 23–27. DOI: https://doi.org/10.33927/hjic-2023-04.

[155] Ashwini Kumar et al. "Development of electric vehicle with permanent magnet synchronous motor and its analysis with drive cycles in MATLAB/Simulink". In: *Materials Today: Proceedings* 72 (2023), pp. 643–651.

[156] Xin Wang. “Field-Oriented Control of Permanent Magnet Synchronous Motors Based on DSP Controller by Qasim Al azze, Bachelor of Science”. PhD thesis. Southern Illinois University Edwardsville, 2014.

[157] Vishal Virani, Swapnil Arya, Jaydeepsinh Baria, et al. “Modelling and Control of PMSM Drive by Field Oriented Control For HEV”. In: *C, Modelling and Control of PMSM Drive by Field Oriented Control For HEV (February 12, 2019). Advances in Power Generation from Renewable Energy Sources (APGRES)* (2019). DOI: 10.2139/ssrn.3442515.

[158] Aminu Babangida and Pèter Tamás Szemes. “Energy consumption simulation and economic benefit analysis for a light duty urban commercial electric vehicle”. In: *2022 IEEE 20th International Power Electronics and Motion Control Conference (PEMC)*. IEEE. 2022, pp. 667–672. DOI: https://doi.org/10.1109/PEMC51159.2022.9962881.

[159] Aminu Babangida Abdullah Waheeb Jaffer Omer Ghareeb and Péter Tamás Szemes. “Dynamic Modeling and Optimization of Permanent Magnet Synchronous Electrical Machine Propulsion Powertrain at Different Modeling Levels”. In: *Acta Polytechnica Hungarica* (2025). DOI: DOI:10.12700/APH.22.3.2025.3.3.

[160] Seong-Cheol Kim et al. “Design and analysis of BLDC motor driver for hybrid electric vehicles”. In: *Next Generation Smart Grids: Modeling, Control and Optimization*. Springer, 2022, pp. 297–311.

[161] Mopidevi Subbarao et al. “Design, control and performance comparison of PI and ANFIS controllers for BLDC motor driven electric vehicles”. In: *Measurement: Sensors* 31 (2024), p. 101001.

[162] Khairy Sayed et al. “Application of Tilt Integral Derivative for Efficient Speed Control and Operation of BLDC Motor Drive for Electric Vehicles”. In: *Fractal and Fractional* 8.1 (2024), p. 61.

[163] Dhineshkumar Krishnan et al. “Optimized Design and Deployment of BLDC Motor Poles in E-Vehicle”. In: *2024 International Conference on Science Technology Engineering and Management (ICSTEM)*. IEEE. 2024, pp. 1–4.

[164] V Sandeep and Sharankumar Shastri. “Analysis and design of PM-BLDC motor for three wheeler electric vehicle application”. In: *E3S web of conferences*. Vol. 87. EDP Sciences. 2019, p. 01022.

[165] Syed Shehryar Ali Naqvi et al. “Multi-objective optimization of PI controller for BLDC motor speed control and energy saving in Electric Vehicles: A constrained swarm-based approach”. In: *Energy Reports* 12 (2024), pp. 402–417.

[166] Aidha Muhammad Ajmal and VK Ramachandaramurthy. “Regenerative Braking of Electric Vehicle with Brushless DC Motor”. In: *Applied Mechanics and Materials* 785 (2015), pp. 280–284. DOI: https://doi.org/10.4028/www.scientific.net/AMM.785.280.

[167] CM Pappalardo et al. “Design and development of a virtual model of an electric vehicle of category L7”. In: *IOP Conference Series: Materials Science and Engineering*. Vol. 568. 1. IOP Publishing. 2019, p. 012114. DOI: 10.1088/1757-899X/568/1/012114.

[168] Mirza Muntasir Nishat et al. “Development of genetic algorithm (ga) based optimized PID controller for stability analysis of DC-DC buck converter”. In: *Journal of Power and Energy Engineering* 8.09 (2020), p. 8. DOI: https://doi.org/10.4236/jpee.2020.89002.

[169] Qian Zhang and Shaopeng Tian. “Energy Consumption Prediction and Control Algorithm for Hybrid Electric Vehicles Based on an Equivalent Minimum Fuel Consumption Model”. In: *Sustainability* 15.12 (2023), p. 9394. DOI: https://doi.org/10.3390/su15129394.

[170] Mathwork. *Generic Internal Combustion Engine*. Mathwork 2024, (accessed on 5 January 2024).

[171] JS Norbakyah et al. “Modeling, simulation and model optimization of internal combustion engine for PHERB powertrain”. In: *Jurnal Teknologi (Sciences & Engineering)* 79.5 (2017). DOI: https://doi.org/10.11113/jt.v79.9262.

[172] Callum J Oglieve, Mahdi Mohammadpour, and Homer Rahnejat. “Optimisation of the vehicle transmission and the gear-shifting strategy for the minimum fuel consumption and the minimum nitrogen oxide emissions”. In: *Proceedings of the Institution of Mechanical Engineers, Part D: Journal of Automobile Engineering* 231.7 (2017), pp. 883–899. DOI: https://doi.org/10.1177/0954407017702985.

[173] Jonker - Huissen B.V.: Gearbox Volkswagen Crafter 2.0 TDI FWD - Gearbox With Gearbox Code TWX New. *https://www.proxyparts.com/car-parts-stock/information/gearbox-code/twx/part/gearbox/partid/20789355*. Proxy Part, (accessed on 23 May 2025).

[174] Aminu Babangida, Chiedozie Maduakolam Light Odazie, and Péter Tamás Szemes. “Fuel economy simulation and development of an online data acquisition system with hil method for a vw crafter hybrid car”. In: *2023 IEEE 32nd International Symposium on Industrial Electronics (ISIE)*. IEEE. 2023, pp. 1–4. DOI: https://doi.org/10.1109/ISIE51358.2023.10227931.

[175] Yurdagül Benteşen Yakut. “A new control algorithm for increasing efficiency of PEM fuel cells–Based boost converter using PI controller with PSO method”. In: *International Journal of Hydrogen Energy* 75 (2024), pp. 1–11. DOI: https://doi.org/10.1016/j.ijhydene.2023.12.008.

[176] Gaber Magdy et al. “Tustin’s technique based digital decentralized load frequency control in a realistic multi power system considering wind farms and communications delays”. In: *Ain Shams Engineering Journal* 10.2 (2019), pp. 327–341. DOI: https://doi.org/10.1016/j.asej.2019.01.004.

[177] Ping Wang et al. “Fractional-order load frequency control of an interconnected power system with a hydrogen energy-storage unit”. In: *Fractal and Fractional* 8.3 (2024), p. 126. DOI: https://doi.org/10.3390/fractalfract8030126.

[178] Krzysztof Parczewski and Henryk Wnęk. “Analysis of energy flow in hybrid and electric-drive vehicles”. In: *Energies* 17.8 (2024), p. 1915. DOI: https://doi.org/10.3390/en17081915.

[179] Javier E Meseguer et al. “Assessing the impact of driving behavior on instantaneous fuel consumption”. In: *2015 12th annual IEEE consumer communications and networking conference (CCNC)*. IEEE. 2015, pp. 443–448. DOI: https://doi.org/10.1109/CCNC.2015.7158016.